CRANFIELD UNIVERSITY

NASR ALMANDHARI

Influence of Centrifugal Compressor System Components on its General Rotordynamic Characteristics

MSc by Research
Academic Year: 2015 - 2016

SCHOOL OF AEROSPACE
Final Thesis Report

Initial registration: 10 April 2014

Supervisor: Professor Pilidis
Supervisor: Professor David Mba

Abstract:

Nowadays most countries are depending on Oil and Gas for their energy supply. In such operations, centrifugal compressors are dominating most of the used critical machines hence it is important to give these turbomachines more consideration in terms of their technical performance and reliability. Centrifugal compressors are one of many turbomachines that require technical solutions for Enhanced Oil Recovery (EOR). The oil and gas fields have different production environments which require adequate selection of compressors to handle the variance in gas and oil specifications and this in turn force the equipment manufacturers to revise their currently used design specifications.

This research presents different types of compressors and their work principles with an emphasis on centrifugal compressor components The literature review carried in this research describes different cases in turbomachinery rotordynamics where failures were encountered at the commissioning and operation stages. Also the literature shows how these machines are improved technically by improving the compressor components performance such using Pocket Damper seals and tilting type bearings.

The aim of this research is to study the factors affecting Rotordynamic behaviour of large natural gas centrifugal compressors. The study will review the influence of various conditions of rotor components such as bearings, seals, impellers, etc on the overall Rotordynamic stability at various process conditions.

The two cases study of this research were selected of four identical centrifugal compressors have been commissioned in May 2010 and since then there were many identical high vibration amplitude issues which consequences the compressor tripped, this issues were investigated numerically and experimentally in this thesis. The first phenomenon was high levels of rotor vibration while traversing its first critical speed during hot start only. The high amplitude vibration occurred while traversing its 1^{st} critical speed during hot

start was investigated numerically. The different rotordynamic affects were rolled out in terms of direct influence on this case such as force coefficients (direct and cross-coupled coefficients) and rotor unbalance effect. The temporary thermal bow was suspected to be the reason of this phenomenon; therefore a detailed investigation has been conducted numerically to investigate the thermal bow effect at 1st critical speed.

The second phenomenon was high vibration appearing on gearbox pinion bearing side during MOCS. The torsional vibration were confirmed by conducting torsional numerical analysis, the interference diagram indicated some of natural frequencies which it could be excited by different harmonics that may be excited by the VFD motor.

Key Words,

Labyrinth Seals, Unbalance, Rotor, Bearing, Instability, Cross coupling forces, Torsional vibration, Lateral vibration, Damping, stiffness, Critical Speed

ACKNOWLEDGEMENTS

I am very grateful to all those who were encouraged me to peruse my MSc. I would like to thank my thesis supervisor Professor Pilidis, Head of Propulsion Engineering Centre School of Aerospace, Transport and Manufacturing, who's always keen to help me whenever needed. Also I would like to thank Professor David Mba who was guiding me technically me throughout my research.

Furthermore I would like to acknowledge my best friend Dr Mohamed Al Yahyai and Mr Saif Al Farsi, PDO Compressor Subject Matter Expert (SME) who were contributing in stimulating suggestions and discussion.

I am very thankful to my parents whom without their prayers and encouragement this project would not have been completed. To my beloved wife and my sweet daughters and sons thanks a lot for your patient, encouragement and support during my study period.

TABLE OF CONTENTS

LIST OF FIGURES

List of Tables

NOMENCLATURE

ζ	Damping ratio
x	Displacement
$\dot{x}$	Velocity
$\ddot{x}$	Acceleration
j	Imaginary number
K	Spring force
m	Mass
c	Damper force
ω	Forcing frequency
α	Acceleration of a body
ϕ	Phase angle
Ek	Kinetic energy
Cc	Critical damping
v	Velocity
My	Bending moment
ωn	Natural Frequency
ωd	Damped natural Frequency
Vz	Shear force
Z	State vector
F	Field Matrix
P	Point Matrix
$\bar{R}$	Amplitude Ratio
Ω	Frequency Ratio (function of shaft speed)
P	Natural Frequency
V	Whirl Frequency
T	Torque
J	Polar moment of inertia
τ	Torsional shear stress

LIST OF ABBREVIATIONS

CFM	Cubic Feet per Minute
UCS	Undamped Critical Speed
PDO	Petroleum Development Oman
EOM	Equation of Motion
EOR	Enhanced Oil Recovery
FEA	Finite Element Analysis
TM	Transfer Matrix
IGV	Inlet Guide Vanes
PDS	Pocket Damper Seal
LPC	Low Pressure Compressor
MPC	Medium Pressure Compressor
HPC	High Pressure Compressor
HPS	Hole Pattern Seal
DGS	Dry Gas Seal
MCS	Maximum Continuous Speed
DTHCS	Diverging Taper Honeycomb Stator Seal
FPDS	Fully Partitioned Pocket Damper Seal
SOG	Stabilizer off gas
API	American Petroleum Institute
DEP	Design Engineering Practice (Shell Standard)
SP	PDO Specification
FAT	Factory Acceptance Test
MRT	Mechanical Running Test
SRDC	Sieh Rawl Depletion Compressor
SM	Separation Margin
AF	Amplification Factor
MCOS	Maximum Continuous Operation Speed
MMSCMD	Million Metric Stander Cubic Meter per Day

Section one

1 Introduction

1.1 General Background of the Research Topic

Compressors have various industrial applications. Natural gas compressors, in particular, are widely used in oil and gas industry. They are also used in power generation, and chemical processing units. Gas Compressors types are divided into different types for different applications such as axial, centrifugal, integrally geared, reciprocating, or rotary. [4] Compressors selection is dependent mainly upon the required process duty conditions such as flow, pressure, temperature, etc. It also depends on fluid properties such as density, mole weight, dew point, etc. of the gas in combination with the total head (compression ratio) and the duty which has to be performed.

This thesis consists of four sections such as compressor types, rotordynamic fundamentals, literature review and Rotor dynamic numerical analysis.

The first section covers different types of compressors used in industrial area classified in two major applications such as rotary flow compressor and positive displacement flow compressor. This section shows the dynamic principle of each type; however the centrifugal compressor design, operation and components were explained to understand their influence on compressor rotordynamic.

The second section highlights the rotordynamic fundamentals mainly on the three rotor vibration modes lateral, torsional and axial. Also the comparison between lateral vibration and torsional vibration was indicated

The literature review on the Influence of Centrifugal Compressor System Components in its rotordynamics is covered in section three as it is divided into three chapter's aerodynamics (Seals), hydrodynamics i (Bearings) and rotor influence. All three affects centrifugal compressor in terms of its reliability and life span, such as instability, unbalance and surge.

Section four describes the selected case study and its corresponding numerical analysis. Both lateral and torsional analyses were discussed in details considering varying operational factors, Moreover the two issues were investigated numerically, the first phenomenon was the high levels of rotor vibration while traversing its first critical speed during hot start only and the second phenomenon was sadden high vibration appearing on gearbox pinion bearing side during MOCS. Numerical analysis were used to study the two phenomenon while field data provides some vibration data mainly from system 1 Bently Nevada for two different rotor configurations where the effect of seals, mounting methodologies and bearings are studied. The results include Undamped Critical Speeds (UCS), damped critical speed and forced response analysis. Also the analysis explores the factors affecting rotor instability and their effect on rotordynamics characteristics.

1.2 **Types of compressors:**

The two major classifications of compressors are:

- Axial flow compressors and Centrifugal flow compressors which are classified from Turbomachines, also known as Rotordynamic machines.
- Positive Displacement compressors which are classified from Displacement machines

These two classifications apply to compressor handling any fluid, the same basic principles apply. However, the working principles of Turbomachines and Displacement machines are fundamentally different. Turbomachines work by putting kinetic energy into the fluid and then converting that kinetic energy into pressure. Displacement machines work by enclosing fluid in a moving part of the machine and transporting both fluid and machine part from inlet to outlet.

Figure 1—1[1] shows a general chart for preliminary selection of compressors in terms of suction Volume (m^3/hr) and Discharge pressure (bara) and also with other specified operating points which shall be selected within the proven

operating envelope such as Flow consideration, temperature considerations and also Fluid type considerations (hazardous classification).

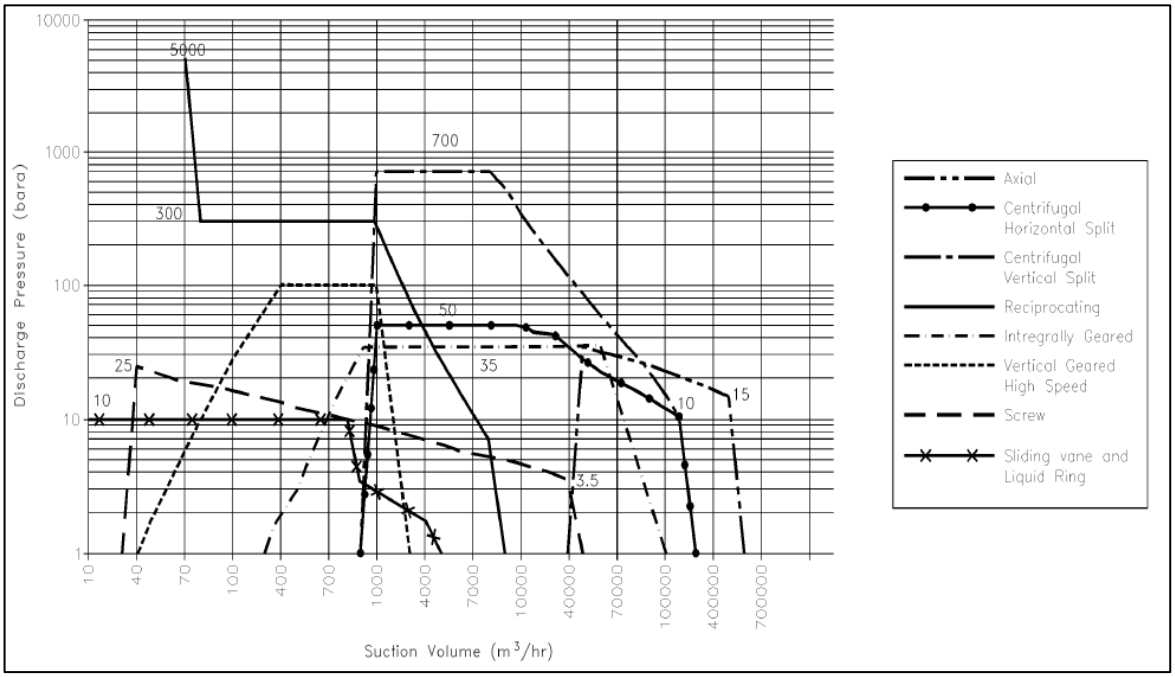

Figure 1—1 PRESSURE/ VOLUME MAP FOR VARIOUS COMPRESSOR TYPES[4]

1.2.1 Axial compressor

Axial compressor can handle larger volume flows and more efficient than centrifugal compressors. However, centrifugal compressors have wider operating ranges and less exposed to surge and disposed to fouling. For that, axial compressors should be selected for high flow applications with consideration of gas quality such as cleanness and non-corrosive.[4]

Axial flow compressor consists of a rotor assemblies with rows of airfoil section blades mounted around it. The rotor mounted between bearings in the casings which are fit in stator blades, also of airfoil section arrangement. A compressor stage consists of a row of rotating blades followed by a row of stator blades Figure 1—2. The compressor is a multistage unit as the pressure increase by each stage is small. At the inlet to the compressor is an additional row of stationary blades known as the inlet guide vanes (IGVs). On some Compressors the IGVs are variable that is the angle of incidence of the blade

can be varied during start up and running. On other compressor the IGVs are fixed, that is the angle of incidence does not change, they are used to guide the air smoothly onto the first row of the rotor blades. There is a gradual reduction in the air annulus area from the low to the high pressure end i.e. from the inlet to the exit end of the compressor. At the exit end of the compressor are usually fitted exit guide vanes. These are used to straighten the airflow, leaving the end of the compressor to remove swirl from the air before entering into the combustion chamber at a reasonably uniform axial velocity.[2]

The air enters through the compressor IGVs with high speed rotor it is accelerated by help of rotating blades and then the air compressed through the Stator blades and it is diffused in to stator passage which resulted kinetic energy convert to pressure, as shown in Figure 1—3.[2]

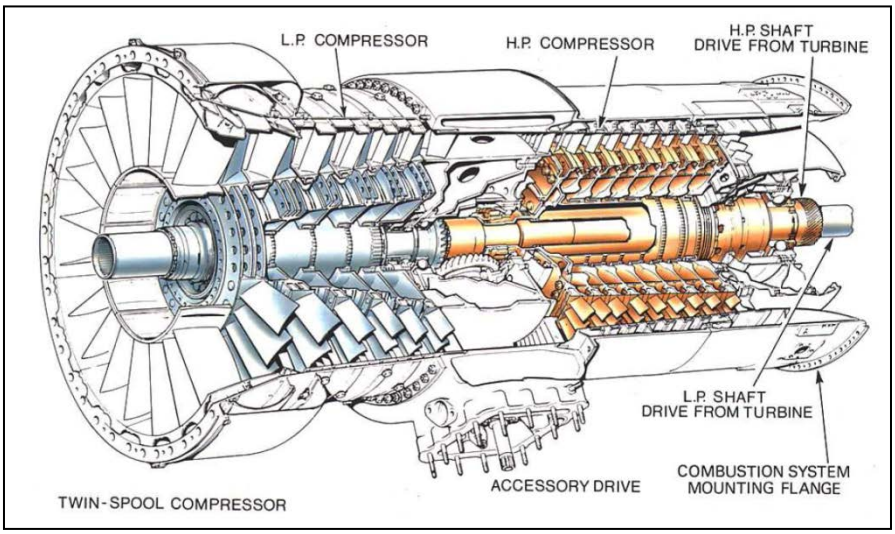

Figure 1—2 Typical axial flow compressor [2]

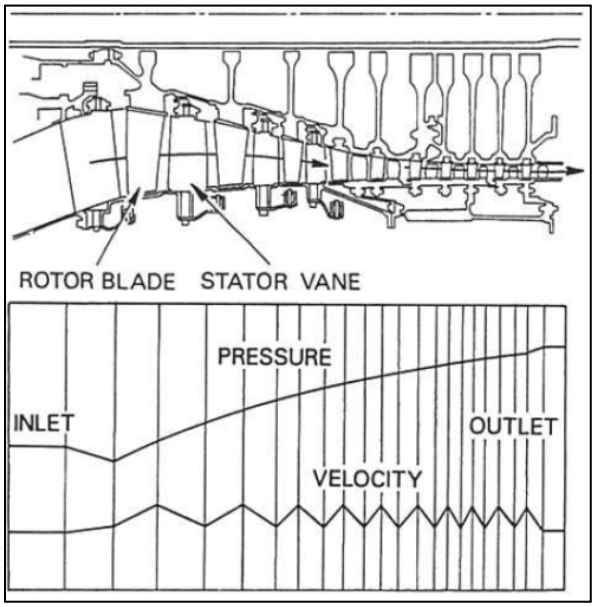

Figure 1—3 Pressure and velocity changes through an axial compressor. (© Rolls-Royce plc 1986) [2]

1.2.2 Positive Displacement compressor

A positive Displacement compressor is mainly selected of high pressure and low volume application process also it can consider on the selection in case the flow required is too small for centrifugal compressor selection or if the head requires an undesirable, large number of stages. [4]

There are two classifications of Reciprocating compressors:

- **Single acting reciprocating compressor.**

In single acting compressor, the forward stroke is the compression stroke and backward stroke is the suction stroke. As shown in the above drawing compression is taking place only on one side of the piston. One forward stroke and one backward stroke make one revolution. A single-acting compressor has one discharge per revolution.

- **Double acting reciprocating compressor. Figure 1—4**

Most heavy-duty reciprocating compressors are double acting. In a double-acting compressor, gas is compressed on both sides of the piston. The double-acting compressor has two nos. of discharge strokes and two nos. of suction

stroke per revolution. Suction stroke and discharge stroke take place simultaneously as compression is taking place on both side of the piston.[1]

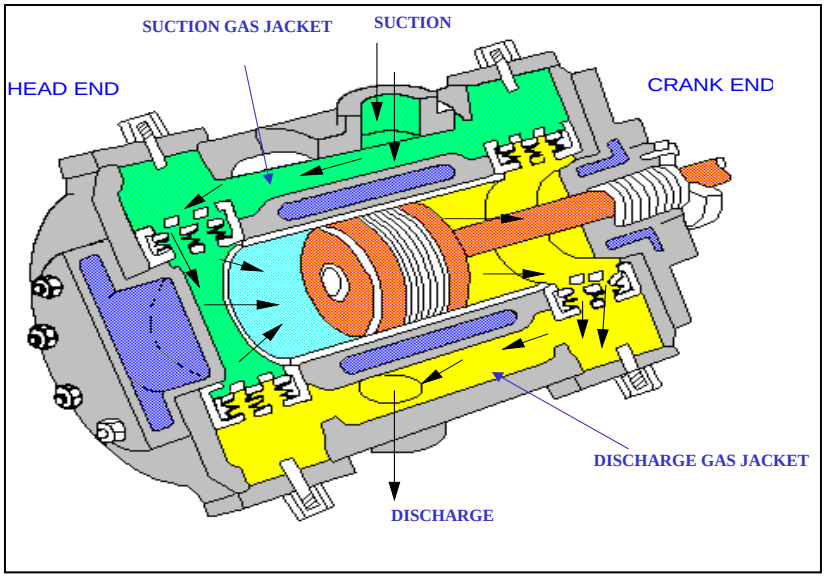

Figure 1—4 Double acting reciprocating compressor [1]

In a reciprocating compressor, a volume of gas is entering into cylinder through the suction valve. The gas is compressed when the piston forces it into a smaller volume Figure 1—5. Then the compressed gas is discharged into the discharge line through the discharge valve Figure 1—6. The cylinder valves control the flow of gas through the cylinder. Cylinder valves act as check valves. They permit flow only in one direction. A compressor valve opens because of pressure differences. For the valve to open, the pressure of the gas in the suction line must be higher than the pressure of the gas in the cylinder. When the pressures across the valve are equal, the valve closes and prevents back flow. Suction valves open when cylinder pressure is lower than the pressure of the gas in the suction line. Discharge valves open when cylinder pressure is higher than the pressure of the gas in the discharge line.[1]

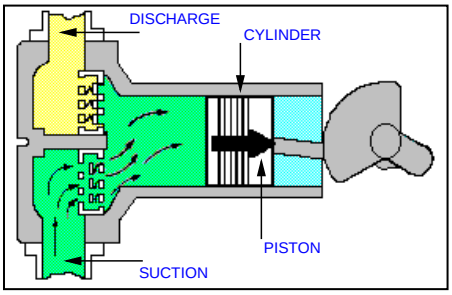

Figure 1—5 suction stroke [1]

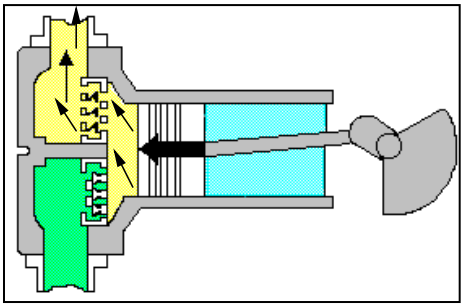

Figure 1—6 Discharge stroke [1]

1.2.3 Centrifugal Compressor

Centrifugal compressors are classified in two different types, vertical split (Bundle type) shows in Figure 1—8 and horizontal split shows in Figure 1—7 . The vertical type is applicable for high pressure Max 700 bara and huge volume Max $300x10^3$ (m^3/hr) and the horizontal split is applicable for less pressure Max 50 bara and similar of vertical spilt volume Figure 1—1.[4]

Figure 1—8 Vertical split type (PDO, Harweel plant 2012)

Figure 1—7 Horizontal split type. (PDO,Lakwair,2003)

The centrifugal machine achieves the compression process with the aid of a rotating impeller possessing several blades. The impeller is mounted on a shaft and is rotated by an external drive unit. The gas enters the casing and with the aid of the impeller, is forced at high velocity to the walls of the casing. Here the energy conversion takes place. That is to say velocity energy is converted to pressure energy as shows in Figure 1—9.

Following are the main components of a centrifugal compressor, Casing (Horizontally split & Barrel type), Diaphragms, Guide vanes, Diffuser & Volute, Rotor, Balancing piston, Impellers, Couplings, Bearings (Journal & Thrust bearings, Seals, etc. In chapter three more details about this components. [3]

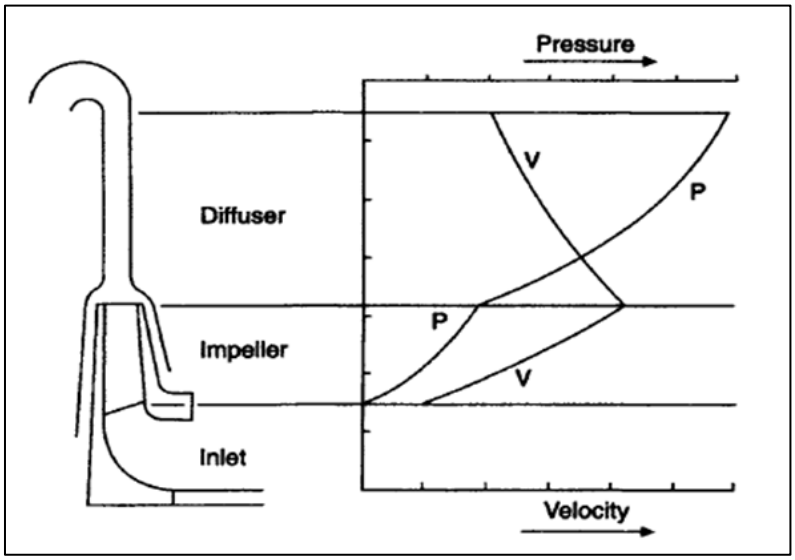

Figure 1—9 Pressure and velocity changes through a centrifugal compressor. [3]

Centrifugal compressor is a machine consists of rotating parts and static part which enclose inside pressure casing, it is always came with complete train (compressor package) of other unties such as speed transmission (gear box, fluid coupling) and driver untie such as an electric Motor or a gas turbine or Engine .

The dynamic principle of the compressor is started from the fluid compassion that the compressor is designed to meet the specified operating envelope of the performance curve shows in Figure 1—10 which it is including the discharge pressure, power, polytrophic head and polytrophic efficiency versus inlet capacity from predicated surge point to 115% rated capacity at minimum operating speed and 80%,90%,100% and 105% speed indicating the effect of specified suction pressures , temperatures and molecular weights .[13]

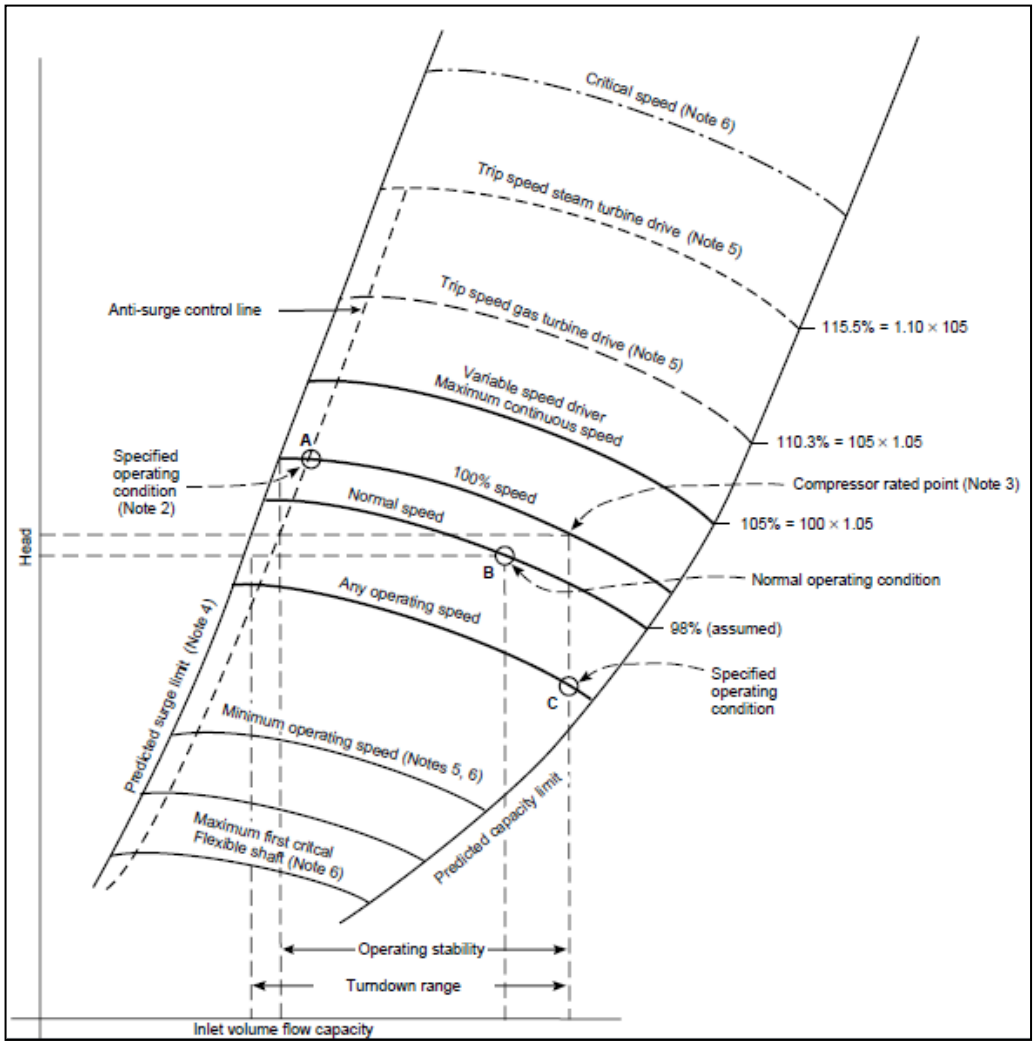

Figure 1—10 compressor performance curve [13]

Figure 1—11 shows compressor cross section which it consists of two-stage centrifugal compressor each stage has 4 impellers .The fluid enters through the converging suction nozzle then the flow accelerates within the plenum inlet by 2-3 times then the fluid enters the first impeller through impeller eye, the impeller with high speed rotation is transferring the mechanical energy to the fluid takes place with increase of the fluid velocity, pressure and temperature. Once the fluid discharged from impeller and enters through the diffuser which it causes the pressure increase more and same as the temperature and this phenomenon is clearly shows in Figure 1—9. After that the fluid requires to flow to the second impeller or can says second stage that after it is crossing the return band then it changes the flow direction by 180º through the vane channel

and a 90º turn to achieve axial inlet into the eye opening of the following impeller. However there is some amount of fluid leakages through the labyrinth seal which it leads to reduce the pressure and the biggest amount of fluid enter into the second impeller eye then it goes through all previous sequences through all stages. The number of stages (impellers) are increasing the pressure until it goes through the volute and then to diverging conical exit diffuser where the fluid is subjected to a further pressure increase.[7]

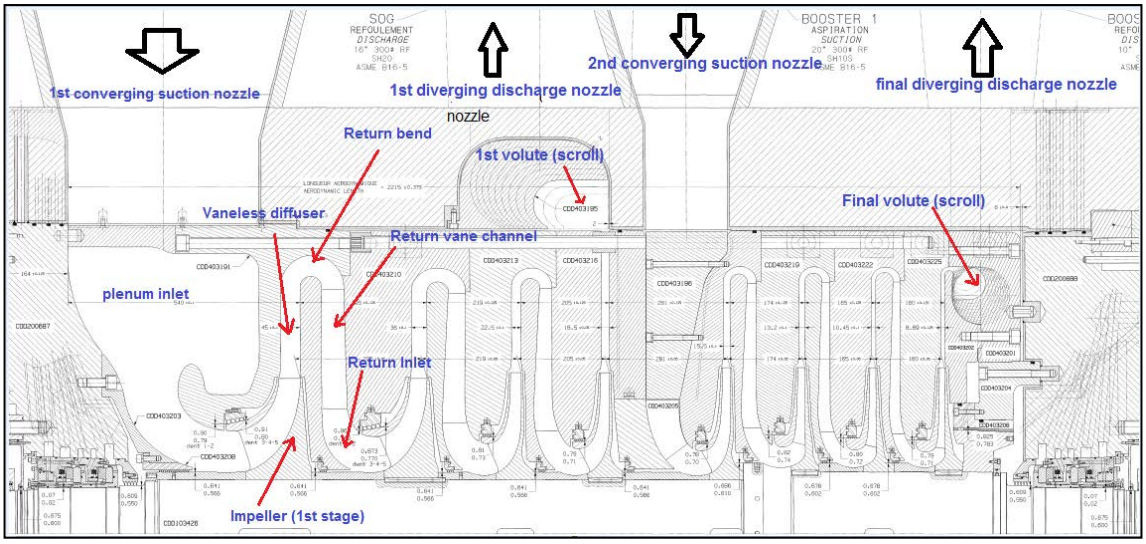

Figure 1—11longitudinal cross section (PDO, Harweel LP compressor manual)

1.2.4 Centrifugal Compressor Components

1.2.4.1 Casing

As mentioned earlier there are two types of compressor Casings (horizontally split and vertically split) the aim of the Casing to protects the internal components and also to prevents gas leaking atmospheric. Indeed during major compressor overhauling is required to reach to the Woking components for repair or replacement for that the casing designed to split types. Casings can be made up different materials such as stainless steel or alloy steels depends up on the pressure, temperature and corrosive nature of the gas.

1.2.4.1.1 Horizontally split casing

The horizontal split casing is split along the centre-line of the machine shows in Figure 1—12. Mostly the main suction and discharge nozzles are built into the lower half of the casing that to be easy to remove the upper half of the casing during the maintenance or inspection of the internal parts such as shaft, impellers, Diaphragms and labyrinth seals. This type of casing is used for low pressure service Maximum 50 bar [4] , since it is difficult to prevent leak from between two parts of censing and also it is not allow using it at high Hydrogen Sulphide (H2S) that to avoid any chance for leakage . [3]

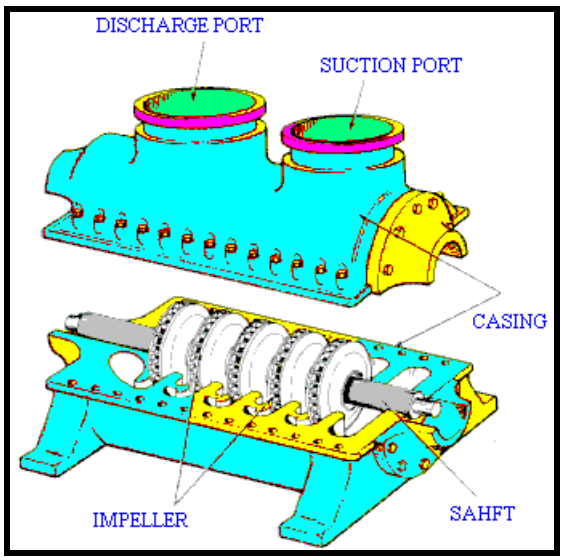

Figure 1—12 horizontally split [3]

1.2.4.1.2 Vertically split casing

Vertical split casing shown in Figure 1—13 is used for higher pressure which it is between 50 bara to 700 bara as per DEP31.29.40.10 standard and also used for high Hydrogen Sulphide (H2S) process application. This type of casing shaped cylindrically which has removable end cover. When end cover is removed the complete bundle can pull out and then by spilt the bundle vertically or some model can do horizontally which then allowed doing maintenance and inspection.

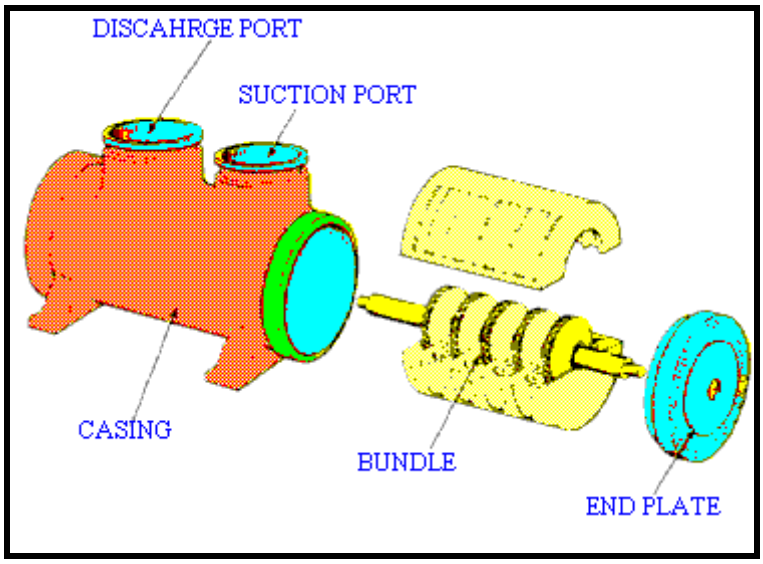

Figure 1—13 vertically split [3]

1.2.4.2 Diaphragms

Diaphragm is the stationary part of the compressor which accommodates volute, diffuser and guide vanes as shows in Figure 1—14. Those diaphragms are separating each stage from other that to avoid gas passing back from one stage to previous stage. Both vertically split and horizontally split casings possess horizontally split diaphragms to permit easier maintenance. Diaphragms can be made of cast iron, cast bronze, cast steel or alloys. Selection of the material depends up on the operating pressure and temperature of the compressor.

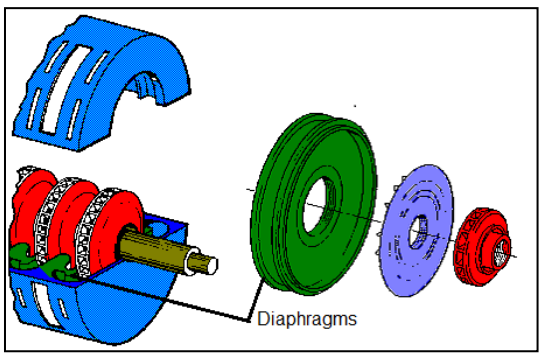

Figure 1—14 Diaphragms [3]

1.2.4.3 Impellers

The impeller is mounted on common shaft to make up the rotor and it imparts the kinetic energy to the fluid. The impellers are mounted on the shaft with different arrangement such as straight through and back-back that some arrangement, all impellers are facing the same way in one direction and other arrangement some impellers face one way and others face reverse direction, respectively. Indeed the back-back arrangement allows a degree of thrust balancing within the machine. [3]

Impeller designs must consider aero-thermodynamics that by assure several disciplines such as volume flow, head efficiency and operating range stress analysis (static and dynamic) and rotordynamics must warrant smooth running. There is different impellers design application and the common used the Shrouded 2D-impeller, the Shrouded 3D-impeller and the Semi-open impeller. [7]

1.2.4.3.1 Shrouded 2D-impeller:

This type of impeller shown in Figure 1—15 a design generally stated to 2D-impeller, shrouded with backward-curved blades with angles between 40°- 50° and the maximum flow coefficient is nearly 0.06; this application were commonly developed that compressor high pressure ratios m low volume flows, high numbers of stages and low rotational speed.

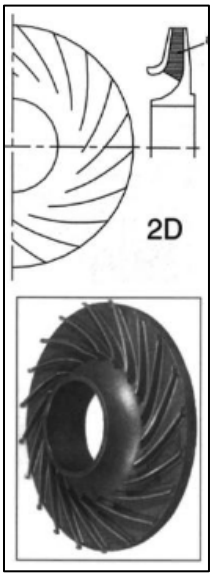

Figure 1—15 2D-impeller, shrouded with backward-curved blades. [3]

1.2.4.3.2 Shrouded 3D-impeller:

This type of impeller shown in Figure 1—16 a design generally stated to 3D-impeller, shrouded with twisted backward-curved blades with angles between 45°-60° this application are considered comparatively high efficiency at a reduced outer impeller diameter, a high rotational speed, an extensive operating range and a reduced maximum number of stages per single shaft compressor casing.[7]

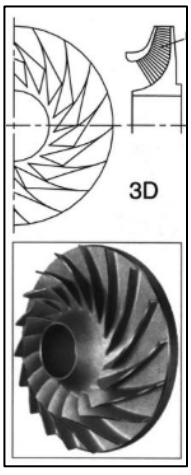

Figure 1—16 3D-impeller, shrouded with twisted backward-curved blades.[3]

1.2.4.3.3 The Semi-Open Impeller:

There are two types of semi-open impeller a design generally stated to S-impeller with backward-leaning blades with angles between 45°- 70° and other type R-impeller that it has wheel with radials ending blades with an exit angle of 90°.This application is considered a highest tip speed, a smaller operating range, lower efficiency and flatter performance curve.[7]

1.2.4.4 Dry Gas Seal

Dry gas seal is importance component in the compressor which is preventing any leak from compressor casing to atmosphere especially if the process specifications with high pressure and high H2S (see Figure 1—17).

Using Dry gas seal has increased significantly in the last two decades because they eliminate contamination and do not use lubrication oil that is more reliable if compare it with oil seal. However it is often used on compressors application in oil refineries, petrochemical and oil & gas processing plants.

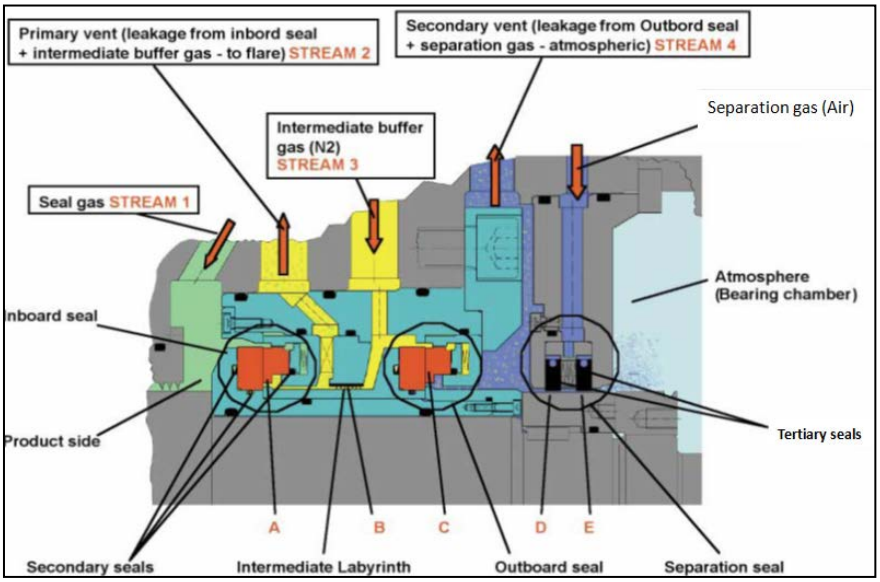

Figure 1—17 Dry gas seal [3]

Figure 1—18 shows Tandem seal with Internal Labyrinth type this seal is basically mechanical face seals, consisting of a mating (rotating) ring and a primary (stationary) ring. During operation, grooves in the mating ring generate

a fluid-dynamic force causing the primary ring to separate from the mating ring, thus, creating a "running gap" between the two rings.

A sealing gas is injected into the seal, providing the working fluid for the running gap and the seal between the atmosphere or flare system and the compressor internal process gas. Inboard of the dry gas seal is an inner labyrinth seal, which separates the process gas from the gas seal. Outboard of the dry gas seal is a barrier seal, which separates the seal from the compressor shaft bearings.

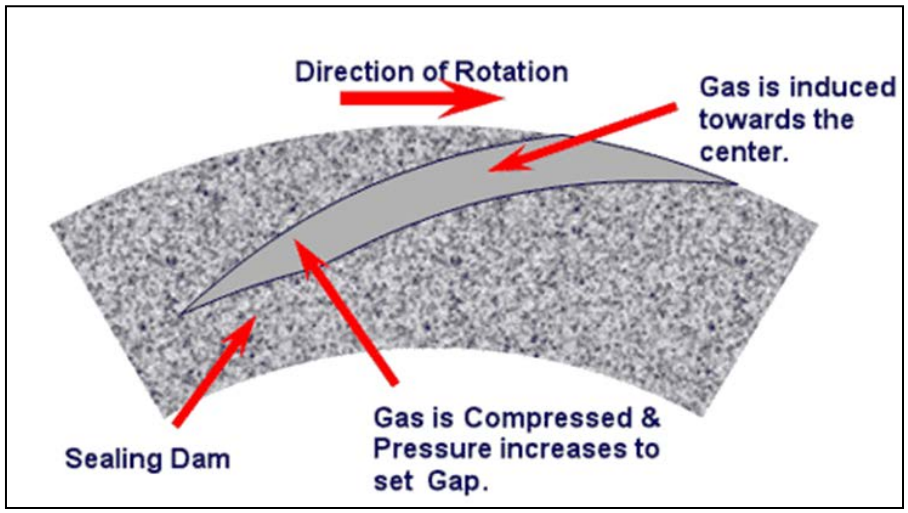

Figure 1—18 Rotary seal face [3]

1.3 **Project definition**

The proposed subject is to study factors affecting the rotordynamics stability of large natural gas centrifugal compressors operating in Petroleum Development Oman. This study will review the influence of various conditions of rotor components such as bearings, seals, impellers, etc on the overall rotordynamics stability at various process duty conditions.

1.4 **Research Aim and Objectives**

The aim of this research to study the Centrifugal compressor components and studying the Rotordynamic influential parameters, components and sub components which will provide the required knowledge to design, evaluate, operate and trouble shoot high speed rotary machines. Experimental and numerical analysis will be used in this study. The objectives set for this research are as follow:

1. Conduct a detailed literature survey to understand what influences the rotor dynamic characteristics of an operational compressor. This will include investigations on the influence of bearing and seal types, their associated clearances and the effect of molecular weight of the compressed gas.
2. Develop a numerical model to predict the centrifugal compressor rotor dynamic characteristics for varying bearing and seal clearness, etc. Compared the results obtained numerically with that observed on operational gas compressors.
3. If any discrepancies are found then a parametric study to map the cause of such variance will be undertaken. The numerical model will allow for prediction of the amplification factor at critical speed for varying levels of unbalance and ‘non-perfect’ assembly (including loss of clearance, etc).

1.5 **Research Methodology**

On this research is using two methodologies, numerical analysis and experimental.

The numerical analysis grants the fundamental rotordynamics instability analysis as well as the performance of the rotor system at different stiffness and damping parameters. Moreover the numerical analysis will be used to study the effect of lateral vibration and torsional vibration on the rotor system. The experimental study provides some vibration data mainly from system 1 Bently Nevada for two different rotor configurations where the effect of seals, mounting methodologies and bearings are studied.

Section Two

2 Rotor Dynamics Fundamentals

2.1 **Introduction**

The rotors have been the main commonly used parts of most of turbomanchines. Rotor is mechanism given rotary motion which stores energy and transfer power through different applications such as belts, gearbox or coupling [53]. However the rotor stability is become the main key of health rotor dynamically machines since the rotor has many sources (forces) that can be involved to disturb rotor stability if not designed properly , those forces (spring force , damping force and perturbation force) are normally appeared between rotor and bearing system [5] . For that, there is greatest concern during rotor operation since there is three vibration modes see Figure 2—1 could occurred on that time, Lateral vibration, Torsional vibration and axial vibration [53]. The most modes concerning about are Lateral and Torsional vibrations since the axial vibration mostly controlled by thrust bearings and balance piston. Intend, in the API617 provides the options for types of analysis which should be considered during centrifugal compressor design such as Lateral analysis and Torsional analysis. As per API617 stability analysis is performed in two level , level 1 stability analysis should be adequate calculated logarithmic decrement is higher than 0.1. Otherwise level 2 analysis becomes mandatory.

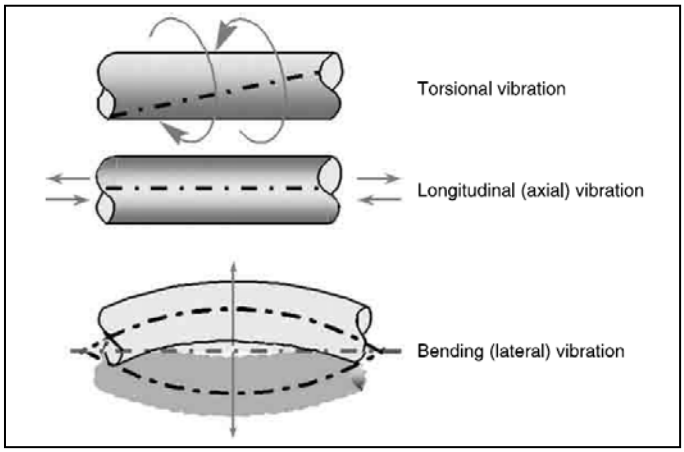

Figure 2—1 Rotor vibration modes [53]

In fact there are many factors can excites vibration modes like unbalance , bent shaft, misalignment, oil whirl ....est. . The most critical factor excites the lateral vibration is unbalance that “when the rotor mass centreline does not coincide with its rotational axis, then mass unbalanced inertia-related rotating forces occur” [53]. The unbalance force generates frequency of the rotor lateral vibrations which will be same as the rotational speed thus the unbalance related synchronous lateral vibration are transferred as 1X vibration . For that, it is vital during the operation states unbalance related synchronous vibration amplitudes are acceptable and with high-speed turbomanchines should be efficiently exceed some lateral balance resonance speeds which known as critical speed [53], in Figure 2—2 shows the limitation of an Amplification factor (AF) [13].

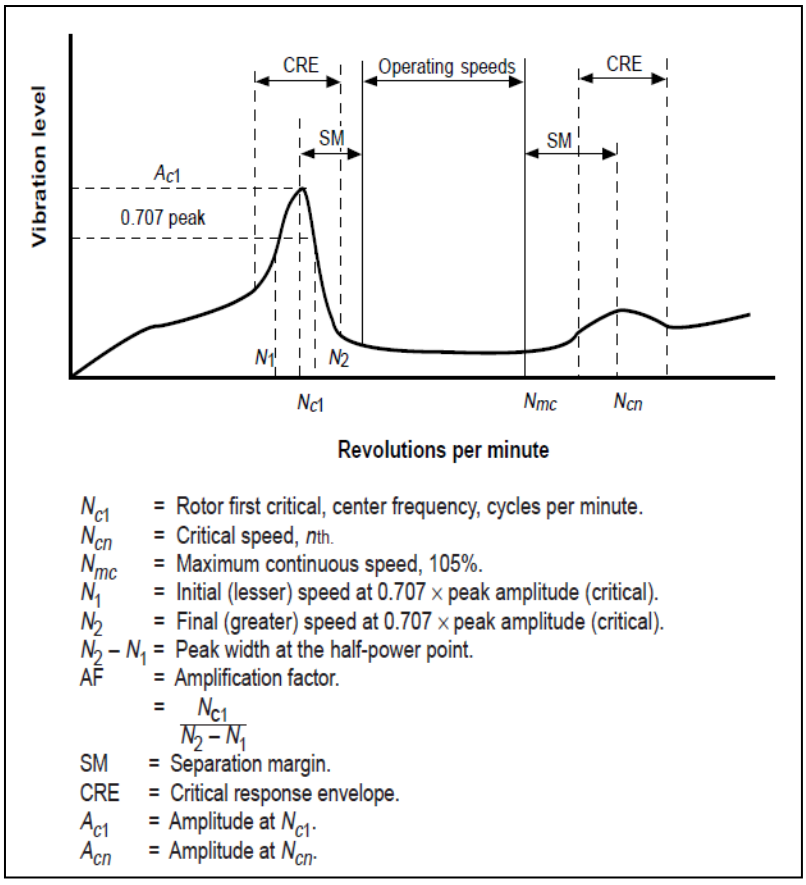

Figure 2—2 Rotor Response Plot [13]

2.2 **Critical speed**

Critical speed is a phenomenon of rotating shaft which has some amount of residual unbalance however even well balanced rotary will get into resonance when it rotates at speed equal to bending natural frequency. For that, during rotor design it vitals to calculate rotor bending critical speed which also should be considered many factors with this calculations such as dissimilar moments of area of the shaft, Gyroscopic effects of disks, coupling between two rotors and stiffness and damping of oil film bearings [54].

2.2.1 Lateral Vibration

For more understanding of the lateral critical speed it is vital to know the basic fundamentals of rotating shaft through the rotor equation of motion which Rao [54] explained them on his rotordynamics book.

In Figure 2—3 shows the geometry of unbalance of single mass flexible rotor in radial rigid bearings (Jeffcott rotor) which consists of heavy disk mass (M) mounted at mid-span of a massless elastic shaft, as seen *E* is indicating the geometric centre of the disk and it is centre of gravity is at a distance *a*.

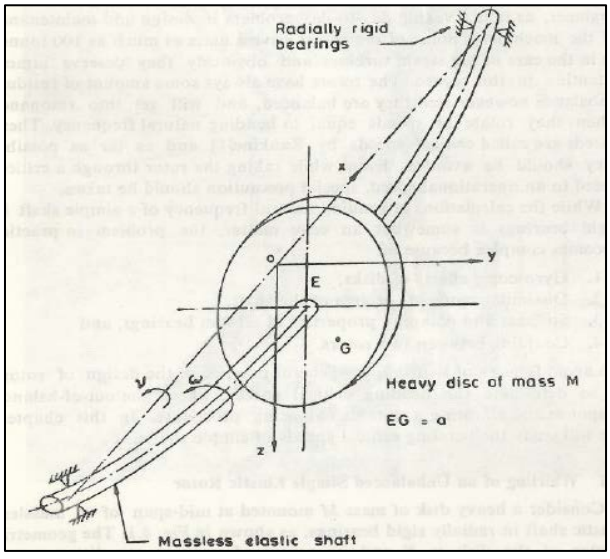

Figure 2—3 Single mass flexible with residual unbalance [54]

In Figure 2—4 shows the geometry of shaft whirl at the disk location of Jeffcot rotor in Figure 2—3, with consideration of the fixed system axis (OYZ) with regards the disk whirl due to unbalance where K is lateral stiffness of the shaft and C is equivalent viscous damping of the system, the equations of motion for the rotor are [54];

$$M\frac{d^2}{dt^2}(z + a\ \cos\omega t) + C\frac{dz}{dt} + Kz = 0 \quad \textbf{(2—1)}$$

$$M\frac{d^2}{dt^2}(y + a\ \sin\omega t) + C\frac{dy}{dt} + Ky = 0 \quad \textbf{(2—2)}$$

Equations (2-1) and (2-2) can be simplifying as below:

$$M\ddot{z} + C\dot{z} + Kz = m\omega^2 a\, cos\,\omega t \quad \textbf{(2—3)}$$

$$M\ddot{y} + C\dot{y} + Ky = m\omega^2 a\, sin\,\omega t \quad \textbf{(2—4)}$$

Where;

$M\ddot{z}$ & $M\ddot{y}$ are indicating as inertia force

$C\dot{z}$ & $C\dot{y}$ are indicating as damping force

Kz & Ky are indicating as Stiffness force; and

$m\omega^2 a\, cos\,\omega t$ & $m\omega^2 a\, sin\,\omega t$ are rotating external excite force due to unbalance.

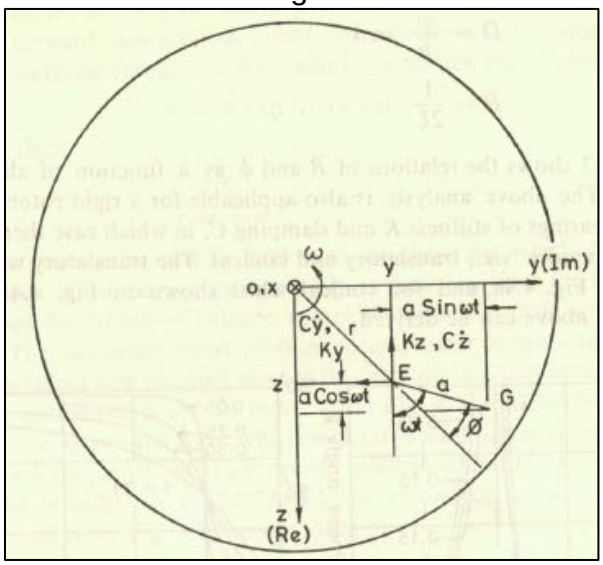

Figure 2—4 Geometry of shaft whirl at the disk location [54]

The whirl radius r can be articulated in a complex amount as:

$$r = z + iy \quad \textit{(2—5)}$$

Thus by combination of two equations (2-3) and (2-4) , a single equation become as:

$$M\ddot{r} + C\dot{r} + Kr = m\omega^2 a e^{i\omega t} \quad \textit{(2—6)}$$

The steady state of the equation (2-6) above is:

$$r = Re^{i(\omega t - \phi)} \quad \text{(2—7)}$$

$$R = \frac{m\omega^2 a}{\sqrt{(k - m\omega^2)^2 + C^2\omega^2}} \quad \text{(2—8)}$$

The non-dimensional structure of equation (2-6) is:

$$\bar{R} = \frac{R}{a} = \frac{\Omega^2}{\sqrt{(1-\Omega^2)^2 + (2\zeta\Omega)^2}} \quad (2—9)$$

$$\phi = tan^{-1}\frac{2\zeta\Omega}{1-\Omega^2} \quad (2—10)$$

Where,

$$\Omega = \frac{\omega}{p}; \quad p = \sqrt{\frac{k}{m}}, \quad \zeta = \frac{C}{C_c}, \quad C_c = 2\sqrt{KM} \quad (2—11)$$

For

$$\Omega = \frac{\omega}{p} = 1 \quad (2—12)$$

$$\bar{R} = \frac{1}{2\zeta} \quad (2—13)$$

In Figure 2—5 shows the relationship between amplitude ratio $\bar{R}$ and Phase angle ϕ as a function of shaft speed (Ω) which illustrates the whirling amplitude at different damping ratios along with the phase shift. It shows in left side that the maximum amplification occurs at frequency ration ω/p = 1.0, this phenomenon is known as resonance. It also illustrates that the amplification is largely influenced by the damping factor ξ. However the lower damping factor ξ, the higher the amplitude ratio $\bar{R}$ and vice versa.

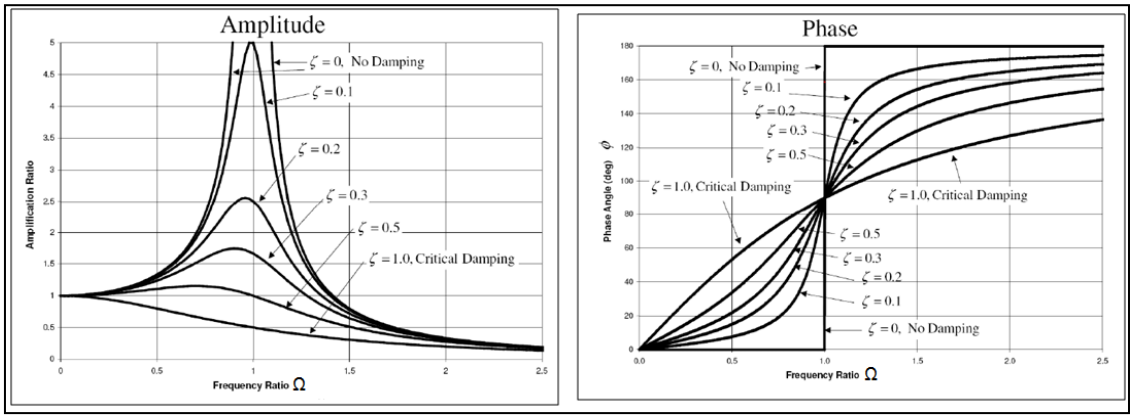

Figure 2—5 Amplitude ratio and phase angle versus frequency ratio[33]

The phase angle ϕ is also named as the phase lag because it measures the lag of the output or system response behind the excitation force. The Figure 2—5 right side shows the phase angle diagram which it indicates the followings:

When $\omega/p < 1.0$ thus, $\phi < 90^o$
When $\omega/p = 1.0$ thus, $\phi = 90^o$
When $\omega/p > 1.0$ thus, $\phi > 90^o$

by solving the equation (2-6), with assumption of forward synchronous whirl that is the whirl frequency (v) is same as rotational frequency (ω)

$$r = R\exp\{i(vt - \phi)\} \qquad 2\text{-}14$$

demonstrating that by:

$$v = \omega, \text{or } v = -\omega \qquad 2\text{—}\ \text{Error! Bookmark not defined.}$$

The rotor is operating as its critical speed when the phase angle ϕ is within 90^o and the highest vibration amplitude (resonance) occurs when $(\omega = p)$ therefore the following can be written,

$$M\omega^2 a = C\omega R \qquad 2\text{—}14$$

Also,

$$\overline{R} = \frac{R}{a} = \frac{M\omega}{C} = \frac{1}{2\zeta} \qquad 2\text{—}15$$

This result is similar as equations (2-12) and (2-13) because of phase angle is equal 90^o , $(\omega = p)$ and $\zeta < 0.25$ that the maximum whirl amplitude can be predicted by equation (2-17) as it take places at a slightly higher frequency than p.

2.2.2 Torsional vibration

2.2.2.1 Introduction

Torsional vibration is twisting of the rotor statically and dynamically about its rotational axis, in fact torsional vibration is more difficult to measure than radial vibration for that it does not get the attention that it should be [5].

Torsional vibration can generate large amplitudes which can occur silently and without any indication or effect on the housing and foundation[18], also it cannot act directly through the bearings since they are designed to reduce the power losses due to friction and they have no spring-like element in the rotational

direction .However, torsional vibration can indirectly cross coupling to radial vibration for that it is possible to indicate any effect of torsional vibration in a radial vibration signal and not recognize them [5].

There are different turbomachines which can develop excessive dynamic stress that in case they run at speed near their natural frequency in torsional vibration which it is oscillatory twisting of the shaft in a rotor assembly. However most of large machines come as full train which it consists of driving and driven units coupled with flexible / rigid coupling and with some cases the gear box untie come between driving and driven units, on this case there are two coupling low speed coupling and high speed coupling which they are connect between motor and gearbox, gearbox and compressor respectively.

Figure 2—6 shows a shaft coupling which used with turbine/motor driven compressor, this type of coupling has a flexible diaphragm coupling transmit power from the driver to the compressor using hub each machine, a flexible metal diaphragm is bolted to the outer rim of each hub, and a spacer connects the two diaphragms. All misalignment is handled by the elastic flexing of the thin webbed diaphragms. There is no relative or rubbing movement of any part of the coupling and no lubrication is required. These coupling can handle fairly large angle of misalignment between the two shafts and also produces lower torsional stiffness, however this coupling can tolerate only slight change in back and forth movement of shaft [3].

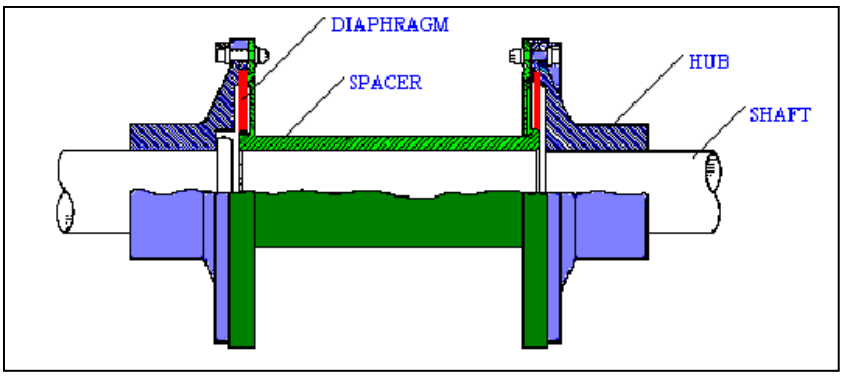

Figure 2—6 Shaft coupling [3]

In fact all rotating machines are generating power delivery needs transmission of torque causes the shaft to twist about its axis, so measurement of torsional vibrations requires angle of shaft twist at different axial position. In Figure 2—7shows three disks are rigidly attached to shaft and because the dynamic forces the equilibrium position represented by the black lines and the angle θ represents the angular deflection of the shaft relative to the equilibrium position [5]. Due to the angular deflection the calculation of the angle of shaft twist preformed that because the angle is increasing caused by spinning shaft. Torsional deflection and vibration involves only amount of twist of the shaft but the spinning shaft makes the twist so difficult to measure [5].

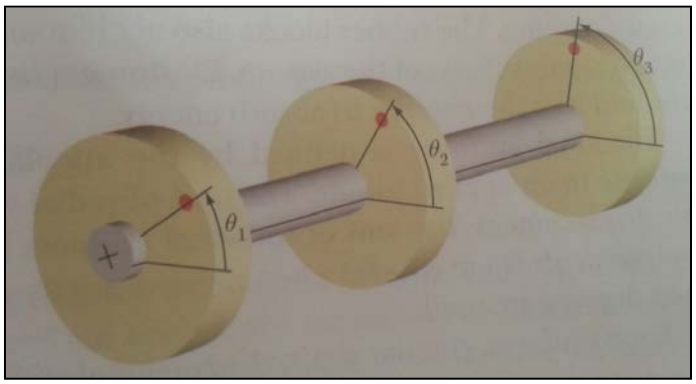

Figure 2—7 measurement of torsional twist (three disks are rigidly attached to a shaft)[5]

2.2.2.2 Comparison between Lateral vibration and Torsional vibration:

The Table 1 illustrated the main differences between the Lateral vibration and Torsional vibration:

Table 1 Comparison between Lateral vibration and Torsional vibration

	Lateral vibration	Torsional vibration
1[5]	Needs to measure displacement relative to an equilibrium position.	Needs to measure the angle of twist of the shaft at different axial positions.
2[18]	Vibration can detect easily through standard instrument devices such as (accelerometer, probes...est.) that can fix them on the housing and foundation.	The instrument device doesn't usually install in the equipment.
3[5]	It has large amplitude which often can indicate on the housing and foundation.	The large amplitude cannot notice on the housing or foundation.
4[18]	It is natural frequencies are influenced by rotating speed.	It is natural frequencies are independent of rotating speed.
5[5]	It can act directly through the bearings.	It cannot act directly through the bearings since they have no spring-like element in the rotational direction.
6[53]	It is damping is high.	It is damping is too low by 10 time than lateral vibration.
7[18]	It is Indicating instability in the rotating machines.	It is very rare to indicate any instability, especially machines without speed control feedback.
8[18]	Its excitation from rotor imbalance (synchronous 1X).	Rotor imbalance no effect on it, only indirectly in machines with gears where the lateral vibration creates dynamic torque.

9[18]	It is analysis can normally be performed on each rotor in the train separately.	It is analysis must include all rotors in the train as rigid.

2.2.2.3 Torsional analysis:

Torsional analysis is using rotor parameters of the angular equivalents of the torque (T), moment of inertia, torsional stiffness and torsional damping .however the lambda is not used with torsional analysis since there is no equivalent to tangential stiffness and also the damping is negligible since it is too low on torsional vibration [5].

Moreover, the torsional vibration analysis is vital to consider during design and even during steady state that because torsional vibration has very low damping which it could leads to very sensitive to change in the rotor integrity for that Muzysnska [53] recommended trending the torsional vibration data on-line after fix torsional vibration measuring device. However the usual engineering objectives of torsional analysis are [18]:

1. The natural frequencies should be predicated.
2. The effect on the natural frequencies and vibration amplitude should be evaluated that in case any changing on the design parameters or components within the train, this usually needs computer simulation.
3. The vibration amplitudes and peak torques should be indicated during steady state torsional excitation, also by using computer simulation.
4. During the transient condition (start-up and shutdown) the dynamic torques and gear teeth load should be computed.
5. The torsional vibration stability of drive trains with automatic speed control should be estimated.

In fact torsional vibration model of the train such as motor driving a compressor should considered as rigid as shows in Figure 2—8which noticed that in the motor rotor and compressor rotor are very little twist .

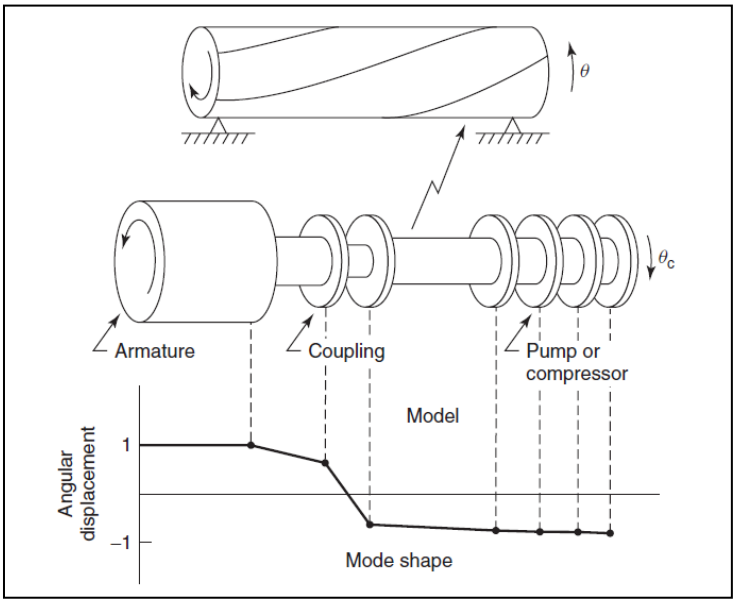

Figure 2—8 Torsional mode shape for a motor driving a compressor [18]

2.2.2.4 Torsional response statically and dynamically:

In fact a machine at steady state the speed is exposed to many torque that are within static balance, the torque appears as an axial position and it creates with in a discrete prime movers which is delivering via a coupling or internally prime mover such as multiple steam or gas turbine or magnetic field . However there same fraction of the total driving torque is input to the rotor at different axial position and the driving torque is balanced by the loads which could be originated by aerodynamic forces in compressor. The rotor speed will be constant in case the equalization to driving torque and the opposite of the load torque. On other hand the rotor shaft will be twisted slightly at a constant angle deflection the below equation finds out the rotor twist amount determined by the load torque as each shaft section [5].

$$\frac{T}{\theta} = K_T = \frac{JG}{L} \qquad (2—18)$$

Where θ is the angle of twist along a shaft section of length L, J is the polar moment of inertia and G is the shear modulus.

The polar moment of inertia for hollow shaft can find it as:

$$J=\frac{\pi}{32}(d_0^4 - d_i^4) \qquad 2—16)$$

Where d_i is the shaft inside diameter and d_0 is the outside diameter.

Equation (2-18) is indicating [5]:

- If the shaft is long the torsional stiffness will by lower.
- If shaft with stiffer materials the shear modulus will be high and it will produce a torsional stiffer shaft.

From equation (2-19), since the polar moment of inertia is related to the 4th power of the diameter, the large diameter shaft is torsional much stiffer than the small diameter [5].

Indeed, most of rotors are not identical in diameter over their entire length thus the torsional stiffness of a typical rotor shaft will contrast with axial position. For that the torsional stiffness on each position will be not identical as well and the total stiffness K_T will be equal of a number of short segments n in series with individual torsional stiffness as [5]:

$$\frac{1}{K_T} = \frac{1}{K_{T1}} + \frac{1}{K_{T2}} + \cdots + \frac{1}{K_{Tn}} \qquad 2—17)$$

There is power delivered as a shaft has product of the torque and the angular velocity the power will be generated:

$$P = T\Omega \qquad 2—18)$$

Where P is the power (watt), T is the torque an in N.M and Ω is rotor speed in rad/s.

On the other hand, the consequence of shaft twist is generating a material strain which is producing a torsional shear stress τ at the outer surface of the shaft and that given as:

$$\tau = \frac{Tr}{J} \qquad 2—19)$$

Where (r) is the radius of outer surface of the shaft.

2.2.2.5 Torsional vibration Simplified models:

In Figure 2—9 shows two machine rotors connected by a coupling and as all rotors in the train are considered as rigid, for that the all shafts have combined torsional stiffness K (in-lb/rad). However the damping in the torsional vibration is

very low which it's always negligible, thus the fundamental of the natural frequency in Hz [18]:

$$\mathbf{f_n = \frac{1}{2\Pi}\sqrt{k\frac{I_{P1}+I_{P2}}{I_{P1}\times I_{P2}}}} \qquad 2—20)$$

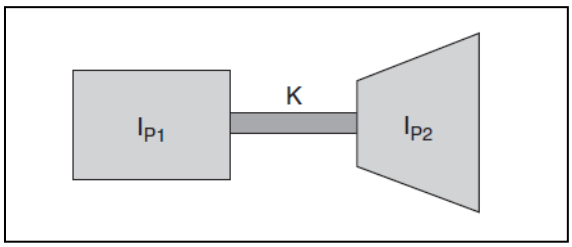

Figure 2—9 a two inertia simplified model [18]

In Figure 2—10 illustrates train with two rotors machine via a gearbox.

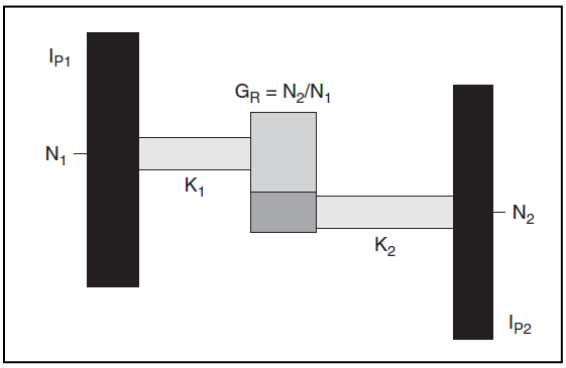

Figure 2—10 a two inertia model with a gearbox [18]

By chosen I_{P1} as driver with reference shaft at speed N_1 and the torsional stiffness K_2 and inertia I_{P2} are at a different speed N_2 , thus the gear ratio G_R squared must be multiplied by torsional stiffness K_2 .

Assume both inertia ($I_{P1}\ and\ I_{P2}$)are much larger than gear inertia, for that the Figure 2—11 indicated the equals model consigned to shaft, both stiffness ($K_1\ and\ K_2$) are in series so the effective stiffness is :

$$\boldsymbol{K_{eff} = \frac{K_1 K_{2eff}}{(K_1 + K_{2eff})}} \qquad 2—21)$$

As $$K_{2eff} = G_R^2 K_2 \qquad 2—22)$$

So the effective inertia of I_{P2} on the reference shaft is:

$$\boldsymbol{I_{2eff} = G_R^2 I_{P2}} \qquad 2—23)$$

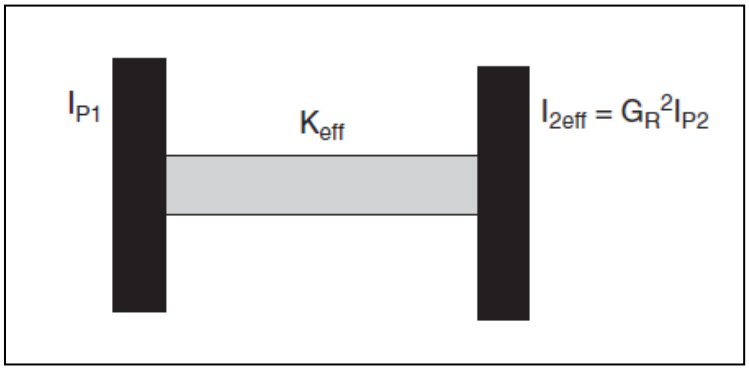

Figure 2—11 an equivalent model for Fig 2-10

The fundamental of natural frequency of torsional vibration is:

$$f_n = \frac{1}{2\Pi}\sqrt{K_{eff}\frac{I_{P1}+I_{2eff}}{I_{P1}\times I_{2eff}}} \qquad 2—24$$

To simplify equation (2-20) further, assume that one of inertia is much larger and I_{P1} has taken as the larger than $I_{2eff}$for that it will be negligible and the model becomes practically one degree of freedom as:

$$f_n = \frac{1}{2\pi}\sqrt{\frac{K_{eff}}{I_{2eff}}} \qquad 2—25$$

The consideration should be taken of the polar inertia of the coupling hubs and the spacer torsional stiffness since they could be have a considerable effect on the torsional model and the consequently of the value for the first natural frequency. In fact this case often happen when rigid coupling changing to a dry flexible coupling and that what indicates in Figure 2—12.

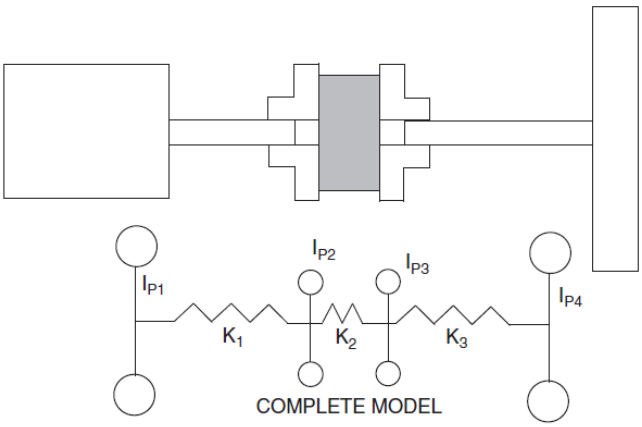

Figure 2—12 model including flexible coupling [18]

In above figure shows a typical driver/ driving an overhung fan or blower via a power transmission coupling. As show in the model consists of four degree of freedom, four inertia (I_{P1}, I_{P2}, I_{P3} and I_{P4}) and three torsional stiffness (spring) (K_1, K_2 and K_3) . in this case of a flexible coupling model that the coupling spacer is much more torsional flexible than the shafts in the driven and driving machine. For that both driving and driven shafts are assumed rigid relative to the coupling spacer, since there is no relative movement between the inertia of driving / driven machines. In fact the hub inertia lumped with machine inertia as shows in Figure 2—13 which it can use the equation (2-18)[18].

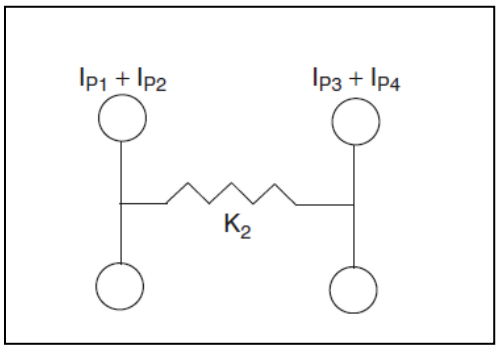

Figure 2—13 a two inertia model when K2 is soft [18]

At the end, the flexible coupling is allows the designer to adjust the natural frequency of the train which they can used it as a tool to shift the natural frequency away from interference with an excitation source.

2.3 **Rotordynamic Numerical Analysis**

In general rotating machine has rotor assembly contributes rotation dynamics which is influenced by gyroscopic moments, cross-coupling and the chance of whirling instability. In fact computer codes have been developed that to give specific rotordynamic analyses. [18]

Rotordynamic analysis become vital for Turbomachines specially during design and operation period that it helps for troubleshooting however there is many of objectives of rotordynamic analysis which Vance 2010 mentioned on his book as such as:

1. Identify the critical speeds by using calculated design data.
2. Verify any design modifications to change critical speeds

3. Expect natural frequencies of torsional vibration in case machine excited by pulsations of the synchronous electric motor via gearbox.
4. Capable to calculate balance correction masses and identify locations.
5. Identify amplitudes of synchronous vibration which it could be caused by rotor imbalance.
6. Identify number of the destabilizing forces which are still not unstated yet.
7. Resolve design modifications to suppress dynamic instabilities.

Indeed an analyse the dynamics of rotating machinery required to use computer simulations which it is usually model the lateral analyses of the shaft supported by its bearings, however there are different types of lateral analyses which can be achieved with consideration of machine conditions and its proposed use such as type of rotor used (rigid, semi-rigid or flexible), balance sensitivities, critical speed position type of fluid film bearings …etc[18]

2.4 **Different types of Rotordynamics models:**

Nowadays the use of a computer to analyse the dynamic of rotating equipment's become more affective to understand the rotordynamic's issues in terms of modal the rotor system with other sources which can influence the rotor stability and this sources can be like bearings , stiffness , damping , cross coupling , unbalance , aerodynamic ….etc. . However the main analysis of the rotor through the computer models is lateral vibration and the torsional vibration, each model has specific influencer for example the bearing supports the rotor and it is playing the main factor on the lateral vibration which can indicates on the critical speed, also other factors of the lateral vibration are stiffness, damping, and cross coupling. On other hand the torsional has different specific influencer such as polar moment of inertia, load torque, stiffness and angular of twist also in torsional analysis has to consider all train on it is model.

There are different types of computer simulations needs to consider during the rotordynamics analysis, the first model to start with rotating assembly (shaft) as

shown in Figure 2—14 the example of multistage compressor rotor with an example of a corresponding computer model. Indeed there is a lot of details are required in the analytical models specially with lateral analysis if compare it with torsional and axial analysis , for that in the lateral analysis needs to consider on this type much elements such as impeller inertia , coupling hub, keyway , weight and dimensions . For the torsional analysis or axial analysis this rotor could maybe passably modelled with just few elements however the model would need to comprise within entire coupling and driving machine [18].

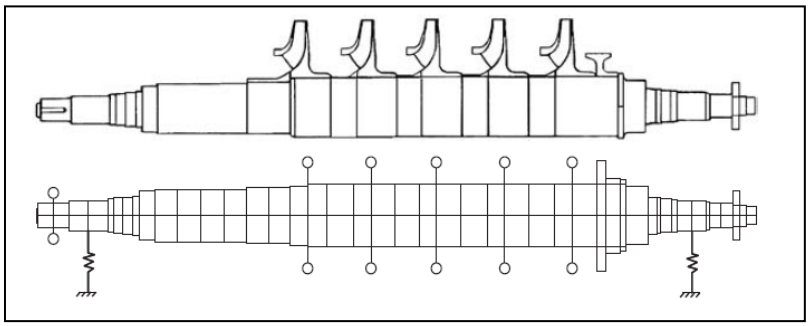

Figure 2—14 Compressor rotor and Corresponding shaft model. [18]

In Figure 2—15 illustrates the second type of rotor model with impeller hubs stiffness contribution which they could be provided to bending stiffness of the shaft. The elements of the hubs are treated as additional layers overlaid on the elements of the underlying shaft [18].

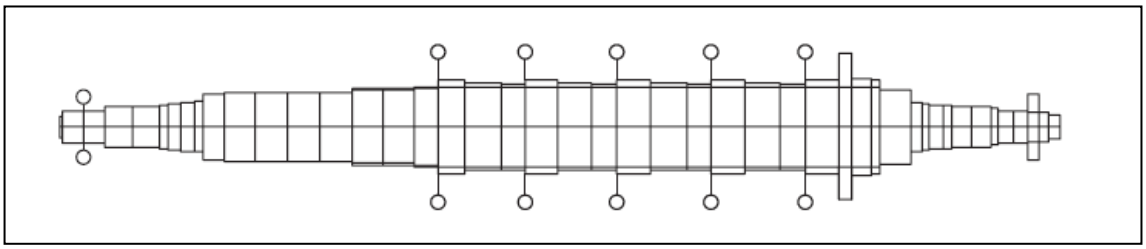

Figure 2—15 Rotor model with impeller hubs stiffness [18].

In the first type and second type the impellers inertia are added directly to the shaft also the five impellers inertia are treated as rigid disks as indicated with five positions to the rigidly shaft , shows in Figure 2—14 and 2-15 [18].

The third type of rotor model needs to be mentioned with bearing which it usually an analysis done separately that to provides bearings stiffness and damping elements connects the shaft, for that this type required details of bearing design such as selection type, diameter, clearance, length , material ..etc.) . In Figure 2—16 shows the modelling of bearing pedestals connecting the shaft with consideration of ground stiffness and damping established for the pedestal. In fact it is valid to consider the both of pedestals and ground which can affect the calculated critical speed of the machine [18].

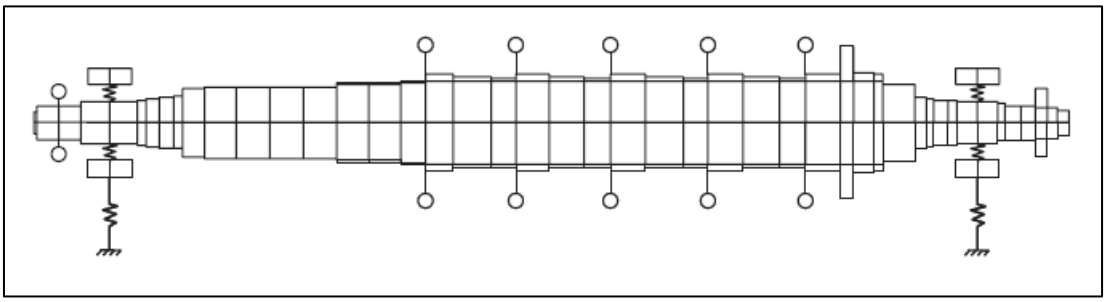

Figure 2—16 Rotor model with bearings connecting the shaft to bearing pedestals. [18].

In addition the high-pressure seal also need to consider with rotor system model since its one of element can affect the rotordynamics of the machine as shows in Figure 2—14 the balance piston seal on the right most impeller in the compressor, in fact the consideration of seal in the computing model is same fashion as bearings that by getting some details such as seal stiffness and damping properties, dimensions and location on the rotor [18].

Section Three

3 Literature Review

3.1 **Introduction**

Turbomachinery has become an important asset in countries economy most, especially those that have greater dependence on oil and gas. Therefore it is important that there is attentiveness in the development of Turbomachinery in terms of design, maintenance, and reliability which in turn brings the research need at the forefront Worldwide many studies and researches demonstrated the extent of machines behaviour in terms of machine components effect. However with different numerical software have been developed to help in and improving such machines such as CFD, Hydrodyne, Xl Laby, Ansys (3 Modeling), …etc

Indeed Centrifugal compressors are widely used and it is one of most influential machine involved in the oil and gas. The aim of this research is study the effect of centrifugal compressor components in the design and off design operation from its rotordynamics point of view. The Objects are:

1. Conduct a detailed literature survey to understand what influences the rotor dynamic characteristics of an operational compressor. This will include investigations on the influence of bearing and seal types, their associated clearances and the effect of molecular weight of the compressed gas.

2. Develop a numerical model to predict the centrifugal compressor rotor dynamic characteristics for varying bearing and seal clearness, etc. Compared the results obtained numerically with that observed on operational gas compressors.

3. If any discrepancies are found then a parametric study to map the cause of such variance will be undertaken. The numerical model will allow for prediction of the amplification factor at critical speed for varying levels of unbalance and ‘non-perfect’ assembly (including loss of clearance, etc).

3.2 **Influence of Aerodynamics on Rotor dynamics:**

3.2.1 Turbomachinery Fluid Seal

3.2.1.1 Floating ring oil seals:

Oil seal rings come as an assembly cartridge with a preload spring, two seals (low pressure and high pressure), Labyrinths seals and drainage paths. This type of seal (see Figure 3—1) functions by allowing clean lubrication it flow between two ring seals known as inner seal and outer seal, the oil pressure always above process suction pressure which it allows passage through the ring seals and rotor shaft then this leakage attempts to atmospheric side and small amount of passage goes through process side outer seal ring. [6]

The ring seal translates laterally with the shaft but it does not rotate. This condition produce huge axial and radial forces at the seal lapped face, normally the seal hydrodynamic forces are larger than the radial frication force otherwise the seal is locked up and can be the source of sub-synchronous vibration [6]. Both sides have oil drainage points and labyrinth seals at end of each side which it helps to drop the pressure.

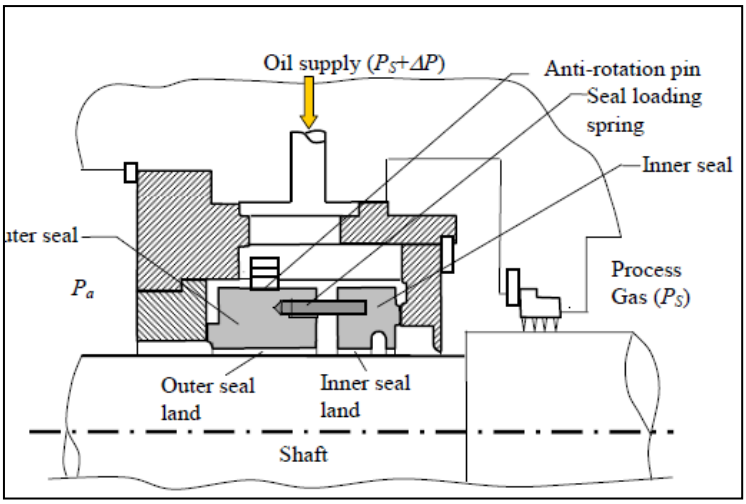

Figure 3—1 typical oil seal multi-ring assembly

3.2.1.2 Effect of floating ring oil seal on Rotordynamic

Floating Oil ring seals are non-rotating components which were mostly used in all turbomachines before Dry Gas seals introduced, wet oil seals are used in multi-stage compressors to minimize the fluid process leakage by utilizing a

pressurized oil seal to form a barrier against the highly pressurized escaping process gas [11]. Wet oil seal generates positive forces (stiffness and damping) to the rotordynamics comportment which is act against the rotor whirl resulting in restoring forces that decrease the rotor vibration amplitude, thus wet oil seal has a very important function to resist the rotor stability [18]. On the other hand, wet oil seal can be one of resource of negative damping mainly when it gains some of the rotor load resulting in reduced bearing cross coupling [34].

Wilcox and Conoco (1998) examined the cause and effects of large subsynchronous vibration (3.5 mils at 3490 rpm) in an FCC wet gas compressor which is driven at 7850 rpm by a 6000 hp electric motor via gearbox. The Compressor outboard bearing vibration increased 2.3 mils and the largest amplitude was at 0.4X to 0.45X, there was many effects considered during troubleshooting such as horsepower, molecular weight, oil pressure and oil temperature but they only achieved limited success, for that decided to performed rotordynamics analysis to find out the cause of the subsynchronous instability. The results that oil seal was determined to contribute the largest destabilizing effect , however an oil bushing seal L/D=0.1875 can float 0.030 inch diametrically in the housing and it has only 3 mil axial movement also it was originally designed with low diametrical clearance of 5-7 mil and additional the support fluid film bearing diametrical clearances of 6-8 mil thus, the observation was the oil seal clearances less than fluid film bearing clearances thus to drop oil pressure 65-70 psi applies roughly 500 lb_f of normal force which its pressing the bushing into the outer ring of the seal housing with contact surfaces frication coefficient μs=0.1to 0.3, the contact force Fc is $\sim$ 50-150 lb_f . However this force can readily lock up the bushing in an unusual position with this seal radial load is not capable to lift the rotor off the bearing which it can affect the rotor stability such as radial load bearings will decrease which lead to reduce bearing stiffness's and cause whirl . The Seal acts as additional bearing support with huge cross-coupled stiffness.

The recommendation to solve this issue as shows in Figure 3—2 it was to cut a 1/16" square groove of inner bushing land diameter which can break up the

hydrodynamic effect which leads the high coupled stiffness also minimize the radial load capacity of the seal [9] [35]. On other hand, test data from Childs et al. (2005-2006) [36] show that thin inner land grooves with depths as large as 15 times the slim land clearance do not effectively reduce the oil seal cross-coupled stiffness's.

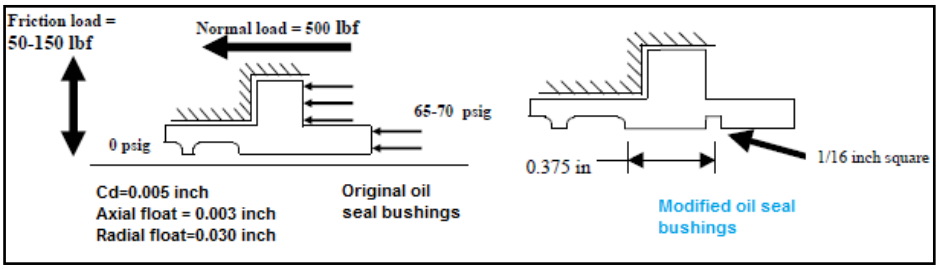

Figure 3—2 Original and modified oil seal bushings [9]

Zeidan et al. (1993) studied two cases of two different type centrifugal compressors, back-to-back type and straight through type on both cases has instability problem. The first case was a back to back compressor with speed of 10000 rpm driven by an aircraft derivative gas turbine with a power turbine via mechanical gearbox. The compressor before modifications was with two stages each one has two impellers with an inter-stage labyrinth seals, floating oil film seals and journal bearing with five pads loading On Pad configuration (LOP). However, because the operational needs the compressor was modified by adding one impeller in each stage thus the total six impellers on the rotor with two segments stepped inter-stage labyrinth seals (balance piston). The stability problems were started immediately after compressor modification for that to solve these problems there were some changing performed such as one of the balance piston seal segment was removed that to reduce the destabilized effects attribute to the labyrinth seals, the bearing were changed to a load between pads (LBP). In 1985 seal oil has problem due to contamination for that it was replaced by Dry gas seal, the stability was good after start-up but become unacceptable after a compressor surge, for that some modifications carried out that to solve the problems by replacing the old journal bearings with a new set which has higher damping through longer bearing pads, Dry Gas Seals were replaced with the old oil seals and Squeeze film dampers were installed to

enhance the damping properties. The compressor started very stable but once surge occurred the machine entered into an unstable condition again.

Finally the problem was solved by replacing the labyrinth seals with new Honeycomb seal which is explained in details on Honeycomb seal section. The main point to highlight that old oil film seals fixed back again that they were playing a stabilizing role through the friction damping action they provided while floating.

The second case was a straight through type compressor which it was almost similar to the above case with an additional of low performance and that due different source, the lockup of floating oil film seal was one of them which it was resulting high cross coupling forces , that what Vance et al., 2010 [18] explained about wet oil seals which have some impact in the rotordynamics (vibration and stability control) that by generate certain sources of optimistic stiffness and damping which could act in conflict of the rotor whirl which leads to reduce the rotor vibration amplitude.

3.2.1.3 Conventional Gas labyrinth Seals

Labyrinth seal is most common used in high speed turbo-machine application, this type of seals either seal teeth-on–stator (TOS) see Figure 3—3 or teeth-on-rotor (TOR) or combination of both TOS and TOR which is known as interlocking configuration see Figure 3—4 & Figure 3—5 respectively and it is non-contacting function with tight clearance that utilized to improve turbo-machine efficiency by reduce the leakage and control the high pressure that to allow fluid to pass to the low pressure region. This passage if not controlled it can causes instability to the rotor and loss machine performance.[14]

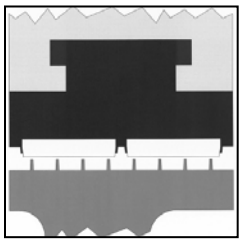

Figure 3—3 Teeth on Stator (TOS) [14]

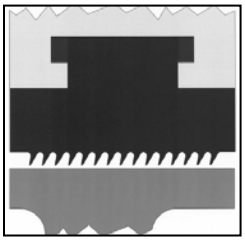

Figure 3—4 Teeth on Rotor (TOR) [14]

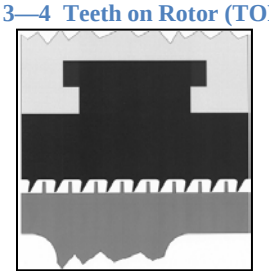

Figure 3—5 Interlocking [14]

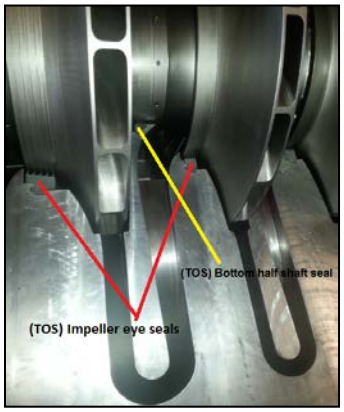

Figure 3—6 Teeth on Stator (TOS) configuration (shaft seal & impeller seal).

This seal utilized in the centrifugal compressors within different positions such as, impeller eye seal, shaft seal and for sealing balance piston cavities (see Figure 3—7). [14]

The purposes of those seals in the compressor are:

1. Impeller eye seal to ensure minimum leakage between the diffuser and impeller that to keep the compressor efficiency steady.
2. Shaft seal to break back pressure which is performed from second impeller that to reduce the axial force which it cans affect the rotor stability.

3. Balance piston to break the discharge pressure that to control the differential pressure between suction and discharge which reduces the impact of highest discharged pressure on axial thrust of the rotor.

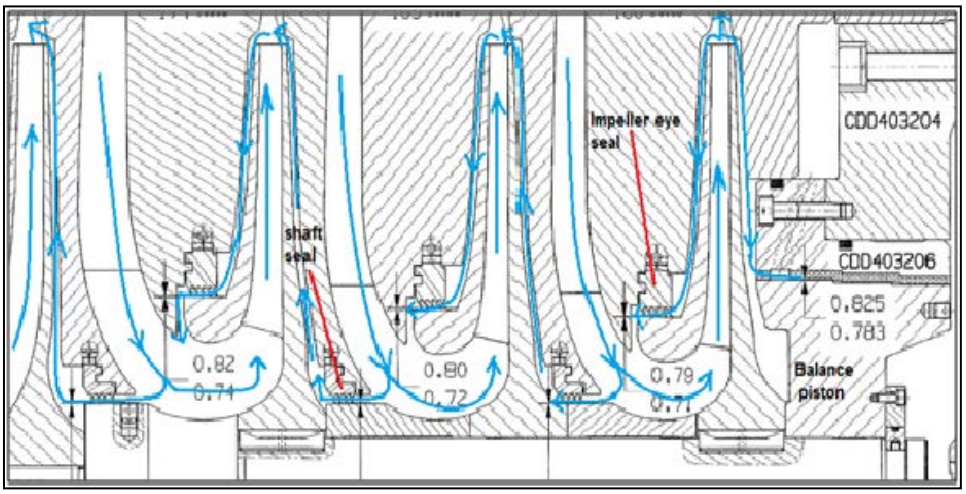

Figure 3—7 Partial section through a typical centrifugal compressor showing Eye, Shaft and Balance piston seal as well as typical leakage paths

.

3.2.1.4 Effect of Conventional Gas labyrinth Seals on Rotordynamic

Alford (1965) [57] wrote a paper which was described the causes Rotordynamic instability of aircraft engine compressor test in 1960s during the U.S.Navy development, his logical model indicated only the assumption of choked flow at two blades seal also on his model that difference pressure goes through the diameter of labyrinth seal without circumferential (cross-coupled not included on his mathematical model) (Jouhn). Also he mentioned on his paper the shape of labyrinth seal clearances it would have effect on the damping, However the direct flows in to the seal with converging clearances (inlet blade clearance is bigger than outer blade clearance) it consequences negative damping coefficients (Cxx,Cyy <0) and seal with diverging clearances(inlet blade clearance is smaller than outer blade clearance) would leads to positive coefficients (Cxx,Cyy >0).

Alford paper was opened the scope for Murphy (1980) [63] to performed his model with multiple (ten) blades and un-choked flow. He selected diverging seal for his model, the seal specifications were 171mm length, 4mm height and 200mm diameter, the blade clearances were 0.15 mm and 0.60mm at inlet and outlet respectively. The seal pressure ratio was 10 with inlet temperature of 182.7Cº and outlet of atmosphere. By using Martin's equation the steady flow was calculated for multi-blade labyrinth seal with equal pressure ratio and was resulted to be 0.224 kg/m-s, with all this conditions the labyrinth seal calculated for a whirl speed of 2500 rpm and amplitude of 0.12mm. Murphy's analysis concluded that converging seal is effect the rotor stability and other hand the diverging seal has positive damping effect which can controllable amount of external damping into a rotor-bearing.

Zeidan (1993) [15], He has separated the gas which flows through the labyrinth seal in two flow models portray, as illustrated in the figure 3-8 the first model is Gap flow dominate and the second model is cork screw dominate, thus the first model has the control at first few cavities of a seal while the second phenomena the most flow circumferential is away from the entrance of the seal which can causes higher cross-coupling and instability in the seals. For that there were many of techniques studies happened to reduce the instability in the seal such as Swirl brakes in the eye impeller depth which is used to reduce the marginal velocity by makes flow straight as the fluid enters the seal see figure 3-9, as high pressure from the compressor enters to the seal section that to minimize fluid rotation .However he described two cases on his paper of two different compressors and he did many analysis on different compressor components such as Bearing, floating oil film seal, labyrinth seal, Honeycomb seal and Rotor. On both cases, the labyrinth seal effect on Rotordynamic during the surge which there was subsequent increase in the labyrinth seal clearance.

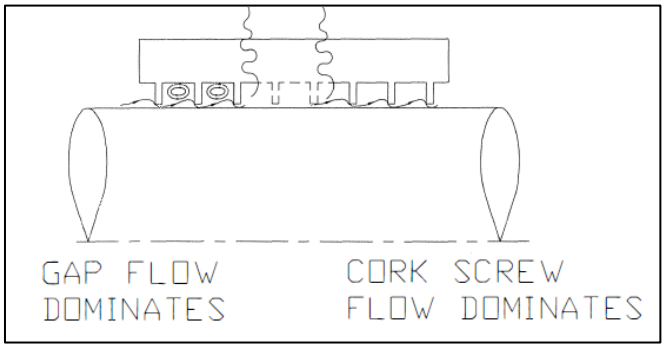

Figure 3—8 Flow in a Labyrinth seal [15]

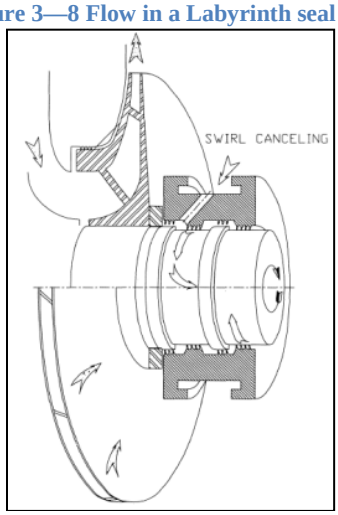

Figure 3—9 Swirl Canceling Device [15]

El Gamal et al (1996) [17], investigated the influence of different type of seals geometrical configurations and operating conditions. This investigations were conducted with four types which are, grooved casing ,grooved shaft , down-the-step and up-the-step seal however the observations was the shaft rotation has impact in all four seals mentioned with different level of effect , thus more effect on the down-the-step and up-the-step seal if compared with grooved casing and shaft . Furthermore, the positive effect of shaft rotation on the up-the-step seal performance where the rate of fluid leakage flow much reduced and the negative shaft rotation accrued on the down-the-step seal.

3.2.1.5 Pocket Damper Seal (PDS)

This type of seal is designed in 1991 at Texas A&M University and it has double determination used as sealing and vibration damping method .it is suitable to use in any application of turbomachine however it has been used to solve

rotordynamics instability issues especially in high pressure centrifugal compressor. [18]

The PDS is playing an effect role beside the bearings in terms of more rotordynamics damping. In Figure 3—10 illustrates the cross section of the original design of the PDS which designed of blades (identical to a labyrinth seal tooth) arranged in axial pairs with divider walls equally spaced around the circumference to form pockets, each pairs of downstream blade has wither a bigger clearance to the shaft or slots to allow leakage flow out of the pockets that not modulated by the shaft vibration more less the slot generates more damping.[18]

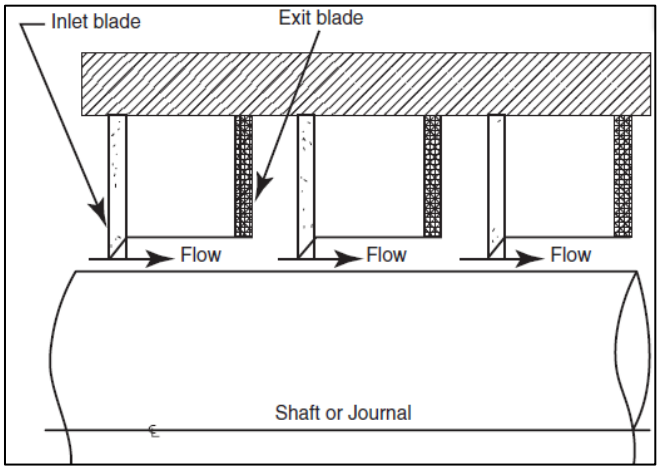

Figure 3—10 A six-bladed pocket damper seal (original design).[18]

3.2.1.6 Effect of Pocket Damper Seal (PDS) on Rotordynamic:

The PDS is used to solve a lot of problem of influences on rotordynamics as approved by Richards et al (1995) [16] on his study to eliminate the sub-synchronous vibration of two identical high centrifugal compressors, those compressors run with Maximum Continuous Speed (MCS) of 11493 rpm and the seal types used a long span traditional Labyrinth at the balance piston. In the low pressure compressor (LPC) observed the sub synchronous vibration frequency was increased above 150 µm and consequence compressor tripped at a speed of 7500 rpm, The sub synchronous vibration frequency was at 61 .25 Hz, which corresponded to the first natural frequency of the rotor.

The rotor design analyses conducted and the result was LPC sub synchronous vibration mode which matches to the first onward mode has a peak positioned at the Balance Piston Labyrinth Seal position see Figure 3—11. Also the spherical pivot, five pads tilt pad journal bearing was analysed numerically to determine its properties at the nominal, minimum and maximum rotor-pad clearance.

The conclusion on this research that mid span Labyrinth seal generated aerodynamic cross coupling forces which it caused high sub synchronous vibration for that the old Balance Piston Labyrinth Seal was changed with new Pocket Damper Seal which it provide more damping forces .

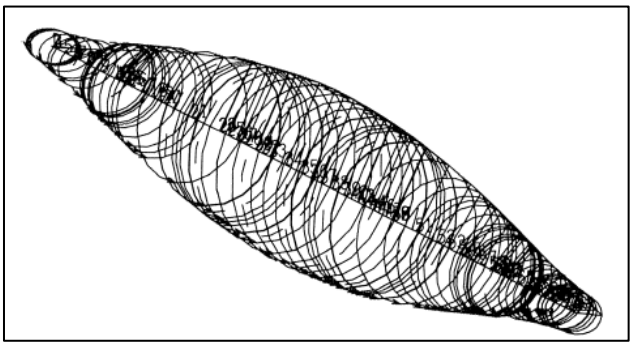

Figure 3—11 First Forward Mode of the LPC.[16]

AMG Eldin (2007) [19] conducted a research of leakage rate and rotordynamic characteristics of the pocket damper seal and labyrinth seals, on this study there were many of consideration on seal types such as seal cavity depth, blade thickness and spacing.

The outcome of this study for the Pocket damper Seals (PDS) are:

- The seal blade thickness and blade spacing has excessive equal influence on leakage drop matched to any other standing seals.
- The results indicated that a best seal depth is active for best performance as in terms of seal performance on leakage rate.
- On pressure test detected that with high pressure test the leakage rate is much lower in comparison to the low pressure due to high eccentricity.

- The PDS arrangement produces its vibration damping property liberated of the fluid viscosity that contributes more reliable.

3.2.1.7 Honeycomb seal

The first usage of Honeycomb seal was in aircraft engine and it was used as an abradable seal which runs against the teeth on the rotor. In 1960s Honeycomb seal used in the compressor which typically have a smooth rotor and rough stator, with this condition it could improve stability of the rotor since it has lesser surface area in the rotor which convey circulation to the fluid and with rough stator can leads to slow the fluid circulation which it cans reduce the destabilizing effect [15].

There are many of advantage of using Honeycomb seal in terms of Rotordynamic which were concluded by Zeidan (1993) [15], such as:

1. It is reducing the leakage by 60% and it helps inferior the thrust force.
2. No much damage (rub) observed on the honeycomb seal (stator) or rotor within compressor which has experienced many surges and also compressor not exposed any instability behaviour.
3. It cans handle high discharge temperature.

As mentioned above, a honeycomb seal has good stability on the rotor due to rough stator and smooth rotor.

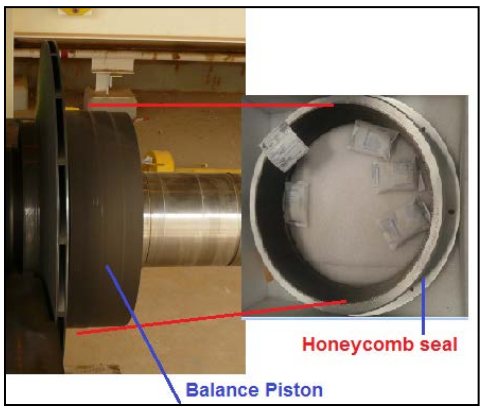

Figure 3—12 Balance Piston and Honeycomb seal

3.2.1.8 Effect of Honeycomb seal on Rotordynamic

Camatti (2003) [20] , published a paper of high pressure injection compressor performance test in terms of Aerothermal and Rotordynamic , the compressor train contents of three stages in 1st and 2nd stages are back-back within one compressor casing each stages have four impellers and the 3rd stage has five impellers , the seals arrangement as below :

- The impeller eye seals with type of Tooth-on-Stator (TOS).
- Back to back (B-B) compressor casing has cylindrical honeycomb seal within inter-stage balance piston and final balance piston with abradable seal (TOS) see Figure 3—13.
- In the 3rd stage casing has only final balance piston with cylindrical honeycomb seal see Figure 3—14.

The outcome of Camatti analysis as below:

- Honeycomb seal without shunt holes were created rotor instability and sub-synchronous highly increased that if swirling gas stopped to entry's into the Honeycomb seal consequently increasing the effective damping since it produce strong cross-coupling stiffness.
- Honeycomb seal, if it is not tapered with converging clearance thus produce negative effective stiffness and its interface with honeycomb seal damping due to lower whirl frequency.

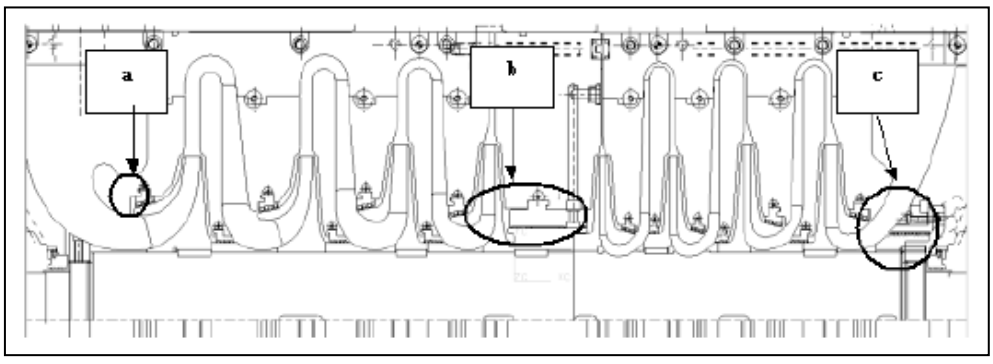

Figure 3—13 B-B compressor casing cross sectional , a) impeller shroud seal, b) Honeycomb interstage seal, c) abradable seal [20]

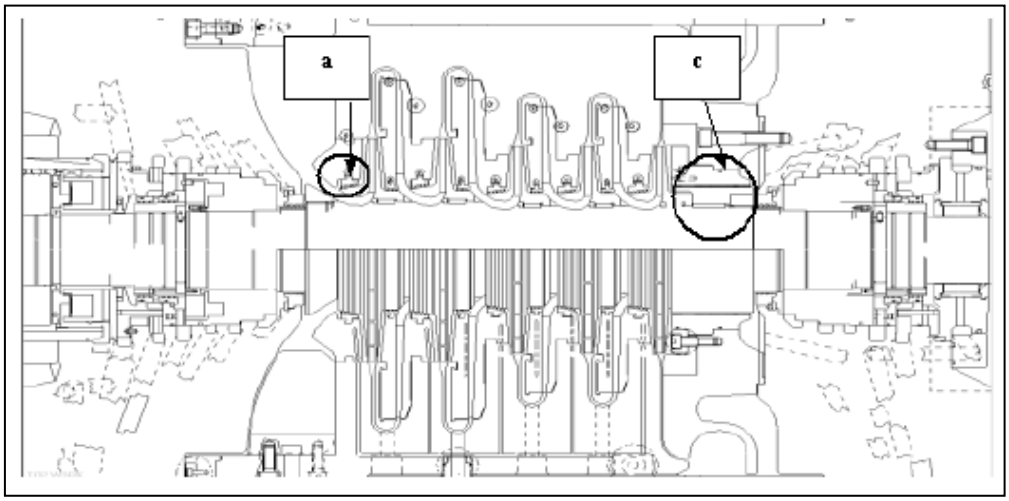

Figure 3—14 3rd compressor casing cross sectional , a) impeller shroud seal, b) Honeycomb seal[20]

Moore et al (2006) [21] investigated the honeycomb seal influences on centrifugal compressors performance at high differential pressure which can expects the effect on rotor stability and on the seal fluid dynamic due to seal deformation. This study conducted on two compressors Low pressure compressor (LP) and High pressure compressor (HP) , both compressors within same train which driven by Gas Turbine and the HP compressor last machine of the train . The LP compressor has to two suctions, each suction with 4 impellers (with tooth-on-stator labyrinth seal with no swirl brake), journal tilting pad bearings and balance piston with a tooth–on-stator labyrinth seal with shunt holes. The HP compressor with back-back arrangement and two sections as well the first section has 4 impellers and the second with 5 impellers , Bearings were similar of LP bearings , honeycomb seal without shunt holes fixed on center balance piston which end without tooth-on-rotor lay seal.

The filed data shows in HP compressor vibration plot with high subsynchronous vibration amplitude which leads to tripped the compressor. The compressor was overhauled and found the severe distorted on the Honeycomb seal that because of negative stiffness coefficient reduced the overall rotor stiffness which dropped off the first natural frequency to a state of low effective damping due to low speed.

The rotordynamics modelling was conducted on the HP compressor that to predict the compressor behaviours and to find the solutions which mentioned below:

- An offsetting convergent seal clearance profile machined that to make sure the clearance high adequate to reduce the critical speed reduction if seals distortion takes place.
- A shunt holes were machined to provide anti-swirl effect at the seal entrance which reduces the destabilizing forces.

Finally this study illustrated that controlling the seal clearance can optimized the stability of Low/High pressure compressor. However by controlling diverging tape can optimized stability without the threat of critical speed reduction in to a negative damping section ,also the labyrinth seal with swirl brakes and the damper seal with shunt holes helps to minimized the cross-coupling .

Kocur and Hayles (2004)[24] investigated a problem of centrifugal compressor which has a high subsynchronous vibration within low frequency; however this compressor was running a period of time with stable rotordynamics and acceptable performance that after changed old Labyrinth seal with a straight through clearance Honeycomb seal. Then the issue of subsynchronous low frequency vibration experienced. However the compressor was overhauled for inspection where it was found that the new Honeycomb seal was extremely fouled mainly at the seal inlet subsequent in a divergence flow path formation.

As above case mentioned the honeycomb seal has big effect on centrifugal compressor rotordynamics stability if gets choked, for that Sprowl and Childs (2007)[23] conducted an experiment to approve the above phenomena . The analyses carried out on Honeycomb seal and smooth seal which exposed with contaminated air that to get seal clogs thus different operating conditions were used for these analyses. The outcomes of this study that the clogged seal has higher leakage rate which consequence stiffness and dynamic stability decreased thus the damping properties get lower. For that Honeycomb seals

should not use with contaminated process that the chances of Honeycomb seal gets clog is high.

Smalley et al. (2006) [25] investigated the dynamic characteristics of the Diverging Taper Honeycomb Stator Seal (DTHCS) compared to the straight through Labyrinth Seal . this study used the non-commercial seal software (ISOTSEAL) developed at Texas AM Turbomachinery Laboratory hence used different loading conditions to get a vision of the seal behavior . The result shows that the Divergent Taper Honeycomb Seal (DTHCS) provides a greater effective damping source at low frequency operation

3.2.1.9 Hole Pattern Seal

Childs was mentioned about this type of seal on two papers, Test results for round-hole pattern damper seals and comparison of experimental Rotordynamic coefficients and leakage characteristics between hole-pattern gas damper seal and honeycomb seal in 1986 and 1998 respectively , the difference between hole-pattern seal and honeycomb seal Figure 3—15 were the hole-pattern seal has accuracy drilled round holes typically like honeycomb seals depth also the special on this seal is the tighter clearances compared with honeycomb seal clearances which its specify leas leakage and more damping.[18]

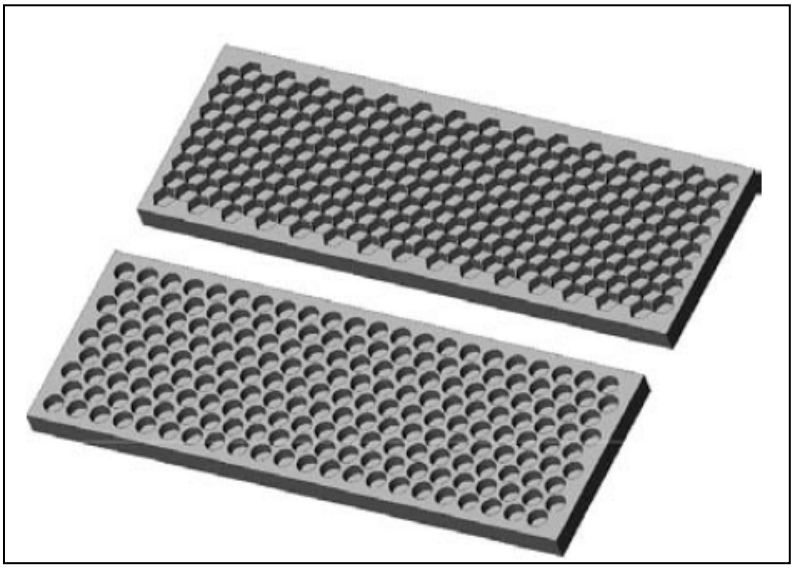

Figure 3—15 Comparison between honeycomb and hole-pattern seals [18]

3.2.1.10 Effect of Hole-Pattern seal on Rotordynamic

Rodrigues (2006) [22] conducted a study on an effect of using hole pattern seal on longer inter-stage seals with long balance piston perspective three variable investigation were conducted to explore the influence of long seals, constant clearance, radial seal clearance, and convergent –tapered seals geometries. However this study performed on two types of compressors back to bake and in line type thus the balance piston fixed in different locations on each compressors the first one in bake to bake type which it fixed on the mid span of the compressor and the second it fixed at 82% of the in line compressor rotor span .

The outcome of this study were indicated on both applications increasing the seals length as well in the L/D seals ratio but on the in line rotor configuration provides high damping and stiffness coefficients and a dramatic decrease in the overall rate of system leakage . On the back to back rotor configuration showed along with L/D ratio improved in the rotor stability. In conclusion On both applications if the seal clearance increases consequence high vibration amplitude.

3.2.1.11 Brush seal

This type of seal shows Figure 3—16 started to be used for jet engines in 2000 , that to increase the efficiency by reduce the leakage by 40-80% compared with labyrinth seal and also the special on it, can hold high temperature since the material usually used alloy (nickel, chromium, cobalt, and molybdenum alloy). this type of seal being replaced the labyrinth seal with some application spicily with higher pressure in comparison jet engines and gas turbines also it can combined with other type of seals such as pocket damper seal used as stand-alone sealing . [18]

Figure 3—16 Brush seals installed in high-pressure steam packing's[18]

3.3 **Trubomachinery Bearings**

3.3.1 Introduction

The fluid film Bearings are most famous used in high speed machines which have been continues developed since 1882 till today. However, the bearings are playing a critical role on the turbo and rotating machinery performance in terms of Rotordynamic, reliability and life. Indeed, as per my field experience on the rotating machines especially with Centrifugal compressors which has different failures some of it due to lack of maintenance, wrong bearing selection and most of it due to design. For that in my literature will focus more in the Film fluid bearings that to understand it works principle and how it cans affect Rotordynamic.

The understanding of fluid film principle done by Tower between 1882 to 1883 while his studying high speed railway engine bearing , in his experimental measurements show the load in the bearing while injecting continue lubricant oil that load was created through the oil film which can separated both surfaces of the bearing and shaft. Tower didn't give any explanation for these phenomena.

In machine with application of high speed and heavy loads and integrate force-feed lubrication should be use radial journal bearings which can support loads for both steady and dynamic state also it can provide stiffness and dampening that to reduce the vibrations, in fact the bearings provide position for rotating

components either radial or axial which by maintained by Journal bearing and thrust bearing respectively. [33]

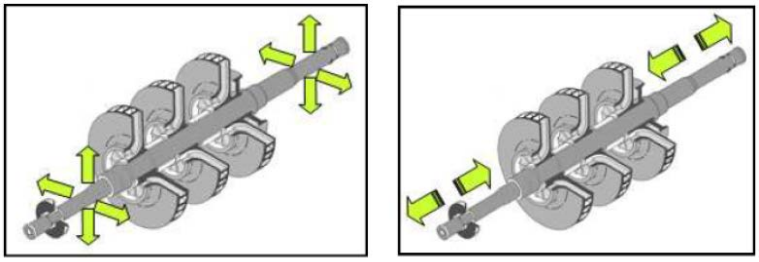

Figure 3—17 Radial and Axial Bearings and Loads [33]

3.3.2 Fluid Film bearings

The fluid film bearings can categories in two types:

3.3.2.1 Hydrodynamic bearing:

In 1886, Reynolds [64] [18] was given good explanations of Tower experimental by developed hydrodynamic lubrication equation that by combined it with Navier Stokes equation. Fluid film bearing principle describes as the very thin film lubricant oil goes between the bearing surface and shaft surface with fully hydrodynamic regime which supported the load to prevent any contact between two surfaces ,however it's very important to use suitable and clean lubricant which is can combined of the three parameters such as speed, loads and oil viscosity, those parameters indicated on the ZN/P curve (Figure 3—18) which it was introduced in 1902, This curve shows the three conditions pass through bearing during speed stand still until the operating speed.

In Figure 3—19 is demonstrated the three conditions Dry friction, Boundary friction and Fluid friction as the shaft on standstill mode (no rotation) the shaft load sets on the bearing which it leads to dry friction as show in Figure 3—19(a) while the shaft started to rotate and the lubricant oil started to mixed which it begins of separation between the shaft surface and bearing surface as seen in Figure 3—19 (b), when the shaft speed increased the hydrodynamic load initiated by dragging the oil film through converging wedge (formed by bearing surface and shaft surface see Figure 3—19 (b)) which it leads to increase the

oil film pressure and the oil film takes place between two surfaces that to supports the static load and dynamic load, this phenomena is called Fluid fraction condition. [18]

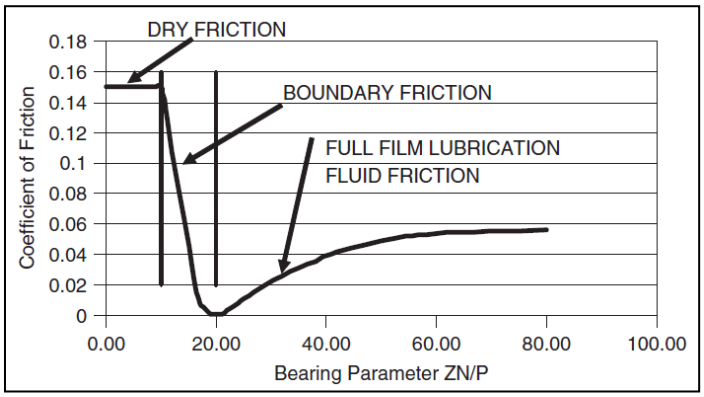

Figure 3—18 The ZN/P curve and the three lubrication regimes [18]

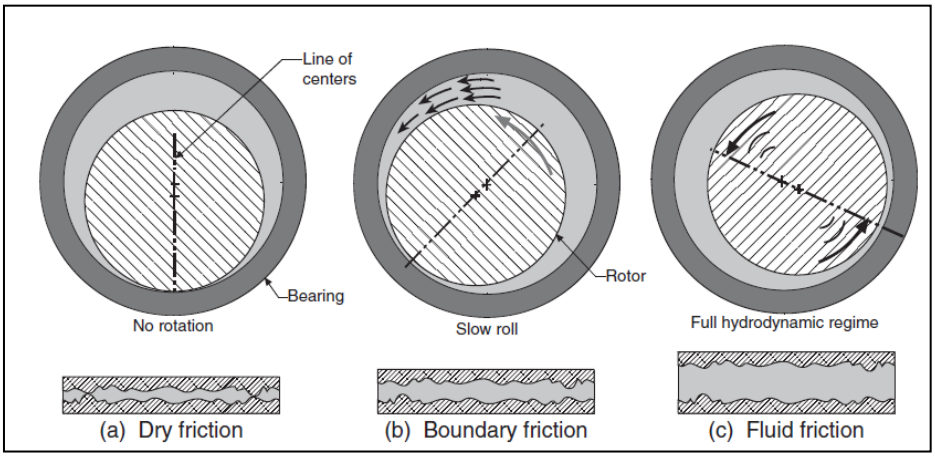

Figure 3—19 Three lubrication conditions in the fluid film bearing [18]

3.3.2.2 Hydrostatic Bearing:

This type of bearing not widely used as the hydrodynamic bearing since it used only with huge equipment which has high torque while start up.

The different between Hydrostatic and Hydrodynamic Bearings mainly on the way of generate the oil pressure which it can left the shaft by certain forces, however on the hydrodynamic bearing the lubricant oil pressure build up by increasing the shaft speed which leads the passage of oil through the converging wedge but on the hydrostatic type the lubricant oil pressure build up

by external pump , the pressurized oil injects through the lower position of the bearing into the bottom of the shaft which it cans lift the shaft on the standstill condition then the oil pressure started to reduce while the shaft speed increased and the fully hydrodynamic regime initiated.[32]

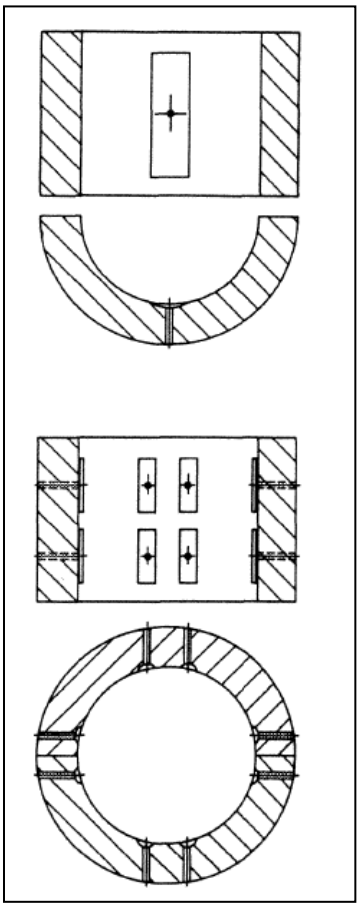

Figure 3—20 Schematic of Typical Hydrostatic bearings. [32]

3.3.3 Fixed geometry/profile sleeve bearing:

The function of fixed geometry/profile sleeve bearing supports large heavy-duty rotating machinery by developing a hydrodynamic pressure through the converging wedge which formed by shaft and bearing surface as shows in Figure 3—21.The oil film draws into a wedge to produce the pressure to lift the load (Hydrodynamic lubrication) that depends on to rotor speed, oil pressure and rotor weight. The oil film should superlatively rotate at speed of 0.5 rpm however with some frication losses which cause the oil film to rotate at 0.42 rpm which it leads to pushes the rotor at angle 7 o'clock if the shaft rotating CW .

These conditions can cause the shaft centre is close to bearing centre which is causing a drop in stiffness and drops in oil pressure or temperature. In this situation, the oil film would push the rotor to opposite position in the shaft. However If this method has continues further and further the shaft would keep getting pushed around within the bearing. This phenomenon is called oil whirl which is naturally unstable since it is increase centrifugal forces that will increase the whirl forces as shows in Figure 3—22.

There are different cases which can induce the oil whirl in the bearing such as light dynamic , excessive bearing clearance , oil properties change , improper bearing design (could be over design for the real shaft loading), change in the internal damping and fluid leakage either of the shaft labyrinth seals or blades shroud. [32]

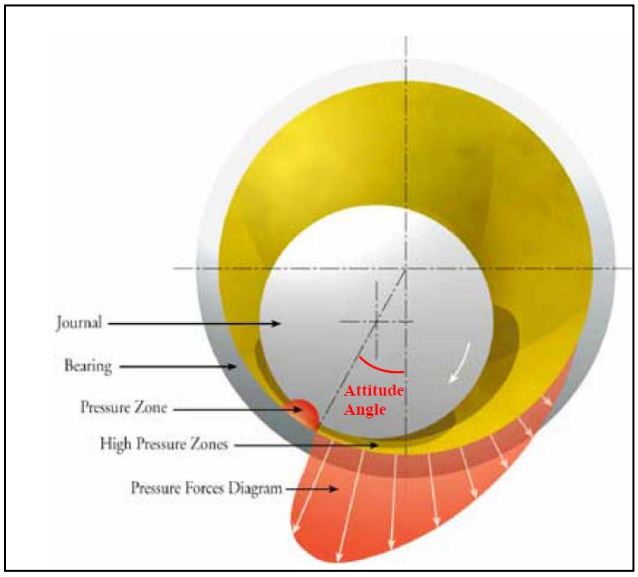

Figure 3—21 Oil Film within a Journal Bearing and hydrodynamic lubrication [33]

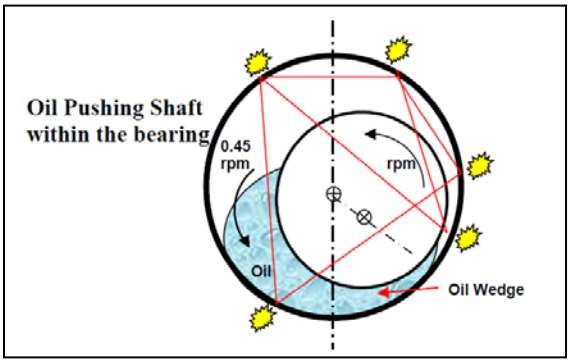

Figure 3—22 Oil Whirl Phenomenon [33]

It is important to understand when oil whirl phenomenon occur during operation time that to take immediately action to prevent any further consequences, therefore if the shaft speed between 40% - 48% the vibration frequency will appear since the sub-synchronous frequency become 0.42X if this phenomenon continues defiantly will lead to severe damage once it reach to oil whip see Figure 3—23. [33]

Oil whip is an unsteady process which can lead to a catastrophic failure this phenomena occur when the oil whirl frequency match with and becomes locked into a system's natural frequency in fact when a machine operated at rotor spins to double the critical speed the oil whirl frequency can be close to the rotor critical speed and so can excite the resonance and cause extreme vibration. [33]

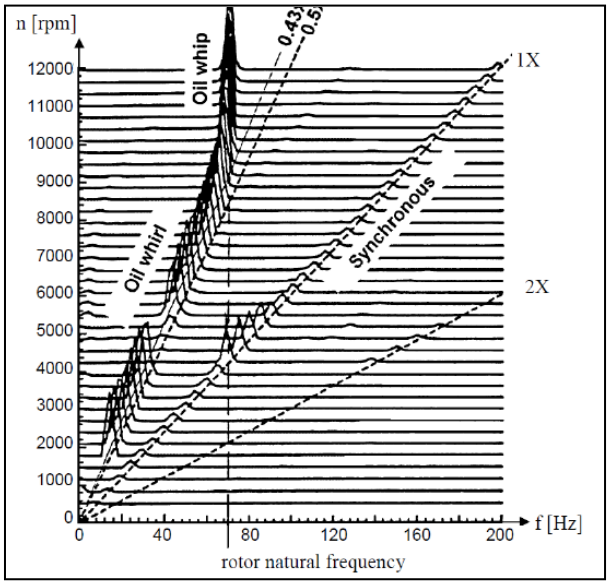

Figure 3—23 Cascade diagram, showing the development of oil whirl just after startup; followed by oil whip from 9,200 to 12,000 rpm.[33]

The cross coupling forces in the Journal bearing to be likely always push the shaft to the reverse side of the converging wedge (formed between bearing and shaft) as shows in Figure 3—24, a combined of stiffness forces (KxyY and KyxX) produce a force that tangential to the circular whirl or it in the direction of the rotation . The circular geometry and the fluid rotation in the bearing are part of destabilizing cross coupled stiffness within a fixed-geometry bearing which these can directly consider and act to the bearing design and configuration. The capability to do change and modify to bearing design and its configuration are helping a lot of achieve a bearing stability therefore to eliminating fluid-induced instability we need to ensure the threshold of instability Ω_{th} should be highest expected operating speed of the rotor, where [5]

$$\boldsymbol{\Omega_{th}} = \frac{\mathbf{1}}{\boldsymbol{\lambda}}\sqrt{\frac{\boldsymbol{K}}{\boldsymbol{M}}} \qquad 3—1$$

By adjusting the parameters of above equation such as decrease the fluid circulation λ, increase the spring stiffness K, or decrease the rotor mass which of course not easily to change it for that to play with other two parameters more reasonable[5], indeed the reduce of the fluid circulation have be done by implemented the bearing geometries such as two axial grooves in Figure 3—25,

Elliptical or lemon bore bearing Figure 3—26 , three-lobe preloaded journal bearing Figure 3—27, four-lobe preloaded journal bearing Figure 3—28 and offset half sleeve bearing figure 3-29. [18]

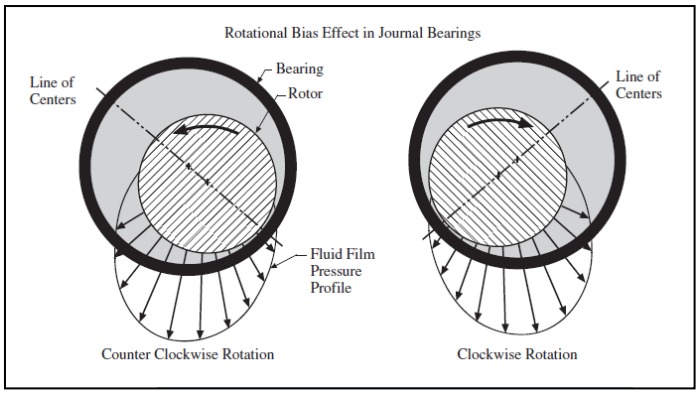

Figure 3—24 Rotational bias caused by cross-coupled stiffness coefficients.[18]

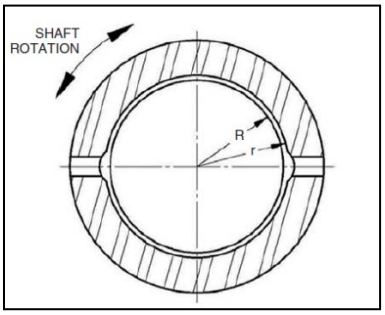

Figure 3—25 Two axial grooves [18]

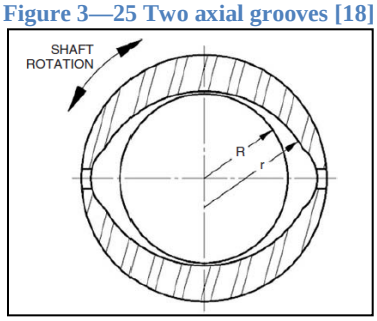

Figure 3—26 Elliptical or lemon bore journal bearing [18]

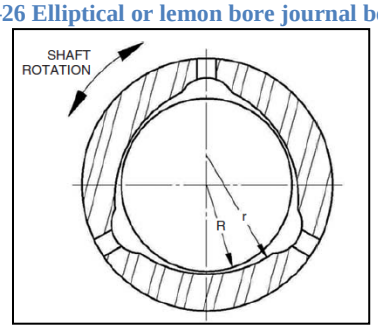

Figure 3—27 Three-lobe preloaded journal bearing. [18]

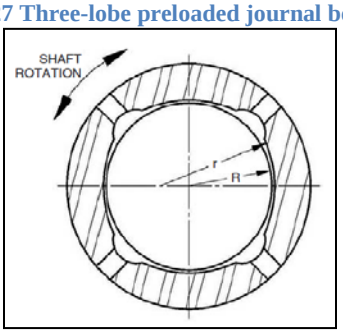

Figure 3—28 Four-lobe preloaded journal bearing. [18]

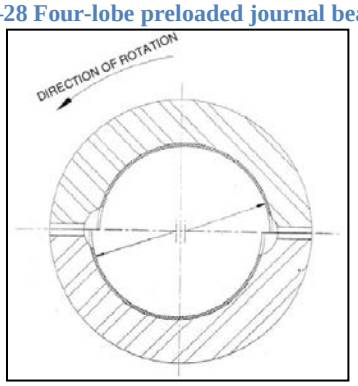

Figure 3—29 Offset half sleeve bearing. [18]

3.3.4 Geometry Tilting Pad Bearing:

Geometry tilting pad bearing are distinction on the stability and less or zero cross-coupling present on it, however the pads pivot reacts to the radial load which is generated from the shaft journal and it will react as a force within the shaft centres, also there will be no attitude angle (attitude angle almost zero) for that there is no cross-coupled stiffness and also the frication and inertia in the pivot will be negligible (See Figure 3—30). [18] Thus, the geometry tilt pad bearings recommend better stability than the fixed geometry sleeve bearings indeed the tilt bearing price a large amount than sleeve type.

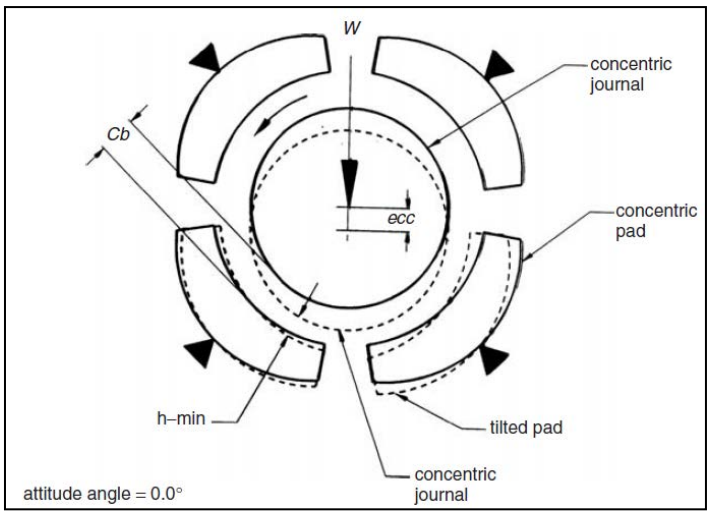

Figure 3—30 Schematic of atilt pad bearing [18]

There are three main designs of tilt pads such as Rocker Pivot Tilt Pad, Spherical Point Pivot Tilt Pad and Spherical Surface Pivot Tilt Pad, each type has speciality thus the Rocker Pivot tilt pad is the cheapest and it is the simplest in term of design since it tolerates tilting movement within circumferential .[18]

3.3.5 Bearing design

there forces which appearing in the rotor within bearing envelop can make a big different on the rotor behaviour if there is any failure in the bearing design or if there is any modification implement after design and the most two characteristics which has changing interface with the rotor stability are Stiffness

and Damping . As the most danger phenomenon to the bearings are whirl and whip which may leads to the major damage.

Basically the consideration of the bearing design is very important to have high performance bearing which Nicholas (1994) highlighted on his paper as below [8]

1. Sleeve bearing load design limits suggested, $L_{u \leq 200\ psi}$ and $L_{u \geq 100\ psi}$ (the recommendation to designed sleeve bearing between these limits thus the bearing with higher loads can perform without any struggle since suitably cool system taken place however the lower load in the sleeve bearing may be lead stress-free (pressure block).
2. The Journal surface velocity recommended design limit as $\mathrm{U_{s \leq 300\ f/s}}$.
3. The bearing clearances range from 1.5 to 2.0 miles of Dia clearance per inch of journal diameter, however the effective damping may reduce if the bearing clearance increased which it leads increasing on the shaft vibration.
4. As shown in the Figure 3—31, the maximum film temperature located near the maximum pressure, for that temperature sensor should fixed close this location which it may at angle of 45 degree with rotation from bottom dead centre for horizontal rotors with vertically downward journal loads. since the bearing Babbitt start melts at 455 °F and it starts to change to soft around 250 to 275 °F thus the maximum embedded temperature sensor proposed as 185 °F design , 200 °F test acceptance ,230 °F alarm and 250 °F Trip . Also need to consider that Max oil temperature will be higher than Max embedded temperature by 20 °F.

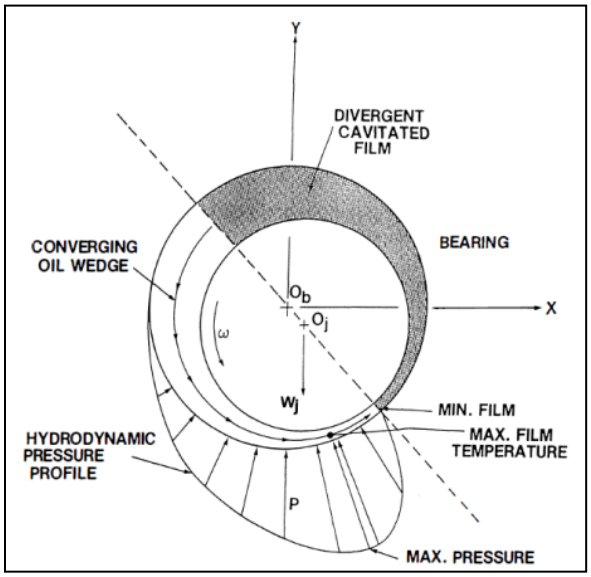

Figure 3—31 Sleeve Bearing Hydrodynamic Pressure Profile [8]

5. All of mentioned limits above apply to tilting pad bearings except the temperature sensor position which it's placed at 75 present of the downstream from the pivot and total pad arc length from leading edge as show in Figure 3—32 that because the maximum film pressure and maximum temperature occurs at some angle with rotation from the pivot as shown in Figure 3—33.
6. The Figure 3—34 shows the pad pivot offset α, which it is centrally pivot by 50% offset usually the offset pivot value from α= 0.5 to α= 0.6 (55% - 60% offset).

$$\alpha = \phi p/x \qquad 3—2$$

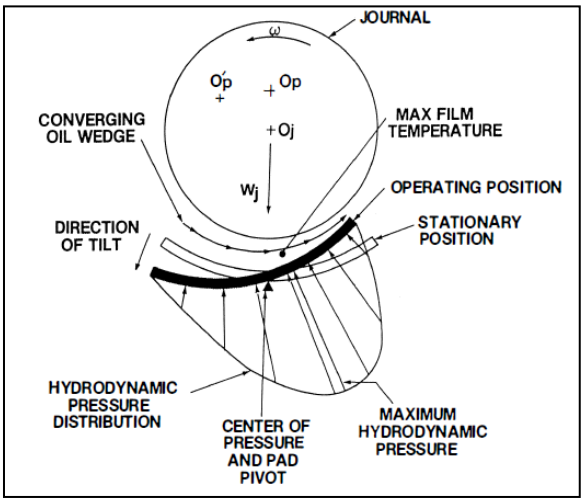

Figure 3—32 Tilting Pad-Angle of Tilt. [8]

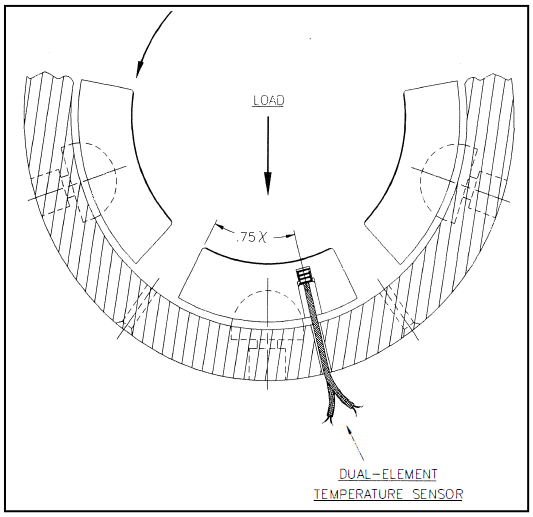

Figure 3—33 Temperature Sensor Location-Load on Pad. [8]

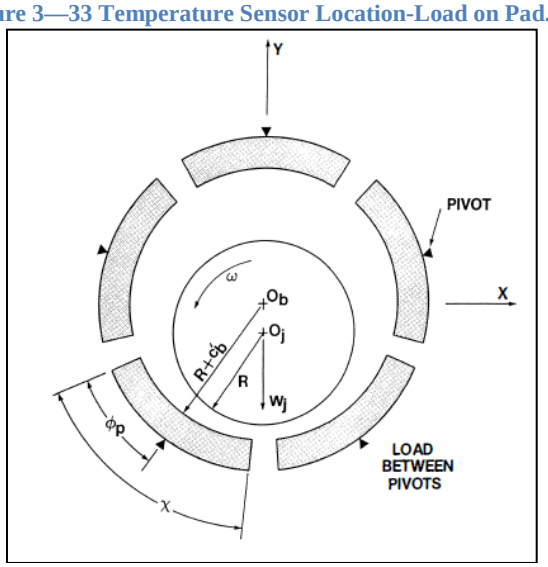

Figure 3—34 Tilting Pad Bearing-Load Between Pivots. [8]

7. Tilting pad bearing preload is defined as m and as seen in Figure 3—35, the zero tilting pad bearing preload where the radius of curvature Rp is equals the Pivot radius Rb and the clearances of the pad Cp , and assembled bearing clearance Cb, are equals thus the, preload = m = 0

$$m = 1 - \left(\frac{C_b}{C_p}\right) \qquad 3—3$$

$$R_p = c_p + R + c_b \qquad 3—4$$

$$R_b = R + c_b \qquad 3—5$$

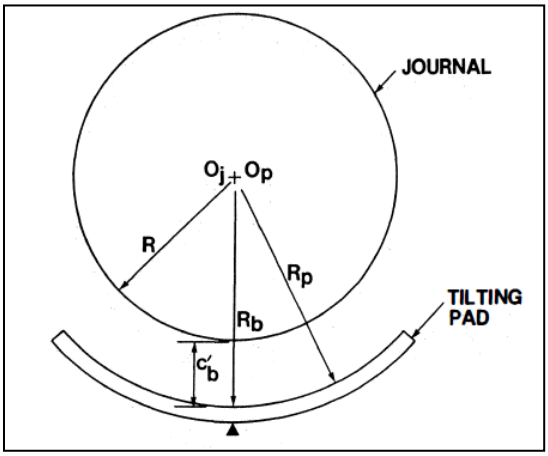

Figure 3—35 Zero Preloaded Tilting Pad. [8]

However if the preloaded tilting pad demonstrated as in Figure 3—36, the Pad clearance c_p is greater than bearing clearance c_b on average the preload values range from 0.2 to 0.6 (20% - 60%) the converging film pass between two surfaces and the pad will create hydrodynamic forces even the bearing load come close to zero.

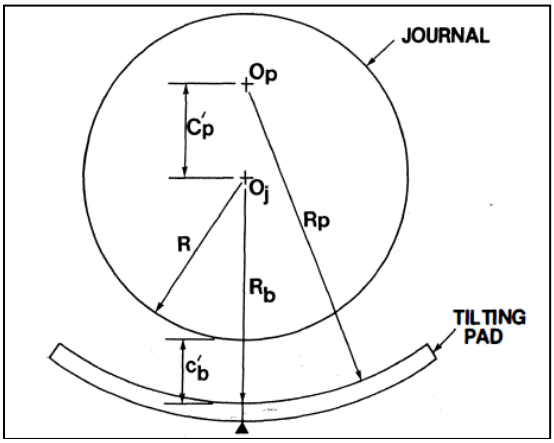

Figure 3—36 Preloaded Tilting Pad. [8]

As preloaded tilting pad bearing reduced to zero or near zero, the damping will increase and bearing stiffness approximately residue steady which will give more stability on the rotor . on other hand, there are some disadvantages of reduce preloaded tilting pad bearing to zero such as the extreme decline in horizontal stiffness and damping (Kxx and Cxx) as the pad preload be converted into negative as shown in Figure 3—37, where the consequent effect on stability can be seen in the Figure 3—38, where the system come close to the unstable regime for preload value under than – 0.1, Also the unloaded of top pad can consequent loss on the damping which leads on rotor vibration

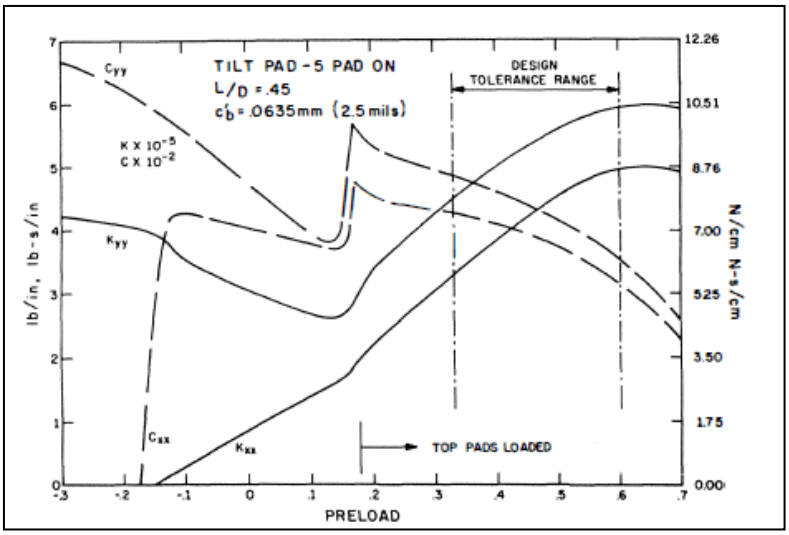

Figure 3—37 Tilting pad bearing, effect of negative preload and unloaded top pads [8]

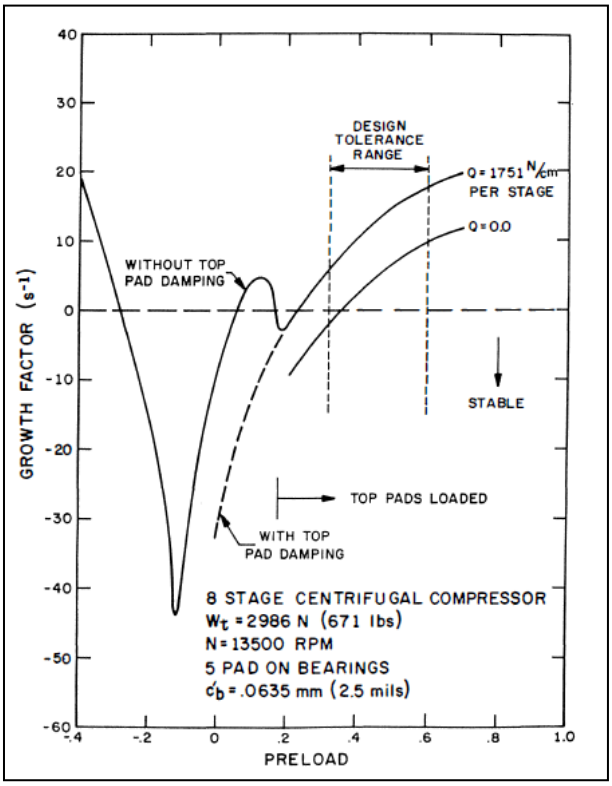

Figure 3—38 Stability vs Preload-Effect of top pad damping [8]

8. The length to the diameter ratio L/D is another strong significant design of tilting pad bearing parameters since it influence directly on the damping, if Pad L/D ratio increases the bearing damping will increase and the stiffens decrease, for that longer pad becomes more popular in the bearing design with consideration of effect on Pad to shaft misalignment for that always self-align pivot recommended for lengthy pads (L/D ratio large).
9. Pivot film thickness calculation must be consider during design , as shown in Figure 3—39,

$$\bar{h}_p = (1 - m).(1 + \varepsilon \sin \emptyset) \qquad 3—6$$

Where, $\bar{h}_p$ is pivot film thickness and ε, is bearing eccentricity ratio:

$$\bar{h}_p = \frac{h_p}{c'_p} \qquad 3—7$$

$$\varepsilon = \frac{e}{c'_b} \qquad 3—8$$

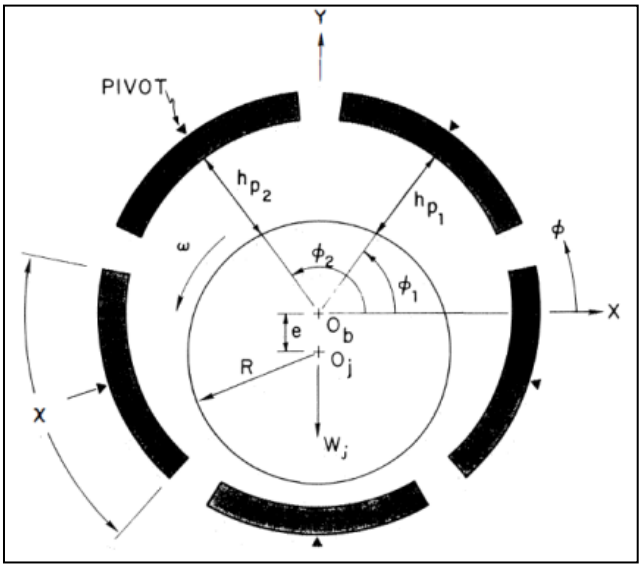

Figure 3—39 Tilting Pad bearing Pivot film thickness [8]

Once the converging film thickness equal or larger than the pad redial clearance the tilting pad become unloaded indeed in this condition no more converging film enters between pad surface and shaft surface so , for an unloaded pad ,

$$h_p \geq \acute{c}_p \qquad 3—9$$

As per the equation (3-14) the pivot film thickness, dim will be

$$\bar{h}_p \geq 1.0 \qquad 3—10$$

If we considered $\bar{h}_p$= 1.0 the preload *m* will be as below equation

$$m = \frac{\varepsilon \sin \emptyset}{1+ \varepsilon \sin \emptyset} \qquad 3—11$$

Also the eccentricity ratio become as,

$$\varepsilon = \frac{m}{(1-m) \sin \emptyset} \qquad 3—12$$

10. The Breakaway torque should consider during design as Nicholas (1994) concluded on his paper that the torque of five pad load between pivot bearing more than sleeve bearings by 24 % and with four pads the torque greater than sleeve bearing by 41 present .

11. Also within same paper the test result of bearing metal temperature reduction for a spray bar design with an evacuated cavity 10% Maximum if compared to a conventional pressurized housing design.

3.3.6 Effect of bearing stiffness and damping coefficients on rotordynamics.

Bearings are significant part which theatre directly on the Trubomachinery performance since most of rotary mechanisms in turn has bearings that to support the Wight and stand the forces associated with rotary motion and vibration however the different type of forces which acts on rotor and bearings definitely affect Trubomachinery Rotordynamic. For that there is a lot of efforts on developing bearing design and also there are continuations of solving bearing issues which already some of them indicated on journals which will highlighted within this Literature.

Nicholas and Wygant (1995)[8] addressed a design method for tilting pad journal bearing pivot (Spherical pivot type) for high load may it goes up to 500 psi. Artless equations were developed to calculate of pivot stiffness and a way to define accurate pivot sizing to avoid pivot failure due to high loads. In their paper concluded lots of concerning on the tilting pad journal bearing pivot design.

Wygant et al. [26] presented the results for influence of two different pivot designs for five rocker back tilting-pad bearings with preload factors ranging from –0.333 to 0.540 and ball and socket types. The measurements were described for a range of speed-load conditions about a range of Sommerfeld* numbers from 0.1 to 4.5 for both on-pad and between-pad load locations. They concluded that pivot type influenced both static and dynamic characteristics because the friction for low loads.

In recent times, Brechting et al [27] extended the range of loads and measured static characteristics for both rocker back and ball and socket bearings. They found that friction characteristics were reduced for high loads. Also they presented a comparison of the measured dynamic coefficients and the measured static characteristics for a tilting pad cross coupling at different loads condition on-pads or between-pads. The result shows the load angle had a moderate influence on operating eccentricity and attitude angle however the speed and load conditions included herein thus the dynamic coefficients were not strongly dependent on load angle on the other hand very importantly the measured results demonstrate the ability of tilting pad journal bearings to satisfactorily operate at off-optimum load angles.

Pettinato and de Choudhury [28] measured the dynamic coefficients of two five-shoe tilting pad bearings one was a key-back and the second was a spherical seat, this measured with load between-pads for a range of Sommerfeld numbers and also the test data included pad temperatures, power loss and operating position. The configuration of those bearings was totally differed in the seat, pad lengths, and pad shapes which indicated the different effect on both stiffness and damping coefficients.

*Sommerfeld $S = \frac{\mu NLD}{W}(\frac{R}{C})^2$ includes the following design parameters; bearing dimensions radius R and radial clearance C, viscosity μ, speed of rotation N , and the inverse of the bearing unit loading or pressure (LD/W) [18]

Yang et all (2005) [29] studied the characteristics of the upper unloaded pad fluttering in journal bearing and its influence on the rotor stability that by experimental preformed on the bearing (Load on pivot (LOP) six tilting pads) with consideration a range of measurements such as film pressure, circumferential, shaft speed, bearing load and vibration comparative between the shaft and the bearing. The result come out from this experiment that ,the pad fluttering characteristics has similar behaviour of oil whip (rotor bearing instability) since it has subsynchronous vibration at a frequency of (0.5X) within rotor speed (1X) also when the shaft speed increase observed the fluttering amplitude of the pad increased and it's frequency stay constant. In conclusion of above observation the Pad fluttering has a direct influence on the rotor stability which it phenomena required to consider for improvement in terms of rotordynamics. One year after Hargreaves and Fillon (2006) [30] performed a practical analysis of a Tilting Pad Journal Bearing to Avoid Pad Fluttering under a light static and dynamic load , in this analysis used three methods to explore the effects . The first method was to establish a preload on the bearing by adding metallic shims, the second method was to control or stop the pad fluttering by install a pad spring and the last method was to generate a pad relief on each pad which should stop any fluttering. From this analysis and with three methods compared that the conclusion was the third method more effective amongst other two methods since it was with simple solution which should not affect the bearing characteristics.

Ronald (2006) conducted an experimental analysis of influence of excitation frequency on dynamic coefficients of a tilting pad bearing; this experimental was carried by using test ring which was based on the concept of free-floating test bearing and a fixed rigid shaft as illustrations in Figure 3—40. the test bearing continent of steel base, rotor support bearing, seals, bearing housing, test bearing with five tilting –pad and rotor as shows in Figure 3—41. The bearing tested with rotating speed of 900 rpm and with static loads ranging from 0.133 to 0.534 kN consequential in range of Sommerfeld numbers of 0.074 to 0.738.

The test bearing had a bearing clearance $C_b$of 81.3 μm , pad clearance C_p of 91.4 μm, preload factor was 0.125 and offset factor was 0.5 , the L/D ratio was 0.75 , the pad length arc was 52°, lubrication viscosity 30.5 mm2/s at 40ºC and 18.60 mm2/s at 55ºC and the specific gravity was 0.846 at 55ºC.

The experimental concluded that the dynamic coefficients of a tilting-pad bearing with a preload factor of 0.125 are frequency dependent and On other hand the Excitation frequencies range from 50% to 200% of the synchronous frequency directly influences the stability of a rotor system . Some specific comments about the trends of measured coefficients are recognized as below:

- In overall principal stiffness's reduced with growing excitation frequency for all Sommerfeld numbers and for both loading directions.
- The excitation frequency indicated little effect on either measured cross-coupled stiffness positions.
- The excitation frequency increased while the damping on pad loading increased as well as Sommerfield.
- As excitation frequency increased Cxy tended to significantly decrease for on-pad loading and less dependence on Between-pad loading.
- There was no any induction of change of principal stiffness with excitation frequency due to lowest Sommerfeld number on the between pad loading.
- No significant Kxy terms were measured for the between pad loading while a small level of cross-coupling, Kyx, was measured the terms did not show any clear trends.

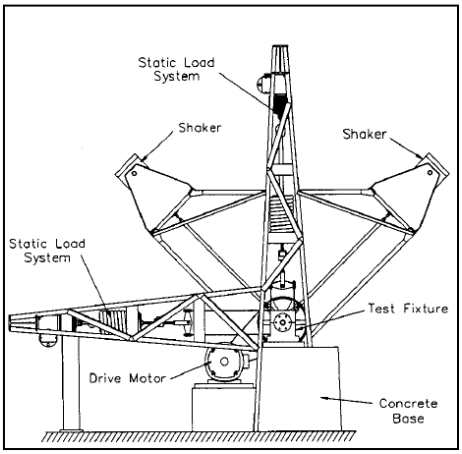

Figure 3—40 Bearing test rig with drive and load systems

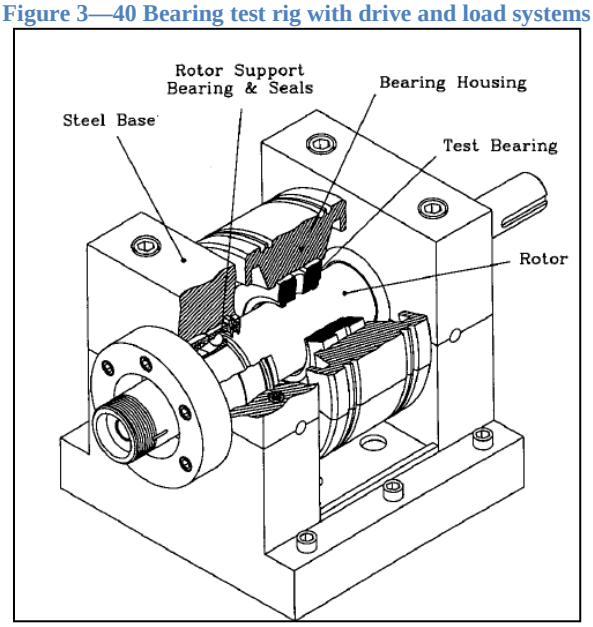

Figure 3—41 Cutaway view of bearing test fixture

S. Kim and K. Kim (2007) [31] conducted an experiment to study the influence of pad-pivot friction on the tilting pad bearing performance, also there was a proposal a mathematical model addressing the affect of friction on the tilting pad bearing performance. The outcome of this study that the friction has a huge influence on the attitude angle of the journal which consequences in a bad bearing performance, furthermore the friction has a direct affect on the fluid film thickness and pressure distribution. To end with the mathematical model confirms that the eccentricity direction of the journal and the load direction do not match when the pad-pivot friction preformed.

3.4 **Centrifugal Compressor Rotor Configuration**

Centrifugal Compressor rotor shall be designed to transmit the maximum torque provided by the driver for that during design must be consider many facts such as the Torque as per horsepower, shaft shear stress, rotor measurements, rotor stiffness, rotor configuration, rotor assembly, rotor balance and materials which the common shaft materials used are ANSI 4140 and ANSI 4340 Steels which have a shear property of 36,000 psi. [37]

As shows in Figure 3—42 the rotor assembly which indicates the main rotor parts such as impellers , spacers (sleeves) , shaft and balance piston however the rotor has different configurations such as single stage overhung , multistage –series (inline) and multistage-opposed (back to back) as shows in Figure 3—43 and Figure 3—44[3]. Moreover, the single stage overhung rotor and multistage –opposed are usually without balance drum due to the rotor thrust values are low enough which could be contained by a thrust bearing. The multistage-series rotor design for high pressure application with balance drum, this arrangement could be cause catastrophic damage in cases failure of balance drum seal [37] for that with this arrangement always recommend [13] fixing proximity vibration probe for axial displacement.

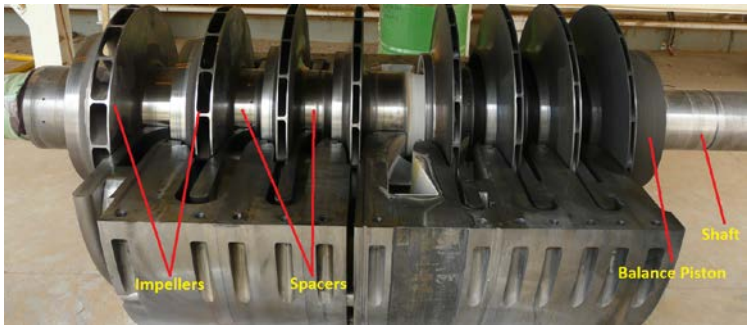

Figure 3—42 Rotor Assembly Harweel, PDO 2014

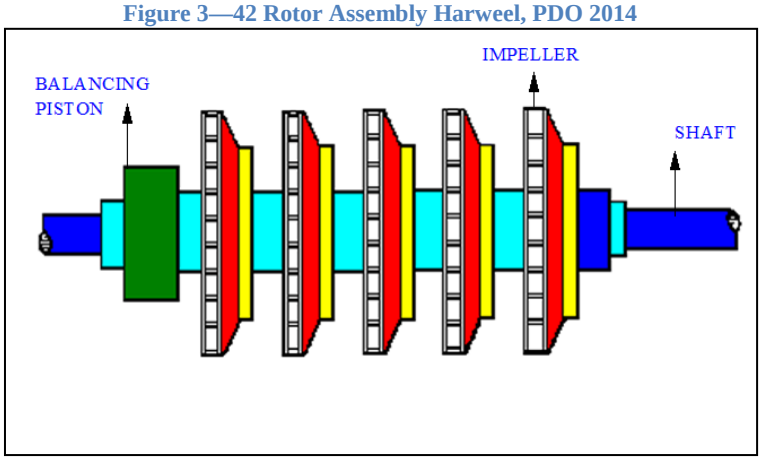

Figure 3—43 multistage –series rotor arrangement [3]

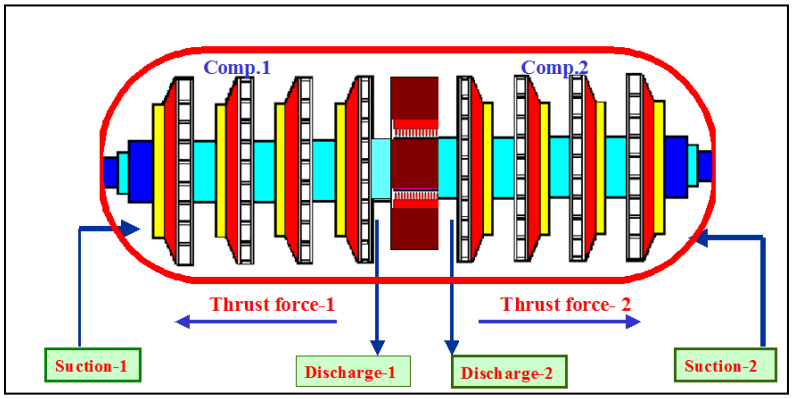

Figure 3—44 multistage-back to back rotor arrangement [3]

The rotor shaft end shall be designed to transmit the Maximum torque (T) provided by the driver which has direct relationship with Brake horsepower and speed thus the torque increases if the Brake horsepower (BHP) increased or speed (N) decreased [37]:

$$T = \frac{BHP}{N}\ x\ 63{,}025\ \frac{in-\text{lbs}-rpm}{H.P.} \qquad 3—13$$

Where: T = Torque (in-lbs); BHP = Brake horsepower; N = Speed RPM

On other hand of rotor shaft design maximum allowable shear stress of the shaft end shall be considered with limit between 12000 psi and 15000 psi, as p the below equation which shows the relationship of shaft shear stress with the torque and shaft diameter for that the thrust collar usually fixed at end of the shaft opposite the coupling however this position of shaft has lowest torque and shaft diameter is smallest.

$$Shaft\ sher\ stress = \frac{16T}{\pi\, D^3} \qquad 3—14$$

Where: T = Torque (in-lbs); D = Shaft end diameter.

3.4.1 Rotor Assembly

Rotor is a main part in the centrifugal compressor consists of a solid shaft, impellers, spacers (sleeves), thrust collar and balance piston. Normally there are two methods using to assembly the rotor components into the shaft; a thermal fit and hydraulic shrink fit process. Hydraulic fit method is mostly using for single stage rotor assembly / disassembly that because most of design need impeller disassembly for seal, the thermal fit method is using for all multistage rotor assembly which it is assembly with vertical position for ease of assembly and to reduce residual shaft stresses .[37]

However, before assembly the impellers into the balanced shaft there is different individual tests as per API 617should be performed on the each impellers:[13]

1. Balancing test; each impellers shall be balanced and the rustles shall be as per specification requirement unbalance Maximum acceptable 5 μ.
2. Penetrate test; each impellers shall be executed through penetrate test that to check for any cracks as shows in Figure 3—45.

Figure 3—45 Impeller Penetrate test, GE 2014

3. Over speed test; as shows in Figure 3—46 the impeller puts inside the over speed test bunker , than it runs with not less than 115% Max continuous speed at duration of minimum one minute as per API617,cluster 4.3.3.[13]

Figure 3—46 Impeller test bunker, GE 2014

4. Dimensional check; each impeller after over speed test should be checked for any deformation on the impeller bore or other critical dimension outside drawing tolerances.

Regardless of the method of rotor assembly the impeller shrink fit values range should be from 0.002–0.003 inches shrink per inch of shaft diameter, on other hand residual stress can deflects the rotor which it cans consequence big amount of rotor unbalance for that the rotor deflection (run-out) must be check and the changes should not more than 0.001–0.002 inches. [37]

3.4.2 Rotor Balance.

Any new design of rotating machinery has Major parts of the rotating element, such as the shaft, balancing drum and impellers, shall be individually dynamically balanced before assembly as complete rotor [13], than final rotor balance must be conducted that by adding or removing mass from a rotor thus that the unbalance-induced vibration falls below a maximum acceptable level [5] which mostly comes under two main standards, American Petroleum Institute API (617) and ISO 10439.

“During the mechanical running test of the machine, assembled with the balanced rotor, operating at its maximum continuous speed or at any other speed within the specified operating speed range, the peak-to-peak amplitude of unfiltered vibration in any plane, measured on the shaft adjacent and relative to each radial bearing, shall not exceed the following value or 25 mm (1 mil), whichever is less [13]”:

$$\boldsymbol{A} = \sqrt{\frac{\mathbf{12000}}{\boldsymbol{N}}} \qquad 3—15$$

Where,

A = amplitude of unfiltered vibration, in mm (mil) true peak-to-peak,

N = maximum continuous speed, in rpm.

However, to get the API rotor vibration average, Original Equipment Manufacturers (OEM) uses the following API regulation to verify the acceptable rotor unbalance rate:

$$Unbalance\ (oz - in) = \frac{4W}{N} \quad 3—16$$

Where,

W= Shaft weight in lbs (at journal bearing locations)

N= Rotor Speed (RPM)

3.4.3 External forces in to the rotor

Bently, 2002 [5] described with simplest way the three forces which are acting in the rotor within fluid film bearing envelop such as spring force (stiffness), damping force and perturbation force and it is nomenclature as F_S , F_D and F_P respectively .

3.4.3.1 Spring Force (stiffness): [5]

The effective spring stiffness, *(K)* is combination of series and parallel of various different sources of spring stiffness which is described as spring force vector, *(Fs):*

$$Fs = -Kr \qquad 3—17$$

As the spring stiffness *(K)* in the above equation is contains all spring stiffness contributions in the rotor system such as shaft, bearing spring stiffness, bearing support stiffness and foundation stiffness.

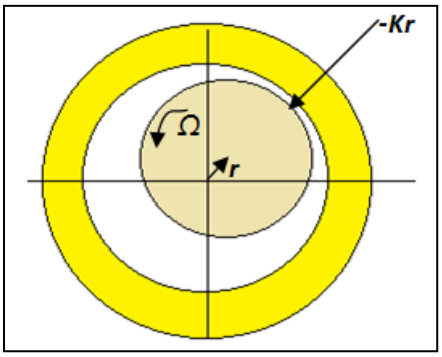

Figure 3—47 Bearing spring force always points in the opposite direction of r

There are two force components perform due to pressure wedge which is the main income of rotor support in Hydrodynamic Journal bearing, this forces are radial component , F_B and tangential component , F_T as shows in below equations and Figure 3—47:

$$FB = - KB\, r \qquad 3—18$$

Where F_B is relative to the displacement and the stiffness which it signs indicates in the opposite direction of r and K_B is the bearing spring stiffness.

$$FT = jD\lambda\Omega r \qquad 3—19$$

Where J indicates the direction of FT (tangential component) which is 90° leading to r in direction of rotation, Ω and D is the damping constant of the bearing, where λΩ is the proportional to the average fluid angular velocity of FT.

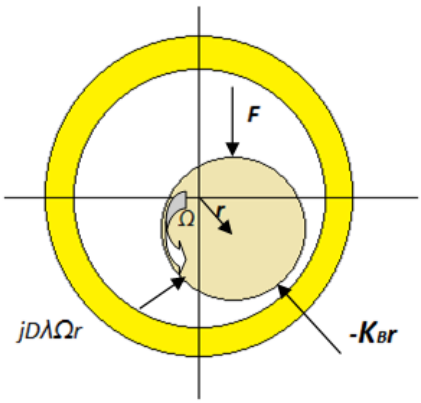

Figure 3—48 two force components behave like forces due to springs FB & FT

3.4.3.2 Damping Force: [5]

The damping force, F_D is a mixture of shearing of the fluid and pressure drag in the Journal bearing where this force is correlated of the rotor interfaces with fluid that surrounds it and the journal velocity.

$$FD = - D\dot{r} \qquad 3—20$$

Where F_D is damping force which comparatives to the damping constant, D and performs in the contradictory to the Velocity vector, $\dot{r}$ as shows in Figure 3—48.

In fact, the damping force is proportional with the velocity if the velocity is large then the damping force will be large for example within the rotor system if a nodal point is located inside fluid film bearing the small vibration at that position will formed a comparatively small damping force .

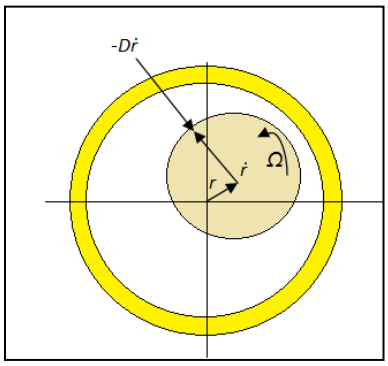

Figure 3—49 Damping force opposite the velocity vector ṙ

3.4.3.3 Perturbation Force: [5]

It is an external forces which disturb the rotor from it is equilibrium position however it can be dynamic force (e.g. change in the magnitude or direction or both) or it can be static force (static defections or change in rotor position or casing deformation and piping strain which leads to shift bearing supports or misalignment) , Figure 3—49 shows the rotor model which it was added small unbalance mass (heavy spot) to the rotor that to generate a comprehensive dynamic vibration reaction , the resulting perturbation force vector, (Fp) :

$$F_P = mr_u\omega^2 e^{j(\omega t+\delta)} \qquad 3—21$$

Where F_P is a nonsynchronous rotating unbalance force vector (ω) squares of the perturbation frequency at any time (t) it points radial outward in the direction given by (ωt + δ).

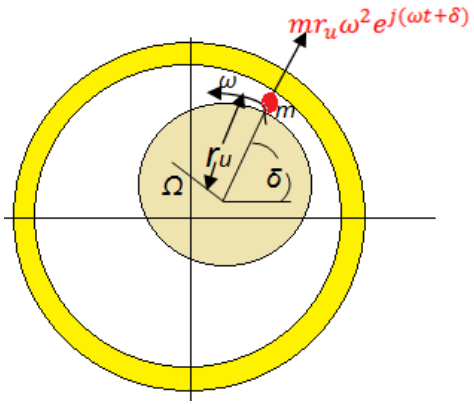

Figure 3—50 Perturbation force, Fp with small mass spot m

All forces which acting on the rotor Figure 3—50(free body diagram) applied by Newton's second low thus, all of them performing on a body is equal to the mass of the body times it acceleration:

$$Fs + FT + FD + FP = M\ddot{r} \qquad 3—22$$

Figure 3—51 shows the free body diagram, Where Fs is the spring stiffness force directs back toward the equilibrium position, FT points 90° from r in the direction of rotation, while FD is damping force which points in direction opposite to the instant velocity vector $\dot{r}$ and the rotating perturbation force FP shows at angular position δ the instant the keyphasor result take place.

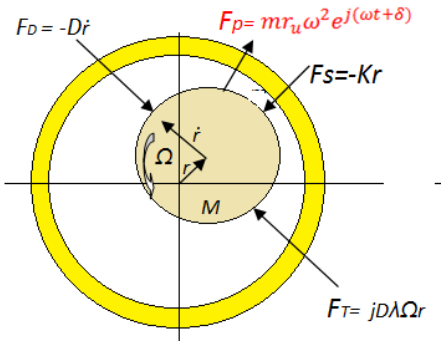

Figure 3—51 Free body diagram

So, the solution of equation (3-6) as below:

$$-K_r + jD\lambda\Omega r - D\dot{r} + mr_u\omega^2 e^{j(\omega t+\delta)} = M\ddot{r} \qquad 3—23$$

Thus, the differential equation of above equation as below:

$$M\ddot{r} + D\dot{r} + (K - jD\lambda\Omega)r = mr_u\omega^2 e^{j(\omega t+\delta)} \qquad 3—24$$

3.4.4 Effect of Rotor Assembly Techniques in Rotordynamic.

The initial design philosophy applied to rotating machinery on rotor analysis by Rankin in 1869 that he published the first calculation of shaft fundamental natural frequencies, his model consisted of a rigid mass whirling in a circular orbit with an elastic spring performing in the radial path however Rankin failed to exceed the first critical speed since he used Newton's second law wrongly in a rotating coordinated system [18]. In 1919, Jeffcott analysis showed the rotors could be operated beyond their first critical speeds with accurate balancing and by replaced the rigid rotor with more flexible models but in fact there were quite a lot of failures while operating at speeds above their first critical speeds [39]. However, Newkirk [38] investigated the failures of compressor which mostly appeared after the first critical speeds, this investigation conducted within General Electrical (GE) research Laboratory in 1924 and the results were the main cause due to whirl at speed above their first critical speed since the whirling rate equal to the first natural frequency where the rotor speed were increased more than its initial whirl speed consequences the whirl amplitude would increase which leads to rotor instability .Kimball (1924)[40] recommended to Newkirk the idea of the internal friction could be the cause of shaft whirling since he demonstrated that under the first critical speeds the internal frication would damp out the whirl motion whereas above the first critical speed it would continue the whirl .since then Kimball and Newkirk worked together and their conducted a lot of experiments on internal frication which they got a many of results such as the onset speed of whirling and the whirl amplitude is unaffected by the rotor balance , whirling is encountered only in the built-up rotors , whirling always occurs above the first critical speed and there is relationship between the unit foundation and whirl threshold speed thus if foundation damping increases the whirl threshold speed dramatically increase [41].

Gunter [42] worked to developing a linear rotordynamics model which in fact as an explanation of some of the experimental results of Newkirk and Kimball's. His model included the effects of bearing and foundation support flexibility and damping and its effect on the internal damping of the rotor. Also he showed on his model the internal friction as a cross-coupled force and the external damping stabilize the rotor bearing system that by increasing its threshold speed instability. However, there is an optimum damping which stabilizes the rotor. Finally, Gunter illustrated the required of external damping source to stabilize the rotor running above the critical speed in case of cross-coupling forces acts due to fluid-film thin pressurized oil films which support the rotor loads.

Walton, Martin and Lund [43] [44] investigated the effect of internal rotor friction through the experimental and theoretical research by using test rotor facility with axial spline and shrink (interference) fit joints. On this experiments, the internal friction model proposed as a system of internal moments rather than the cross coupling forces. They concluded from this study, both joints method cause rotor sub-synchronous and super-synchronous instability during the rotor first critical speed, however the comparison of data from both test joints showed that super-synchronous vibration amplitudes were generally larger for the shrink fit joint than for the axial spline joint. Also within their results the dry film lubrication in the axial joints causes the instability. Finally the main conclusion from this research was that the rotor balancing does not reduce the sub-synchronous.

Kimball [45] [46] explained on his experimental measurements of internal friction in different rotor materials property and both used with and without shrink fits. The Internal hysteresis in a material was assumed during rotor spin which will cause the shaft deflection sideways in the direction of forward whirl. He used sideways deflection of a loaded overhung shaft spin to measure the magnitude of internal frication force, he concluded from those measurements that the sideways deflection is sovereign of the spin velocity and the shrink fits because larger deflection of the shaft as compared to the case of no shrink fit on the shaft. Finally, these experiments demonstrated that shrink fits instead of

material internal hysteresis are much more imperative mechanism of the forward whirl instability.

Black [47] performed different internal friction models to investigating the effect of internal frictions on the stability of a flexible rotor supported on damped flexible bearings with no cross coupling such as coulomb friction , viscous friction and hysteresis friction . The model outcomes demonstrate that for the coulomb friction shows that the rotor-bearing system after passing the first critical speed becomes unstable since the condition of rotor relaxation strength parameter is greater than twice the external damping ratio. For the Viscous friction model shows the threshold speed instability which it is higher than the first critical speed and that the threshold speed is reliant on both external and internal damping resource of the system. Finally, the hysteretic friction model predicts a range of speeds (above the first critical speed) in which the rotor-bearing system becomes unstable but above that range the operation becomes stable. Black concluded from those models that the hysteretic friction and Coulomb friction are more realistic as compared with the viscous friction model. On other hand, Black conducted other analysis within same experimental which shows the effect of bearing stiffness asymmetry on the rotor and the results where the bearing stiffness asymmetry promotes the rotor stability while the damping asymmetry.

Ehrich [48] analyzed internal friction stresses which acts at a 90 degree angle to the shaft deflection plane and that their magnitude is comparative to the rate of change of strain of the shaft strand. However the model shows the ratio of the threshold speed of instability to the first critical speed depends upon the amount of internal and external damping of the rotor. Also on his analysis expects that the instability above multiple critical speeds and proves that it is not necessarily the first mode of the rotor-bearing system which is always excited in an unstable whirl caused by the internal friction other than it cans be any mode higher than the first mode that can be excited.

Vance and Yang [49] studied through an experimental the effect of shrink fits in the rotor stability by using a test rig which is consisted of two disk steel rotor with an aluminium sleeve having two shrink fit interfaces. This test conducted on the transient state (start-up/shutdown) and steady state. The results showed similar of Balck's model which indicated the coulomb frication which the critical speed is crossed forward whirl instability. Also during the transient state was observed instability on the speed ranges. At the end , they utilized a heat gun in the steady state to heat the aluminium sleeve above the first critical speed and the observation was violent instability of the rotor that because the loosens of the shrink fit interface due to possible slipping between the disks and the sleeve which was caused by the thermal expansion of the aluminium .

Mir [50] preformed an experiment on a single disk rotor with an adjustable interference fit mechanism. The experimental results demonstrated both Coulomb and hysteretic damping due to interference fit in the rotor and the amplitude of rotor excitation. Also it showed that logarithmic decrement of the time traces of rotor vibrations decreased by increasing the tightness of the fit, however the conclusion of all that the hysteresis damping coefficients vary with the rotor speed.

Srinivasan [51] preformed free-free analysis on a single disk rotor with interference fit joints through his experiments he analysed the time traces of the logarithmic decays and the equivalent the rotor damping coefficients for internal friction that by using XLRTCTM software to modelled it and as results the instability threshold speed through the converted experimental damping values .

Murphy [52] preformed a numerical analysis to study the effect of cross-coupled stiffness and damping coefficients as well as direct stiffness coefficients on the stability of a simple rigid rotor model which is mounted in horizontal and vertical directions within a linear bearing. This analysis resulted that the direct stiffness asymmetry much more stabilizes the rotor while the cross-coupled stiffness cause instability due to that the they are equal and opposite in sign and exceed certain range of values.

Jafri [41] worked on his Dissertation presents a theoretical and experimental to investigate the effect of variance shrink and interference fit values on rotor system stability. The test rig tests consists of two different rotor setups that are studied are a single-disk rotor mounted on a uniform diameter shaft as shows in Figure 3—52 and a two-disk rotor with an aluminium sleeve shrink fitted to it at the outer surface of the two disks as shows in Figure 3—53. On his experimental he showed clearly the rotor instability due to shrink fit slippage that it has a sub-synchronous vibration which appeared at the first natural frequency of the rotor bearing system. The rotor instability destroyed completely the test rig as shows in Figure 3—54 that to shows and approves the potentially dangerous of vibrations to the safe operation of rotating machines.

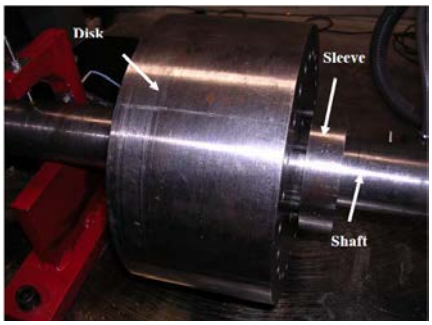

Figure 3—52 Close-up view of a single-disk rotor bearing system tested at the Turbomachinery [41]

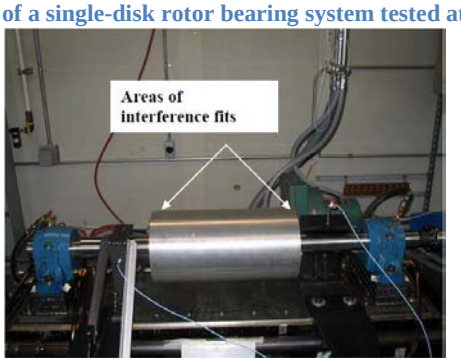

Figure 3—53 Two-disk rotor installed on the ball bearings at the Turbomachinery Laboratory [41]

Figure 3—54 the two-disk rotor with an aluminum sleeve shrink fitted destroyed [41]

Section Four

4 Rotordynamics numerical analysis

4.1 Section Overview

This section describes the one selected case studies and it is corresponding numerical analysis. Both lateral and torsional analyses were discussed in details considering varying operational and design factors, Moreover the numerical analysis were used to study the effect of torsional vibration and it appeared as lateral vibration during MCOS and on the pinion gear. The experimental study provides some vibration data mainly from system 1 Bently Nevada for two different rotor configurations where the effect of seals, mounting methodologies and bearings are studied.

The results include Undamped Critical Speeds (UCS), damped critical speed and forced response analysis. Also the analysis explore the factors affecting rotor instability and their effect on rotordynamics characteristics

4.2 Case Study

4.2.1 Introduction:

The case study covers rotordynamic analytical study and root cause analysis of high vibration amplitude issues of a 27 MW compressor trains installed in one of the depletion compression plants in Oman. The study will be aided with actual data taken from field and also from records of the Factory Acceptance Tests performed for these compressors. At the end of this study a thesis report will be issued. Thesis shall describe in details the issue and the analysis methodology and procedures, conclude final results and provide recommendations to the engineering team in PDO.

4.2.2 General arrangement of the SRDC1 depletion compressor train:

SRDC1(Sieh Rawl Depletion Compressor) trains are 4 identical compressors installed at Oman gas Central Processing Plant (CPP) to take care of the continuously depleting gas fields hence to sustain the productivity of gas and meet the continuous demand.

Each compressor train consists of a single stage Centrifugal compressor set driven by synchronous motor through a Variable Frequency Drive System (VFD) and a fixed speed ratio gearbox mounted on common base frame appropriate to the process requirement specified and complete with the following, refer to Figure 4—1,Figure 4—2,Figure 4—3 and Figure 4—4:

a) Fixed ratio speed increasing, double helical, parallel shaft, gearbox unit.
b) Dry gas seal system comprising of two dry gas seal cartridges, one Seal Gas Instrument Panel and one Seal Gas conditioning skid per train including the strainers, filters, valves, heaters, etc. and related instruments as specified in the equipment Data Sheets.
c) Separation air system for bearing with associated piping, control valves, valves and instruments.
d) Low-speed coupling as installed between the motor driver and the fixed speed ratio gearbox.
e) High-speed coupling installed between the compressor and fixed ratio gearbox.
f) Common base plate for the compressor-gear-motor train.

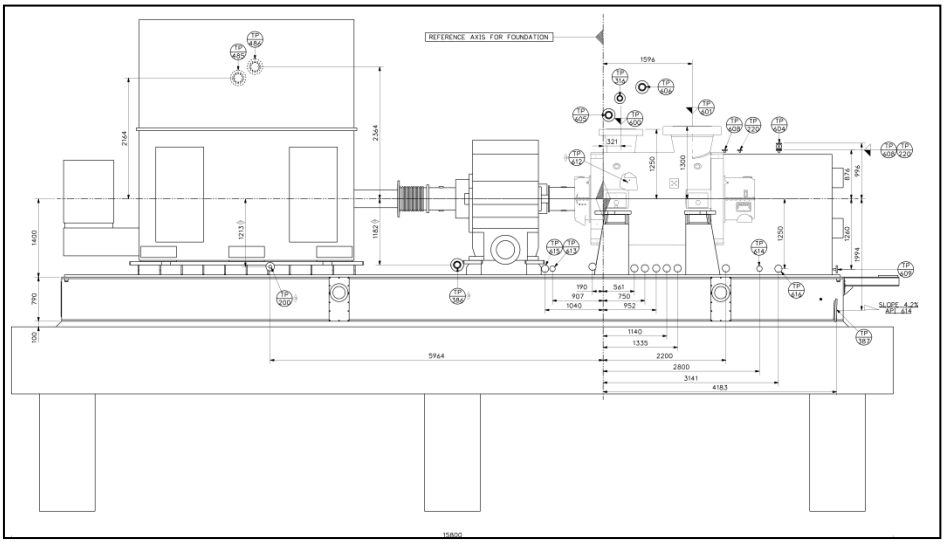

Figure 4—1 Side View of SRDC1 Compressor Train

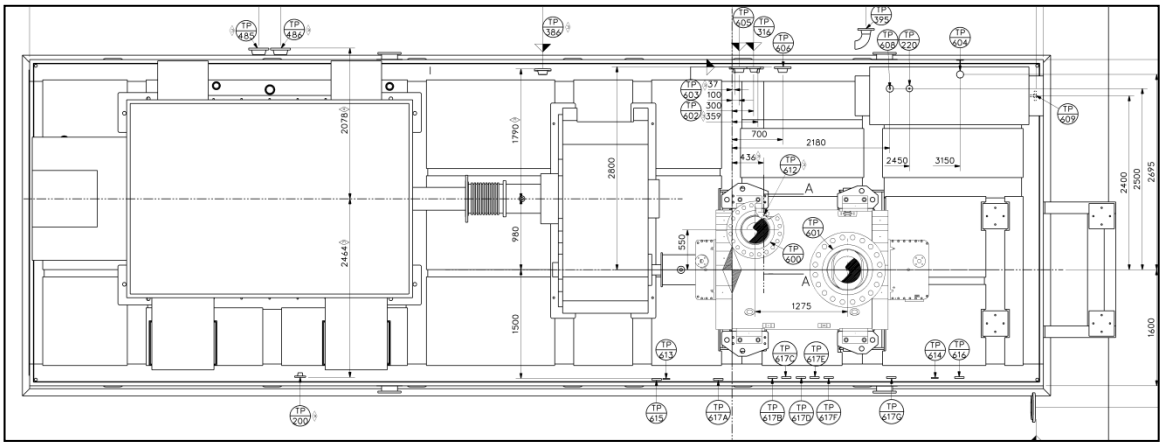

Figure 4—2 Plan View of SRDC1 Compressor Train

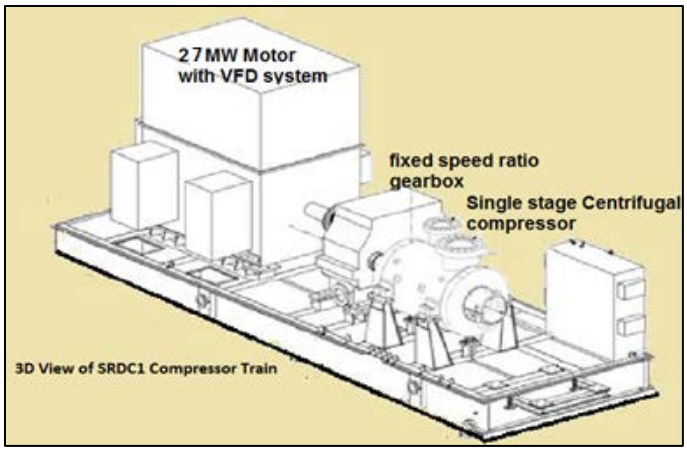

Figure 4—3 3D View of SRDC1 Compressor Train

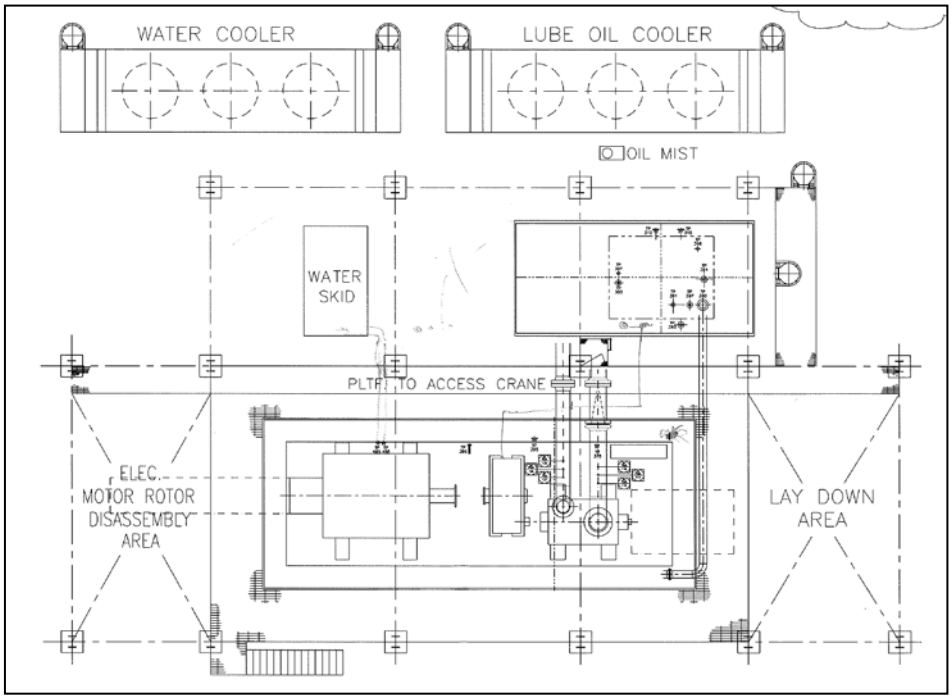

Figure 4—4 GA of Compressor Train and Auxilaries (L.O.conole, L.O. cooler, motor-water recooler, cooling water circulation skid)

4.2.3 Process schematic of the SRDC1 train:

Sieh Rawl Depletion Compression plant consists of 4 identical centrifugal compressors, each one is designed at rated flow of 12.25 MMSCMD of wet gas with suction pressure varying between 35 bara to 65 bara and discharge pressure of 100 bara.

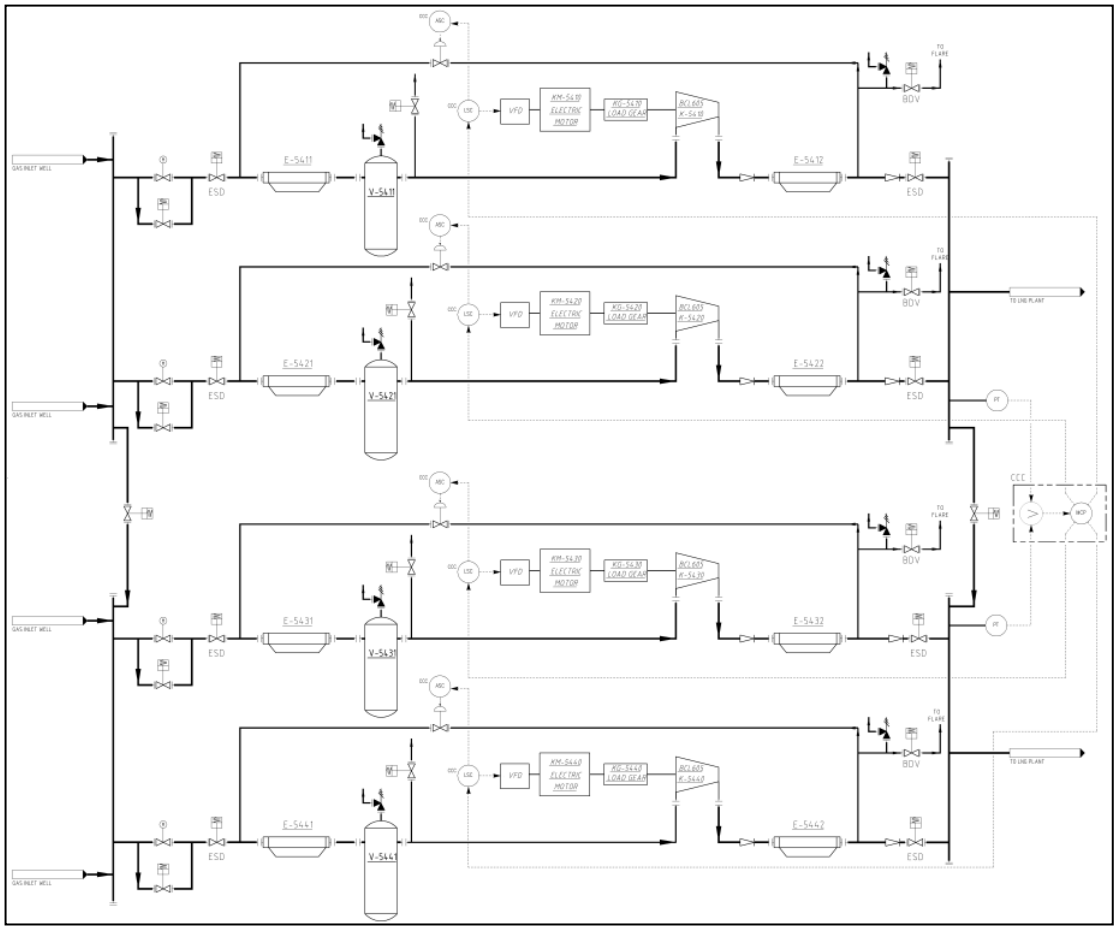

Figure 4—5 Process schematic of the SRDC1 depletion compressor trains

Each compression train is aided with process suction and discharge coolers, suction knock out drum, anti-surge and capacity control valve and hot-gas bypass valve (see Figure 4—5).

Figure 4—6 shows the process schematic of a single SRDC1 depletion compressor, The process gas is compressed from 35.0 Bar abs (3500 kPa abs) to 97.9 Bar abs (9790 ka abs) by a compression stage utilizing a centrifugal compressor of type BCL 605/N. An anti-surge valve (54UCV 124) is installed in the gas suction line. A strainer and a separator are provided in the gas suction line. Coolers are provided in the gas suction/ discharge lines. Instruments and separators are provided on the suction/discharge lines to take the pressure, the temperature and the gas flow. The capacity at suction of compressor shall always be higher than the capacity at which the pressure and flow pulsation phenomenon

begins (surge), as indicated on operation curves. The alternative stresses which the compressor rotor undergoes under such an abnormal operation, may seriously damage bearings and seals of compressor.

Surging effect occurs when at determined revolutions per minute (R.P.M.) the compressor capacity at suction falls below a certain limit value.

In order to avoid surge conditions the compressor unit is equipped with one automatic anti-surge control system that keeps the capacity at suction above the critical value at which surge takes place. If surging problems will occur during start-up or shut-down of the compressor unit, or during mainly changes of compressor unit load, the anti-surge system operates recycling a part of the discharge gas line into the suction gas line. The anti-surge valve that operates the recycling of the process gas is open or closed by means of air pressure signals becoming, through solenoid valve, from an electric to pneumatic signal transducer which receives inputs from a flow controller which receives inputs of gas flow temperature and pressure of the suction line and gas pressure of the discharge line. In case of trip the solenoid valve will interrupt the gas pressure to the anti-surge valve so that this will be completely open.

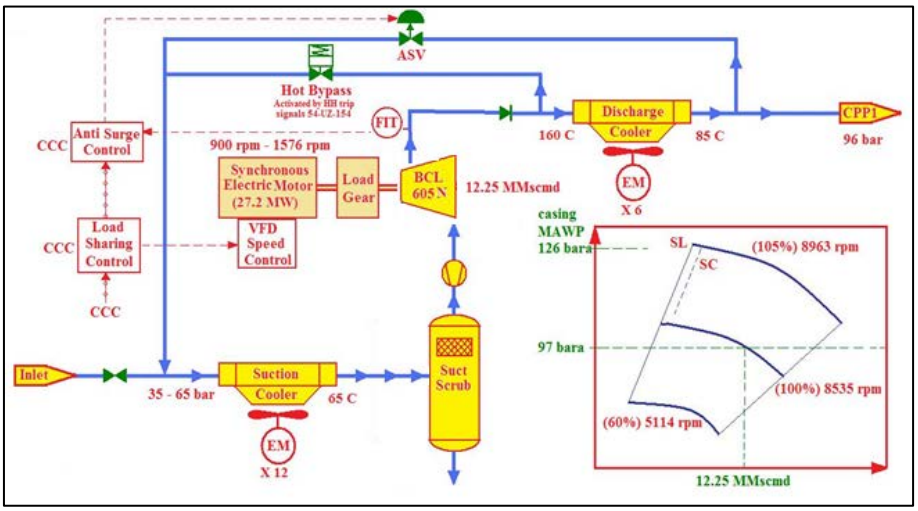

Figure 4—6 Process schematic of a single SRDC1 depletion compressor train

4.2.4 Overview of Compressor Train

The Saih Rawl Depletion compressor train, illustrated in Figure 4—7, is driven by a Variable Speed Drive (VSD) electrical motor which is connected to a Gear Box which in turn drives a centrifugal compressor.

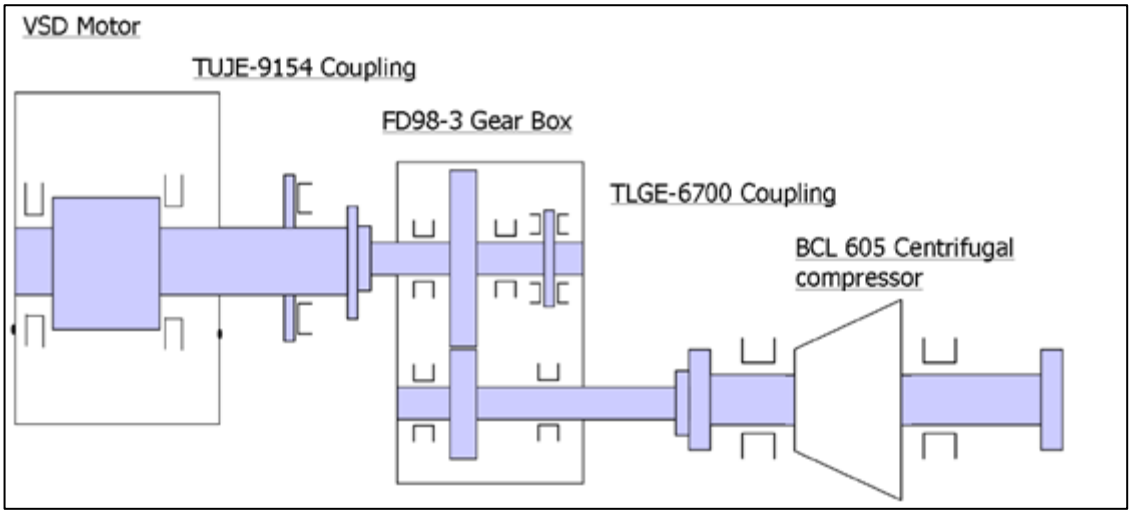

Figure 4—7 SRDC1 compressor train

4.2.5 The Technical Data of Compressor Train

VSD Motor

Type Variable Speed Drive
Speed range: 750 - 1575 rpm
Nominal speed: 1500 rpm
1st lateral critical speed (predicted)
(at bearing foundation stiffness 10^{11} Nm) : 1900 cpm
2nd lateral critical speed (predicted)
(at bearing foundation stiffness 10^{11} Nm): 3402 cpm
Nominal absorbed power 27.23 MW

LSS Coupling

Type: TUJE-9154
Torsional stiffness: 2:0 ¢ 10^{8} Nm/rad

FD98-3 Gear box

Type: Single stage, double helical
Rated input speed: 1495 rpm

Rated output speed: 8508 rpm
Gear ratio: 5.682

HSS Coupling

Type: TLGE-6700
Torsional stiffness: 1:2 ¢ 10_8 Nm/rad3

BCL 605 Centrifugal Compressor

Type: Straight through
Inlet pressure: 35 Bara
Discharge pressure: 97.9 Bara
Journal bearings: Tilting Pad
Thrust bearing: Flooded
Rated speed: 8535 rpm
Max. Continuous speed: 8962 rpm (105 %)
Min. Governor Speed: 5114 rpm
Trip speed: 9410 rpm

Lateral Critical Speeds

First lateral critical speed (predicted): 3750 cpm (Minimum support stiffness)
3950 cpm (Normal support stiffness)
4200 cpm (Maximum support stiffness)

Torsional Critical Speeds

First torsional critical speed (predicted): 1757 cpm
Second torsional critical speed (predicted): 3763 cpm
Third torsional critical speed (predicted): 13782 cpm

4.2.6 Compressor rotor design:

The rotor arrangement is shown in Figure 4—8 which it is straight through with five impellers enclosed type hot shrink fixed, balance piston position on last stage (discharge side) with a Abradable labyrinth, inter-stage labyrinth with solid teeth grooved, Journal bearings with five tilting pad with load between pad (LBP) configuration is used with 60% pivot offset, six pad on Double Acting self-Equalizing thrust bearing.

Compressor rated speed is approximately 7893 RPM while the Maximum Continuous Speed (MCS) is around 8962 RPM, the first lateral critical speed is recorded at 4100 rpm and second critical speed naturally damped (meeting API criteria i.e. AF<2.5), the first torsional critical speed at 1763 rpm and second/third at 3764 and 13823 respectively. The compressor train overall pressure ratio is 54.

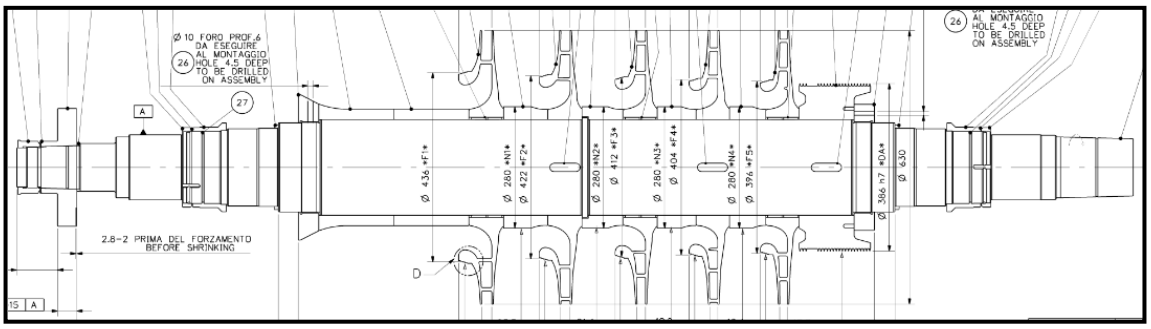

Figure 4—8 SRDC1 Rotor overviews

4.2.7 High-Speed, Parallel Shaft Gear Unit

The gearbox is designed as single stage assembly between Motor and compressor, parallel shaft gears all gearings are manufactured from high alloy steels, hardened and ground.

The gear box is shown in Figure 4—9 which it is consist of pull gear (low speed) with 165 teeth and pinion gear (high speed) with 29 teeth, the speed rate of each rotor is 1495 rpm and 8506 rpm respectively. Both gear rotors are holding by 4 tilting pad LBP bearings two numbers in each rotor and one thrust bearing (tilting pad) is located on NDE side of pull gear.

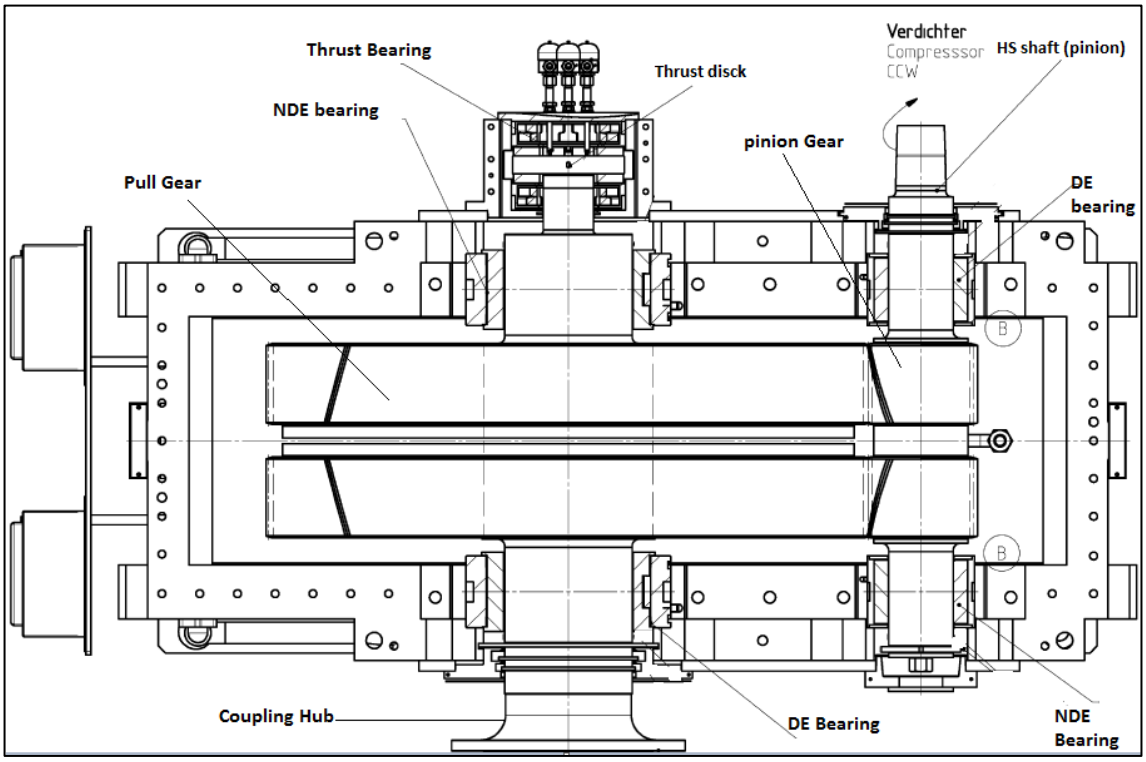

Figure 4—9 SRDC1_GearBox

4.2.8 Description and Field Observation:

All four identical centrifugal compressors (K-5410-KC, K-5420-KC, K-5430-KC and K-5440-KC) have been commissioned in May 2010 and since then there were many identical high vibration amplitude issues which consequences the compressor tripped, this issues were investigated numerically and experimentally in this thesis, the first phenomenon was high levels of rotor vibration while traversing its first critical speed during hot start only and the second phenomenon was sadden high vibration appearing on gearbox pinion bearing side during MOCS .

Figure 4—10 & Figure 4—11 show the filed trends of all four compressors indicates the similarity of behaviour of vibration amplitudes during compressor cold-start and hot-start conditions for that compressor K-5430 was selected to investigate about those issues throughout the numerical analysis.

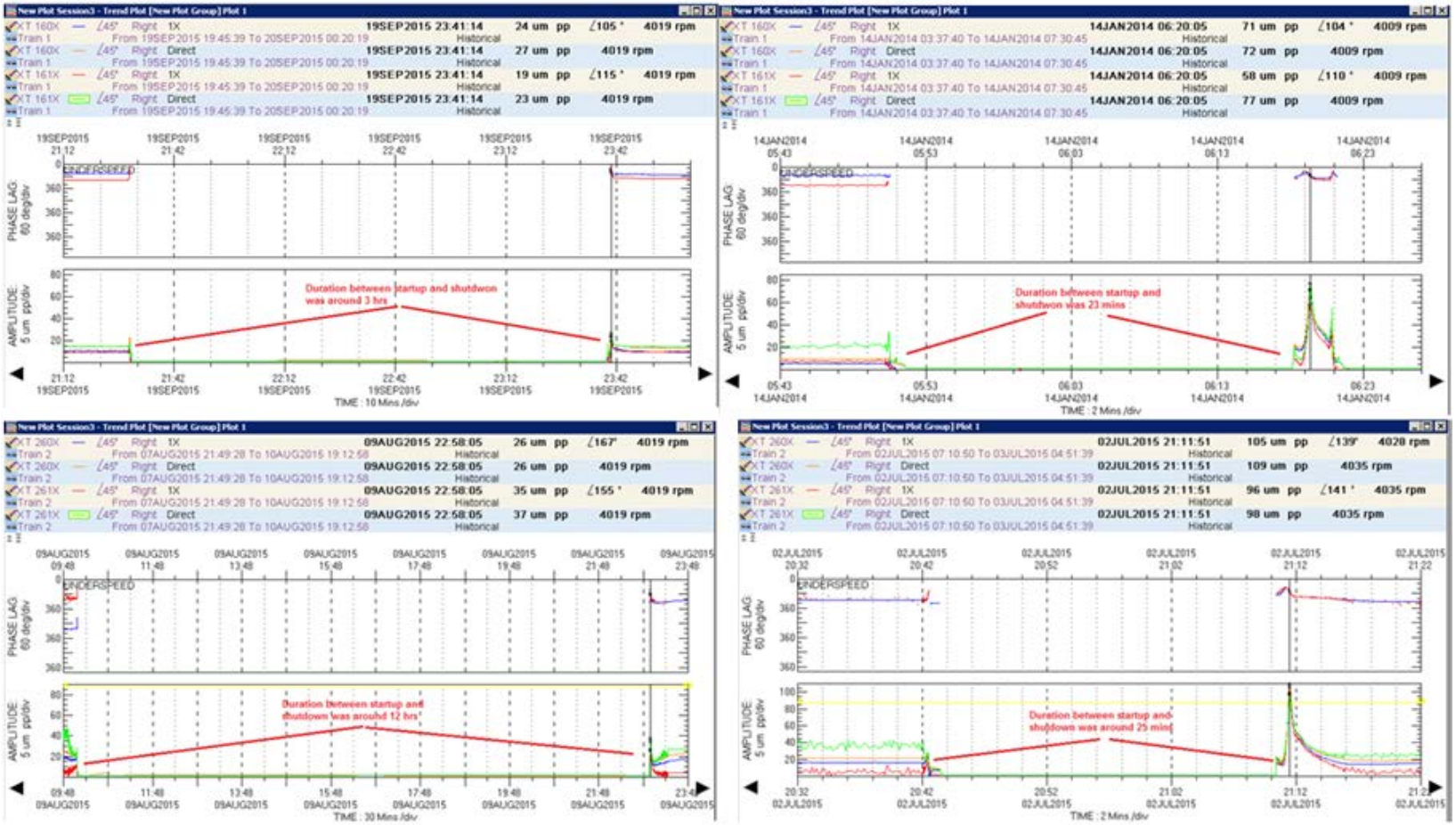

Figure 4—10 Top trends for K5410 (right trend during hot start ; left trend during cold start), bottom trends for K5420 (right trend during hot start ; left trend during cold start).

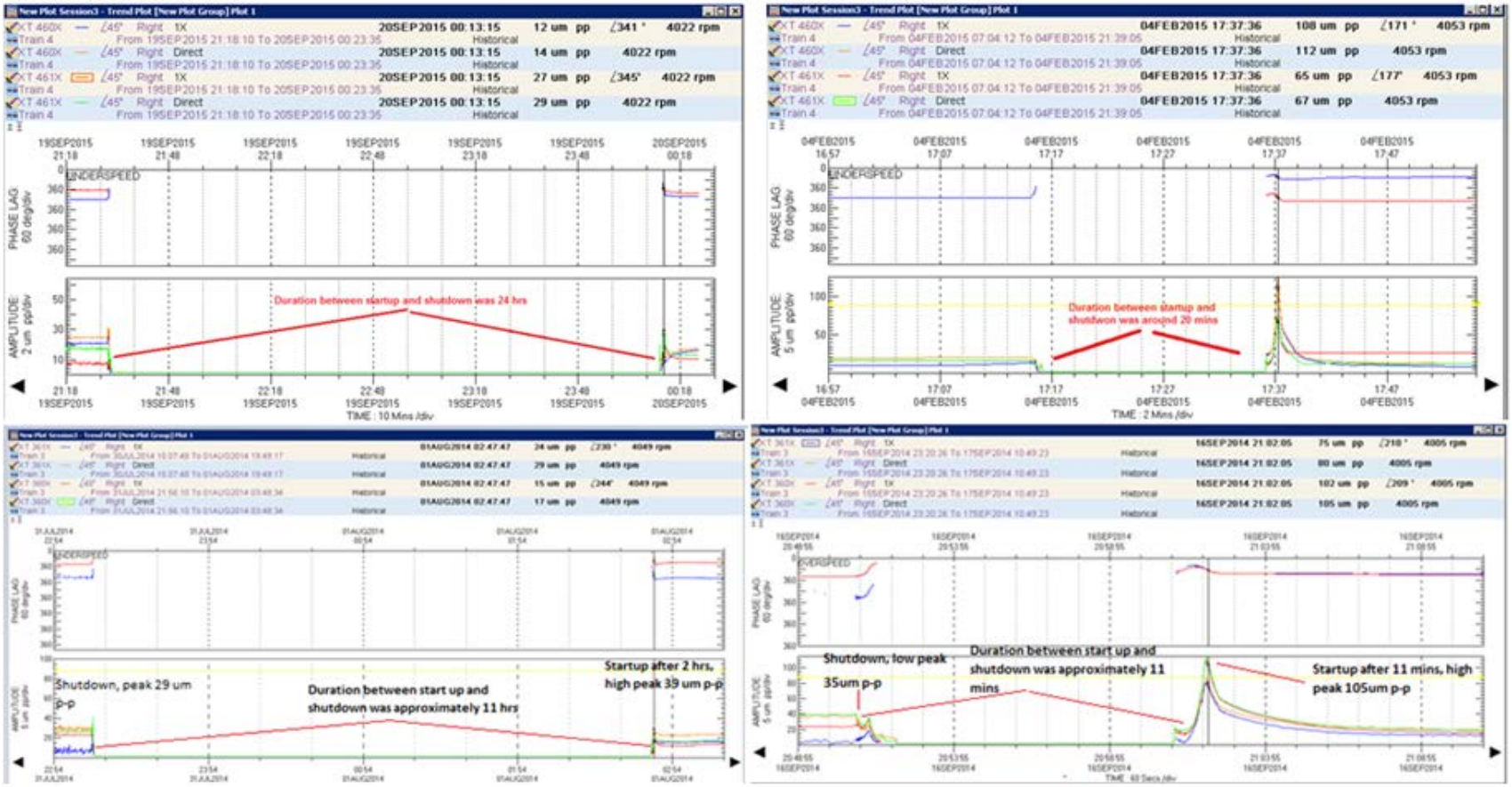

Figure 4—11Top trends for K5440 (right trend during hot start;left trend during cold start), bottom trends for K5430 (right trend during hot start ; left trend during cold start).

Figure 4—12 shows vibration trends of second phenomena which high vibration was gradually appearing on gearbox pinion bearing side of SRDC1 compressors during operating speed, each compressor has slightly difference speed.

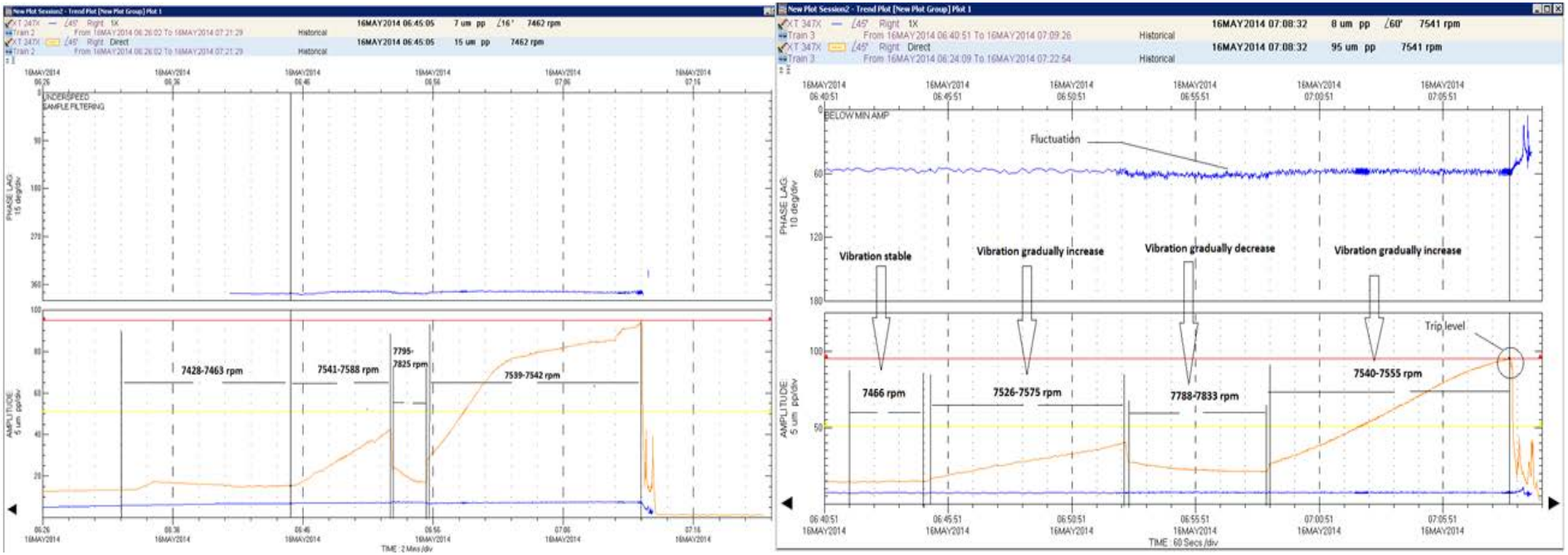

Figure 4—12 vibration trends of second phenomena

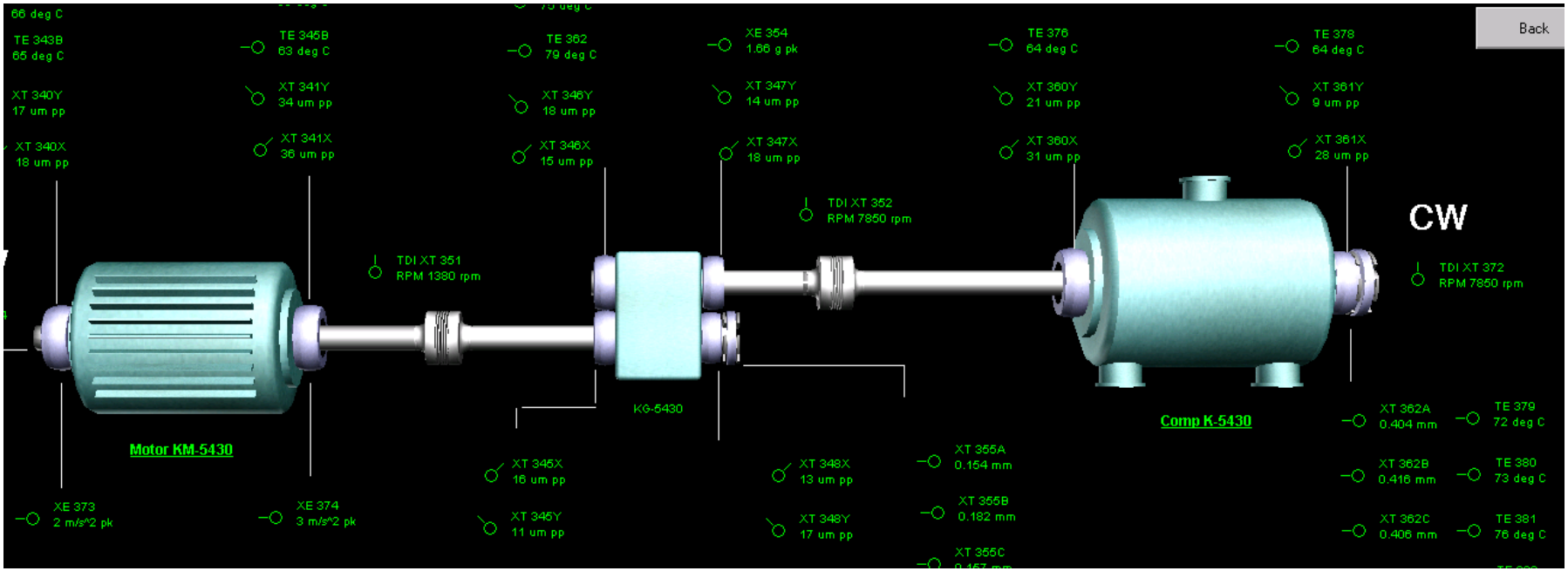

Figure 4—13 layout train from System 1

4.2.8.1 Case-1: Field Observation on variance and high levels vibration amplitude phenomena of compressor rotor while traversing its first critical speed:

Since commissioning in May 2010, the centrifugal compressor (gas compression unit K-5430-KC operated for almost 5 years with variance vibration amplitude phenomena at the first critical speed, the variance in the vibration amplitude was quite evident and in some cases a unit shutdown was triggered particularly at some start-up events.

The bar chart shown in Figure 4—14 illustrate the variance in the vibration amplitude within seven start-up events. Vibration amplitude Units are measured in um pk. In terms of cases variance, all seven start-up cases (vibration amplitude at 1st critical speed) were not constant and also the difference between vibration amplitude between DE bearing and NDE bearing were observed hence the DE bearing was higher by almost 20 % than the NDE bearing.)

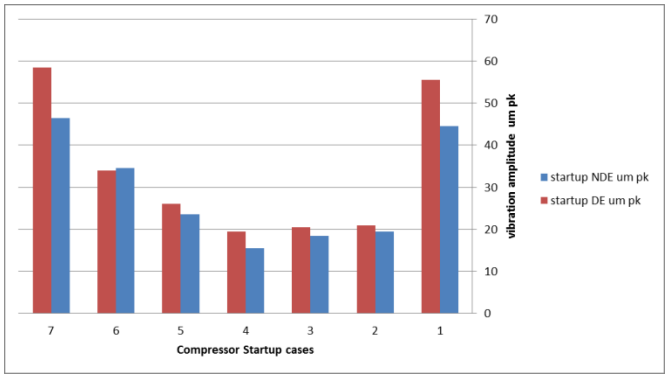

Figure 4—14 vibration amplitude at 1st critical speed during startup

The second bar chart, Figure 4—15 demonstrates less variance in terms of the seven shutdown cases as the vibration amplitudes almost closer from each other and the difference between vibration amplitude at DE bearing and NDE bearing were observed hence the DE bearing was higher by almost 40 % than the NDE bearing.

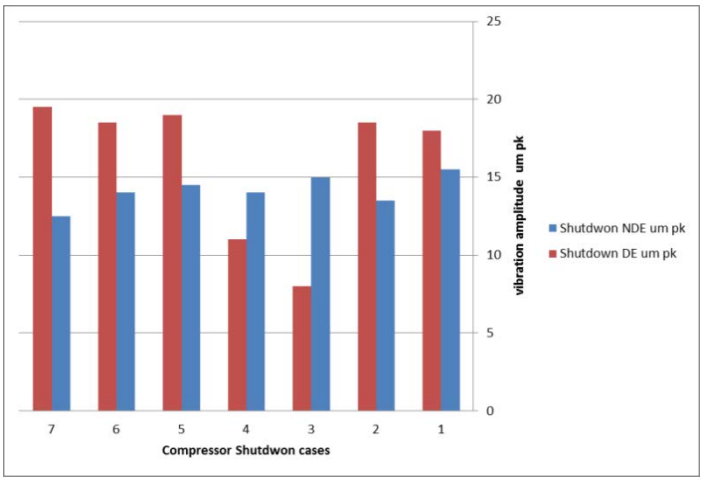

Figure 4—15 vibration amplitude at 1st critical speed during shutdown

Figure 4—16 show the comparison between the above two bar charts of the seven cases of each startup and shutdown in terms of DE bearing vibrations amplitudes at 1st critical speed. The DE bearing was selected because it has the highest values in both cases (startup/shutdown).Overall observation, in all cases the vibration amplitudes during startup was higher than that during shutdown. In terms of startup events, the amplitude in case one and case two were extremely high 120 um p-p and 119 um p-p respectively and case 6 was almost half value of them . On other side the other startup cases almost within same range values of vibration amplitude (40 um p-p to 50 um p-p). However all the shutdown cases were within acceptable vibration amplitudes in terms of variance and values.

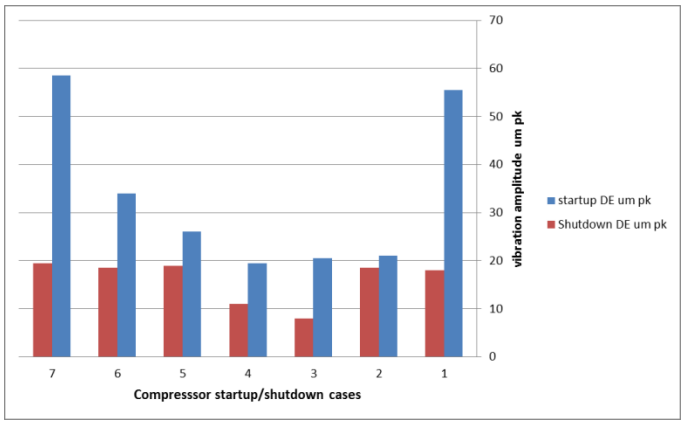

Figure 4—16 comparing between the vibrations 1st critical speed during startup/shutdown

The first event is indicated in Figure 4—17 which has been taken from Bentley Nevada system 1 vibration monitoring software, in this trend plot both startup

and shutdown events are shown related to K-5430-kc centrifugal compressor. The trend consists of vibration signal (amplitude um p-p) of the DE bearing (XT-360X) and NDE bearing(XT-361X) , different observations are observed from this trend due to the fact that the difference between the start-up and shutdown events is 20 minutes only which makes it an important information in comparing both events from a vibration characteristics perspective. One of the most important phenomenon in rotordynamics is the rotor critical speed and in this trend plot the critical speed can be seen while ramping up and coasting down. From Figure 4—17 the first observation is the 1st critical speed at shutdown was much lesser than start-up as the vibration amplitude was around 40 um p-p and 119 um p-p respectively, second observation is the vibration amplitude value of the DE bearing was more than NDE bearing side.

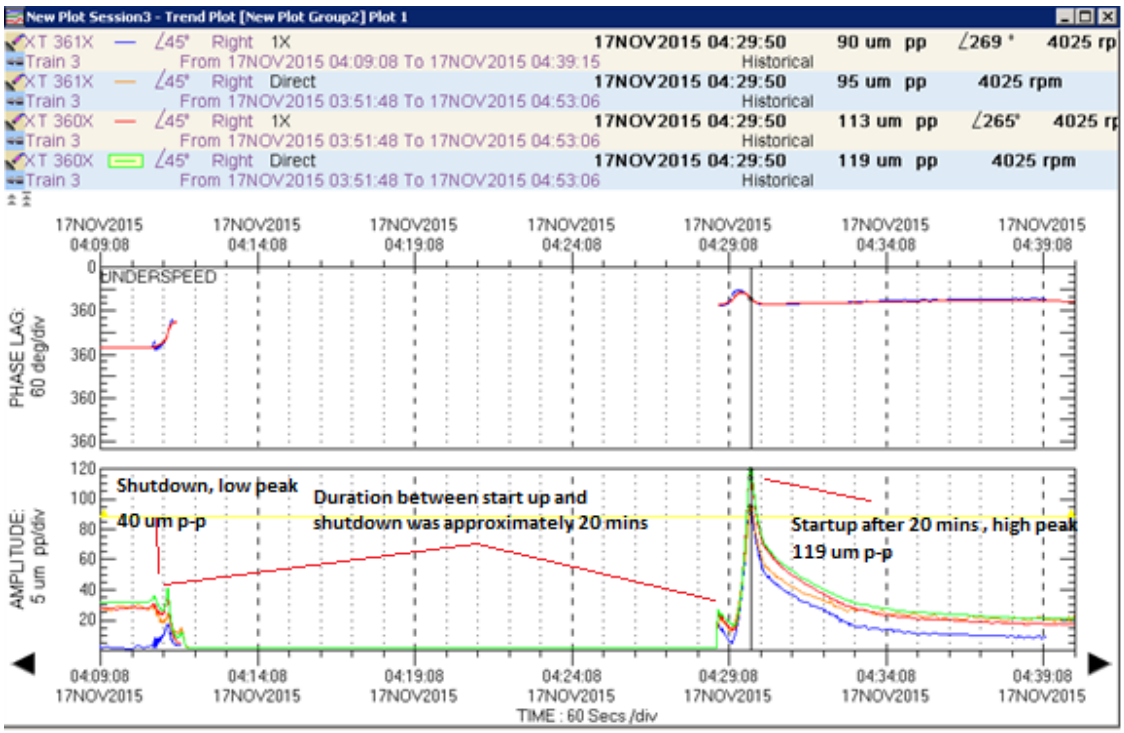

Figure 4—17 First events trend plot

On the same first event the vibration amplitudes were taken and summarized in Table-1 which is clearly indicating the higher amplitude on DE direct signal at 1st critical speed(4072 rpm) during compressor start-up (59.5 um pk) . On the other hand other vibration amplitudes on the MCOS and Low speed were almost within close amplitude values if compared between startup and shut-

down at an average of 11 um pk in MCOS and 7 um pk in Low speed. The amplitude value in MCOS indicates a good compressor rotor balancing as there was no much change between startup and shutdown, also the amplitude values in low speed indicates a low um out values.

Table2 first event higher amplitude on DE direct signal at 1st critical speed during compressor start-up

	SHUTDOWN RESPONE			**Time between shut/start**	**STARTUP RESPONE**		
Event one	LOW SPEED (1800 rpm)	N1 (38950 rpm)	MCOS (7889 rpm)		LOW SPEED (1800 rpm)	N1 (4072rpm)	MCOS (6883rpm)
DE um pk (1X)	3.5	17.5	14	20 mins	8.0	**55.5**	9.0
DE um pk (direct)	5.0	19.5	16.0		9.5	**59.5**	11.5
NDE um pk (1X)	2.0	8.5	1.5		3.5	**44.0**	4.5
NDE um pk (direct)	6.0	12.5	13.5		7.5	**46.5**	11.5

Figure 4—18 shows the second event which has been taken within the same compressor (K-5430-kc) to indicate the difference between start-up and shutdown within 11 minutes which, the shows similar observation such where the 1st critical speed at shutdown was much lesser than start-up as the vibration amplitude was around 35 um p-p and 105 um p-p respectively, second observation is the vibration amplitude value of the DE bearing was more than NDE bearing side by almost 5 um. Table-2 summarizes the trend plot shown in Figure 4—18 which is also clearly indicating higher amplitude on DE direct signal at the1st critical speed (4005 rpm) during compressor start-up (54 um pk) and the amplitudes on the MCOS and Low speed were almost within close amplitude values if compared between startup and shut-down at an average of 10 um pk in MCOS and 6 um pk in Low speed.

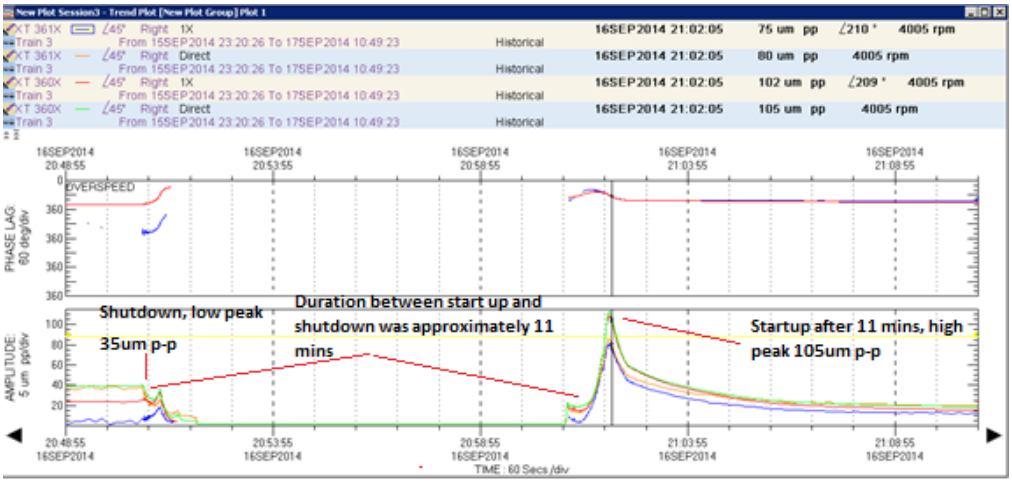

Figure 4—18 Second events trend plot

Table-3 second event of higher amplitude on DE/NDE at 1st critical speed during start-up

	SHUTDOWN RESPONE			Time between shut/start	STARTUP RESPONE		
Event two	LOW SPEED (1800 rpm)	N1 (3925 rpm)	MCOS (7466 rpm)		LOW SPEED (1800 rpm)	N1 (4005 rpm)	MCOS (7117rpm)
DE um pk (1X)	3.0	16.5	8.5	11 mins	5.0	54.0	11.0
DE um pk (direct)	4.5	18.0	20.5		10.0	55.5	13.5
NDE um pk (1X)	3.0	11.5	1.0		2.0	37.5	2.0
NDE um pk (direct)	6.0	15.5	20.0		6.5	44.5	14.5

The observation of the third and fourth events are shown in Figure 4—14 and Figure 4—19 with theirs results (vibrations amplitude) were recorded in table-3 and table-4 respectively. Both events were selected within long period between shutdown and startup (11 hours and 2 hours, respectively). Observation, the results of 3rd and 4th events were extremely different from the first and second events in terms of vibration amplitude during start-up where the values indicate vibration amplitude of 39 um p-p. Hence this vibration amplitude was observed while ramping up and coasting down of both events. The vibration amplitude at MOCS and Low speed of 3rd and 4th events were almost closer to previous events which provides another sign of good balancing and good rotor concentricity.

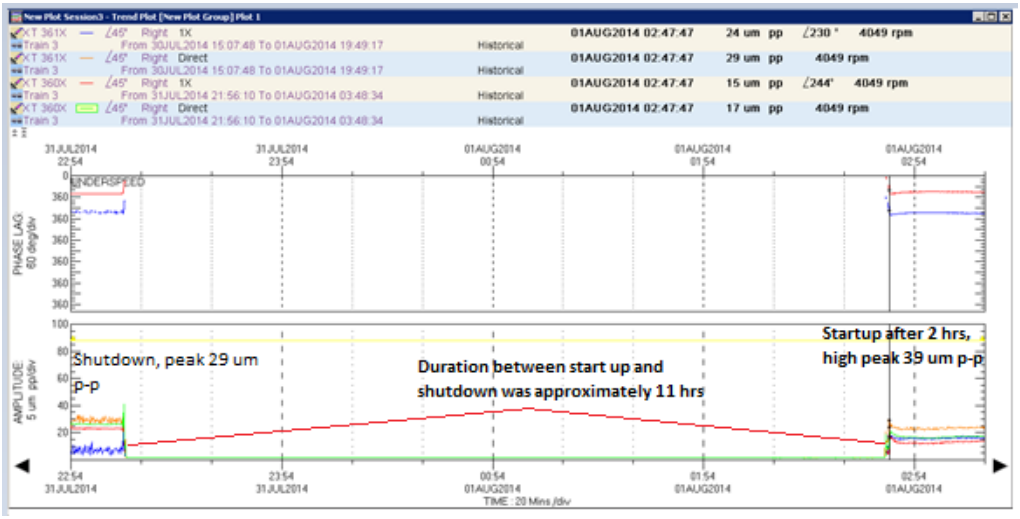

Figure 4—19 third events trend plot

4 Table- Third event low amplitude on DE/NDE at 1st critical speed during start-up

	SHUTDOWN RESPONE			Time between shut/start	STARTUP RESPONE		
Event three	LOW SPEED (1800 rpm)	N1 (3893 rpm)	MCOS (6953 rpm)		LOW SPEED (1800 rpm)	N1 (4045 rpm)	MCOS (5163rpm)
DE um pk (1X)	2.5	10.0	8.5	11 hrs	4.0	17.5	9.5
DE um pk (direct)	4.5	11.0	10.0		5.5	19.5	11.5
NDE um pk (1X)	2.0	11.5	7.5		2.0	11.5	4.5
NDE um pk (direct)	6.0	14.0	11.0		6.5	15.5	13.0

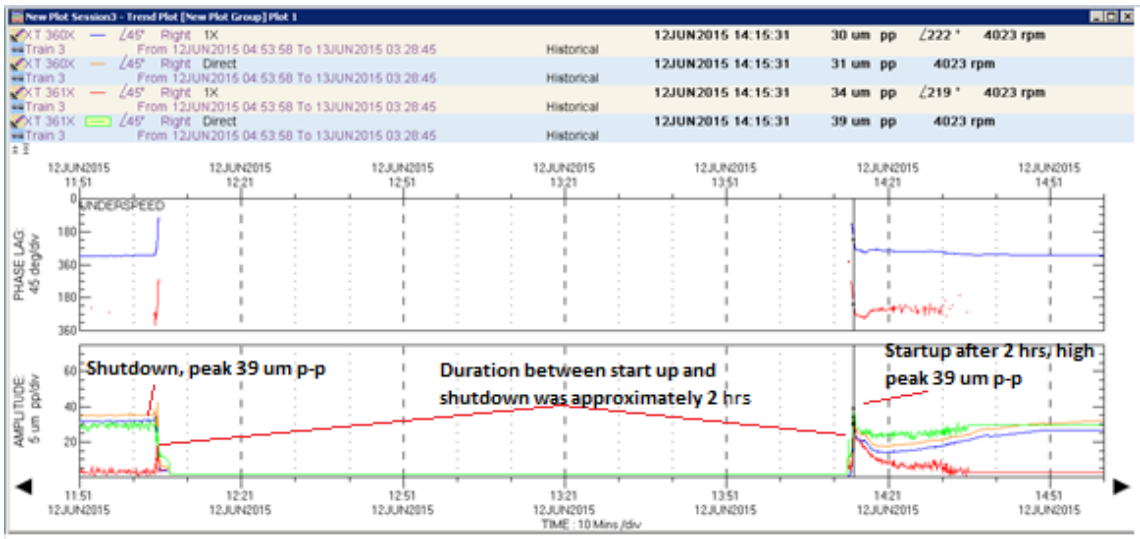

Figure 4—20 Fourth events trend plot

Table 5 fourth event low amplitude on DE/NDE at 1st critical speed during start-up

	SHUTDOWN RESPONE			Time between shut/start	STARTUP RESPONE		
Event four	LOW SPEED (1800 rpm)	N1 (3838 rpm)	MCOS (7483 rpm)		LOW SPEED (1800 rpm)	N1 (4023 rpm)	MCOS (4748rpm)
DE um pk (1X)	3.5	19	16.5	2 hrs	2.0	15	10.5
DE um pk (direct)	5.0	20	18		30	15.5	12
NDE um pk (1X)	2.0	10.5	1.5		2.5	17	2.0
NDE um pk (direct)	6	13.5	15.0		6	19.5	15.0

The high vibration amplitude (>100 um p-p) and normal vibration amplitude (< 39 um p-p) phenomena's which were observed from the previous evidences were investigated in detail through Bentley Nevada system 1 vibration monitoring software to understand the variance between them. Figure 4—21 shows bode plot of both scenarios as the right plot has an amplitude of 30 um p-p which is similar as FAT Acceptance Test result (see Figure 4—43) and the left plot indicates high amplitude of 120 um p-p which exceeds the trip value of 100 um p-p as per OEM table-13. On the other hand the amplitude on the MCOS and Low speed were almost within close amplitude values when compared between the left plot and right plot in Figure 4—21 at an average of 11 um pk in MCOS and 7 um pk in Low speed.

Considering other factors it can be seen that the lube oil temperature of both scenarios indicate similar values of 57°C as shown in Figure 4—21, it be concluded that in this particular case the lube oil temperature has no influence on the observed high vibration amplitude.

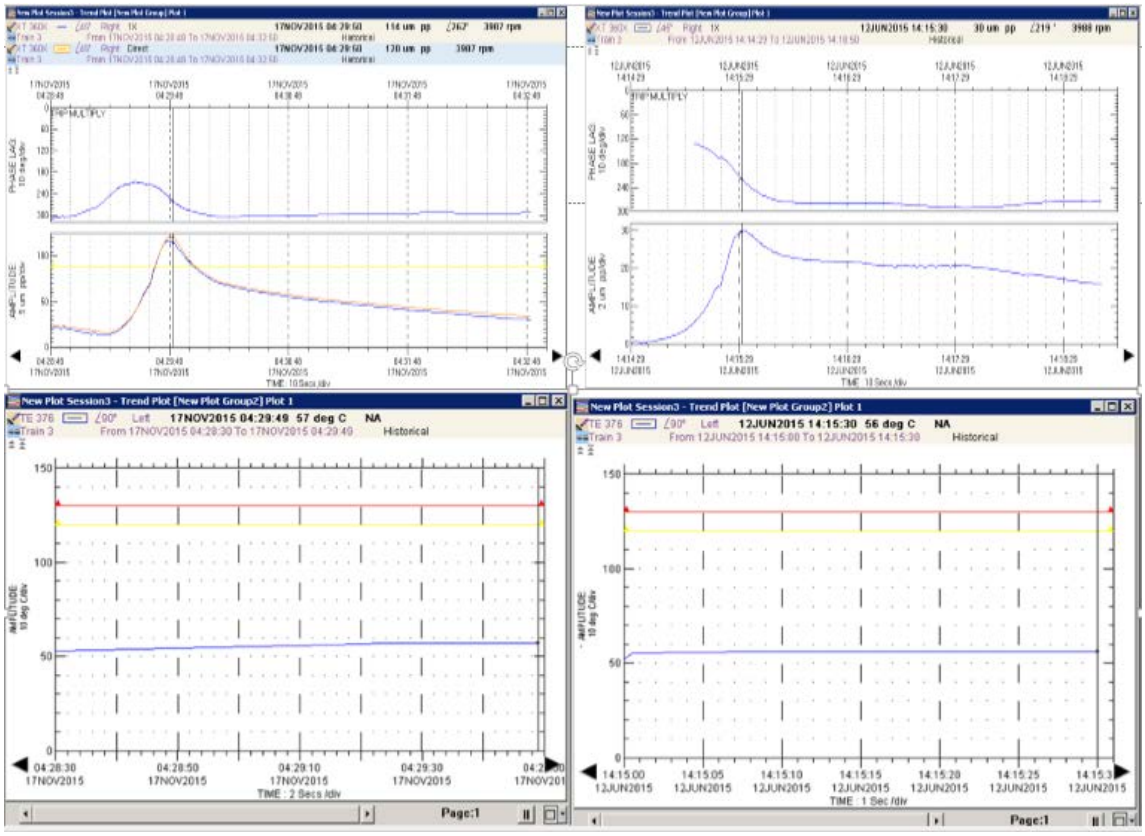

Figure 4—21 trend plots of scenarios, normal amplitude (right side) and high amplitude (left side) bottom plots shows DE bearings temperatures.

The spectrum plot had shown in Figure 4—22 (left) shows synchronous vibration amplitude of around 107 um p-p at the 1st critical speed. This phenomena was investigated through numerical model that to see the forces of (stiffness, damping and inertia).

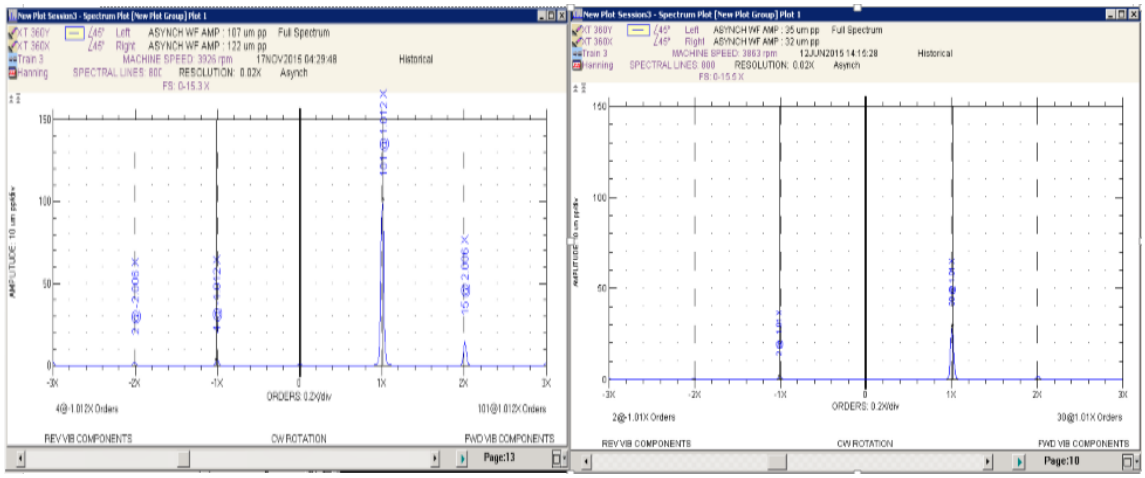

Figure 4—22 spectrum plot

4.2.8.2 Technical data sources

The technical data and the drawing with most of dimensions of this centrifugal compressor have been taken form OEM data sheet and technical manual.

However some data was not available for that many calculations have been done by using the below equations to find the data required in this model such as stages power of each impellers , the gas density of each stages and the Suction/Discharge absolute pressure. The stages power of each impellers and gas density of each stages were used on XLImplr that to model the impeller aerodynamic and the suction/discharge absolute pressure was used on XLGasLaby that to model the labyrinth seal aerodynamic.

The below table - 9 shows the total of calculated stages power of each impellers (23684 kw) which it gives almost similar value of actual power (23724 kw) which it is mentioned in the K-5430 API data sheet.

$$\boldsymbol{Density} = \frac{\boldsymbol{Molecular\ weight}}{\boldsymbol{23.644}} \qquad 4—1$$

$$\boldsymbol{Smass\ flow} = \boldsymbol{density\ X\ St\ flow} \qquad 4—2$$

$$\frac{\boldsymbol{n-1}}{\boldsymbol{n}} = \frac{\boldsymbol{k-1}}{\boldsymbol{k*eff}} \qquad 4—3$$

$$\boldsymbol{Hp} = [\boldsymbol{n}/(\boldsymbol{n}-\boldsymbol{1})][(\boldsymbol{ZRT})/\boldsymbol{MW}]\ [(\boldsymbol{Ps}/\boldsymbol{Pd})^{\frac{\boldsymbol{n-1}}{\boldsymbol{n}}} - \boldsymbol{1}] \qquad 4—4$$

$$\boldsymbol{Power\ Stages} = \frac{\boldsymbol{Smass\ flow\ X\ Hp}}{\boldsymbol{Eff}} \qquad 4—5$$

Table 6 process data and stages power of each impellers

stages	Psuct(N/m2)	Pdish(N/m2)	ΔP	R(KJ Kmol)	Tsuct (F)	Tdish (F)	Suction Density (kg/m3)	Dish Density (kg/m3)	stage power (Kw)
1st impeller	4E+06	4315500	1.23	8.315	333.2	343.2	1263.55	1512.55	4273.87
2nd impeller	4E+06	5321012	1.23	8.315	353.2	363.2	1469.72	1762.27	4495.65
3rd impeller	5E+06	6560807.2	1.23	8.315	373.2	383.2	1715.04	2059.45	4726.94
4th impeller	7E+06	8089475.3	1.23	8.315	393.2	403.2	2007.07	2413.33	4968.15
5th impeller	8E+06	9974323.0	1.23	8.315	413.2	423.2	2354.92	2835.00	5219.71
Total									23684.32

Table 7 Bearing operating conditions

Clearance	Diametrical Assembled Clearance (mm)	Preload (%	Oil Supply Temperature
Minimum	0.17	52.7	40
Nominal	0.185	56.1	55
Maximum	0.212	60	65

Table 8 Labyrinth seal clearances

Code indicate seal clearance position from below drawing		Clearance data at assembly (mm)			Max allowable value during operation (mm)
		MIN	NORM	MAX	MAX
A1	Labyrinth seal clearances on impellers	0.5	0.53	0.56	0.69
A2		0.5	0.5	0.54	0.66
A3		0.5	0.48	0.51	0.64
B1	Labyrinth seal clearances on Spacers	0.3	0.35	0.38	0.49

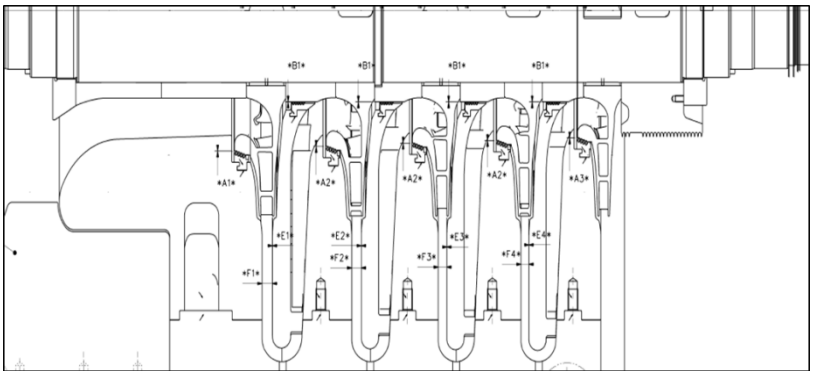

Figure 4—23 Rotor cross seciton drawing

Table 9 Seals Span

Hub(mm) Seal span	Shroud (impeller eye) (mm)	balance piston (mm)
0.005	0.04	150

Recorded vibration levels are evaluated against the manufacturer's alarm and trip levels as listed in Table 10 below.

Table 10 Alarm and Trip of manufacturer's

Unit	Alarm [¹m PP]	Trip [¹m PP]
VSD Motor	**280**	**316**
Gear LSS	**88**	**164**
Gear HSS	**51**	**95**
Compressor	**86**	**100**

4.2.8.3 Compressor rotordynamic model – Lateral analysis

Different factors have been reported in causing centrifugal compressors rotordynamics deficiency such as rotor flexibility, high rotor span with high number of impeller stages and high process pressure on the impellers, cross coupling forces generated by impellers and seals.

However a forced response analysis compacts totally with resonance, critical speeds and their corresponding vibration amplitude [58]. There are a lot of concerns during design stage with regards compressor rotordynamics behaviour due to residual unbalance, critical speed(s) and system stability at operating speed [59].

SRDC1 rotor (Figure 4—8) was modelled using 53 stations (Figure 4—25) which includes a single stage having five impellers, half Coupling additional weight, dry gas seal (DE&NDE), the shaft is modelled based on the rotor detailed drawing shown in (Figure 4—8). XLRotor software is used to conduct the rotordynamics analysis, the software uses Polynomial Transfer Function and Finite Element Method to solve for Undamped critical speeds (UCS), Eigenvector, Eigenvalue, Imbalance Response...etc.. In all of the analysis carried different bearing fluid film temperature was considered (see Table 7). As per the filed data observations different vibration amplitudes were noted at different durations between shutdown and start-up. The analysis shall focus on the root cause of such high vibration amplitude.

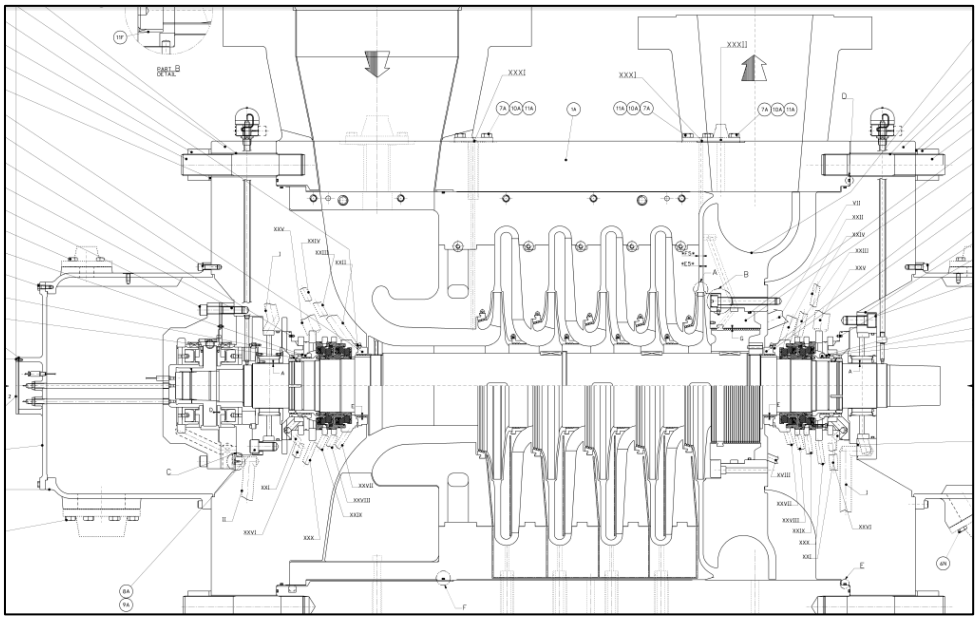

Figure 4—24 K-5430 Cross Sectional Drawing (PDO, 2010)

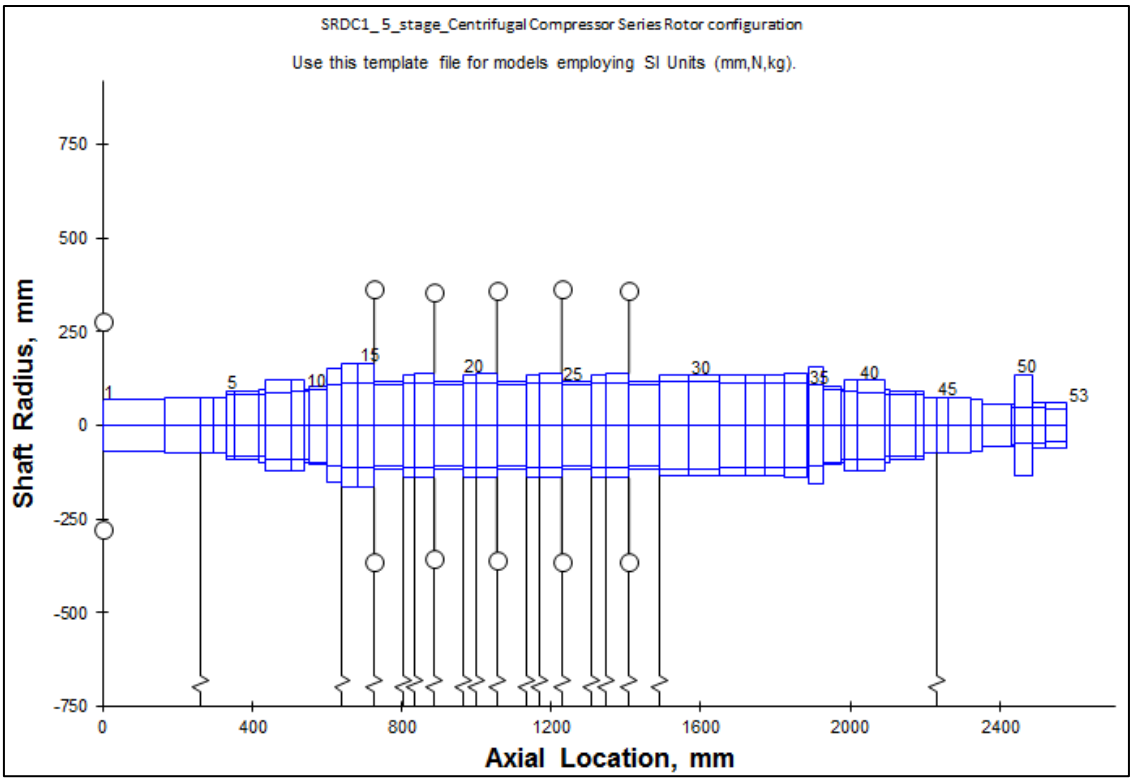

Figure 4—25 SRDC1 rotor-bearing model

Table 11 Rotor added mass and correspondent inertias

Added Mass Description	Added Weight (kg)	Added Ip (kg-m2)	Added It (kg-m2)
1st impeller	55	0.551	0.303
2nd impeller	55.73	0.518	0.306
3rd impeller	54.32	0.505	0.299
4th impeller	46.12	0.429	0.254
5th impeller	46.12	0.429	0.254
Coupling	29.5	-	-

Bearing stiffness and damping coefficients were considered for the different bearing clearances; preload and temperature. The preload and clearances have significant influence on the bearing damping and stiffness characteristics and this in turn affects the general rotor dynamics behaviour of the rotor. Table 12 are shows variance cases selected of bearing preload and bearing clearances at variance temperature which was provided by the OEM (nominal bearing preload with nominal bearing clearance, minimum bearing preload and maximum bearing clearance, maximum bearing preload and minimum bearing clearance) all conditions analysis with variance lube oil temperature condition such as minimum, nominal and maximum (40°C, 55°C and 65°C respectively).

Table12 different cases used to calculate Bearing stiffness and damping.

Cases	Temp °C	Bearing preload	Bearing clearances
Case 1	40	Nominal	Nominal
Case 2	55	Nominal	Nominal
Case 3	65	Nominal	Nominal
Case 4	40	minimum	maximum
Case 5	55	minimum	maximum
Case 6	65	minimum	maximum
Case 7	40	maximum	minimum
Case 8	55	maximum	minimum
Case 9	65	maximum	minimum

Figure 4—26 shows bearing stiffness characteristics at right side and damping characteristics at left side for all nine cases as stated in table 12. The highest

stiffness values are observed at case 6 (minimum bearing preload & maximum bearing clearance at 65°C) and case 9 (maximum bearing preload & minimum bearing clearance at 65°C) whereas the damping characteristics show comparatively small variance between the clearances.

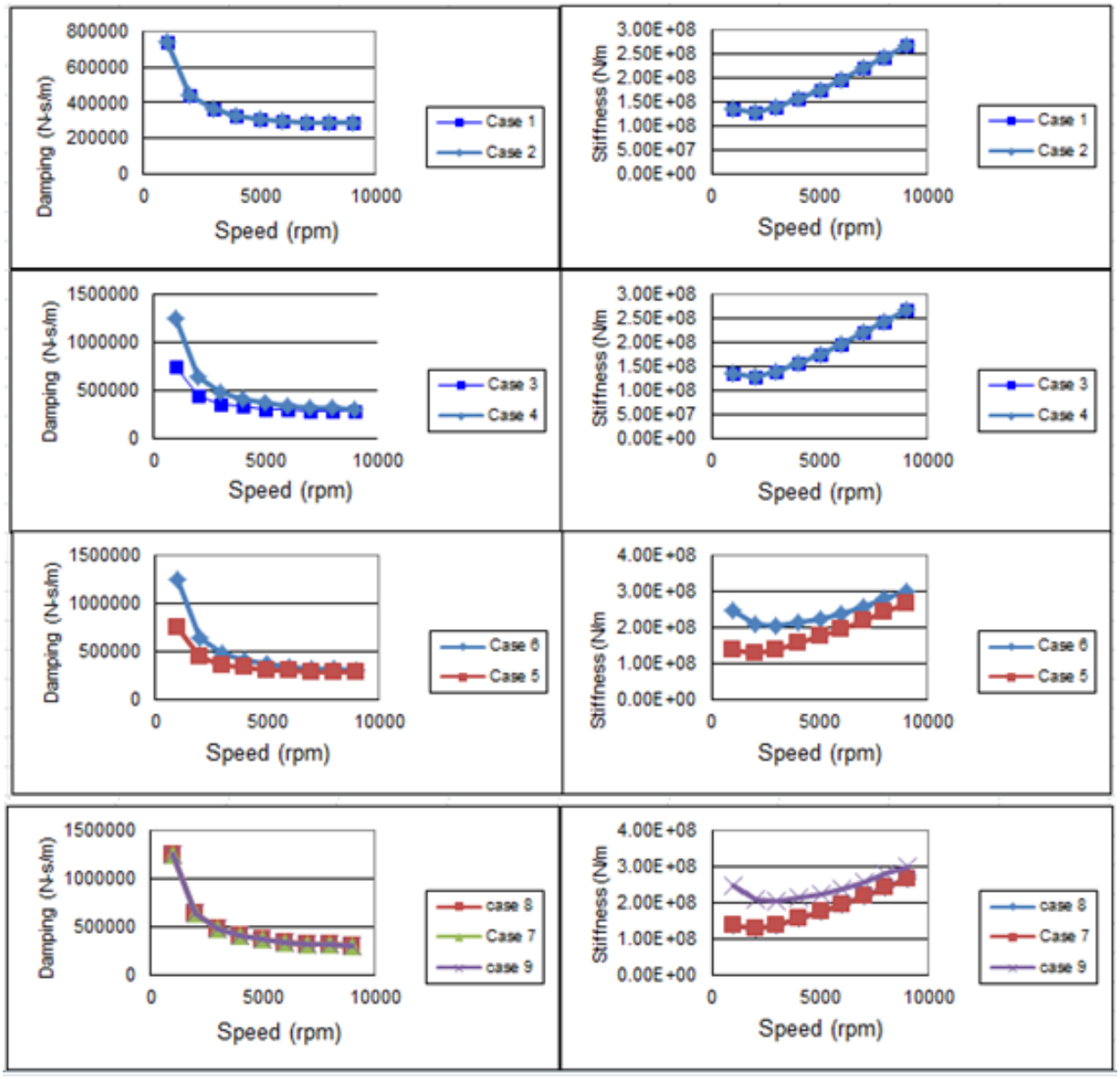

Figure 4—26 bearing stiffness and damping characteristics of all 9 cases selected

On the other hand Labyrinth seals forces are considered as per the Seal clearances provide by OEM (table 8). The Max allowable seal clearance during operation (0.66mm) was considered in model as it can be seen in Figure 4—27

& Figure 4—28 which shows the direct and cross coupling stiffness and damping coefficients generated by the labyrinth seals.

Interestingly labyrinth seals are well known for their negative effect on the overall compressor stability mainly in high pressure ratio machines where the cross coupling forces can be significantly high and this in turn reduces the positive direct stiffness and damping expected by the bearings [21].

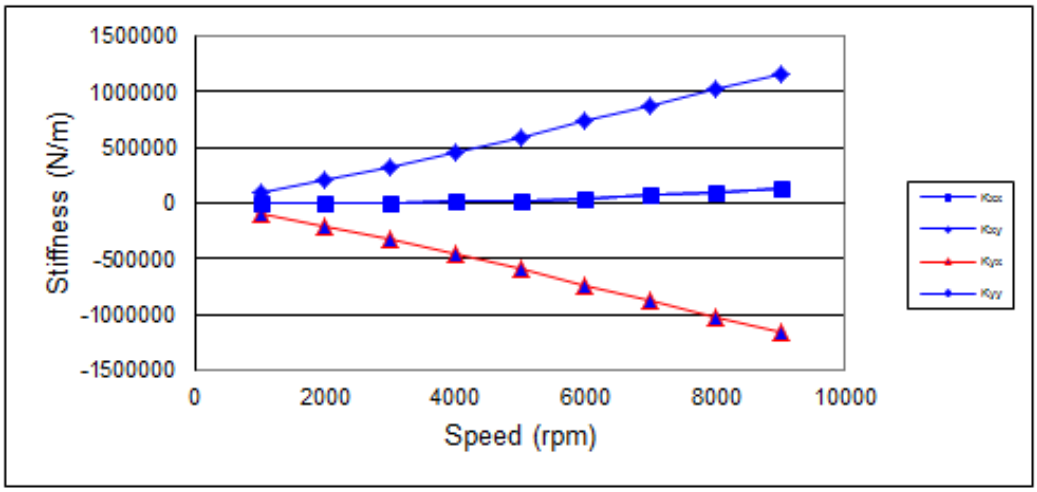

Figure 4—27 Labyrinth seal stiffness coefficients

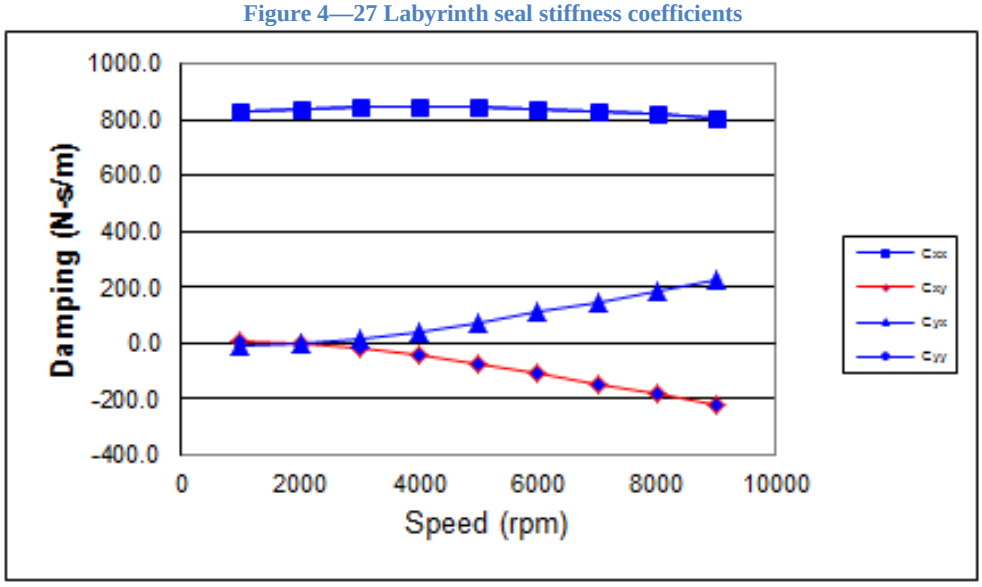

Figure 4—28 Labyrinth seal damping coefficients

4.2.8.4 Results and Discussion

To confirm whether the created rotor model is capable to simulate and predict the compressor rotordynamics behaviour, standard analyses for the compressor

rotor-bearing system is conducted including the ordinary design procedure such Undamped Critical Speed (UCS) and Synchronous Response Analysis. Undamped Critical Speed (UCS) Map illustrates the interface among rotor and bearing stiffness. It is a basic analysis used to show the influence of support stiffness on rotor natural frequencies and their corresponding mode shapes. UCS has different assumption such as:

- Both bearings (DE&NDE) are Undamped Axisymmetric Springs such that (K)_xx=K_yy and (K_xy=K_yx=0).
- The rotational speed of the rotor is equivalent to eigenvalue frequency this is by exchanging the value of the rotor transverse inertia (It) with the transverse inertia (It) minus polar inertia (Ip) [18].

There are two methods to identify the rotor critical speeds, Eigenvalue analysis and linear forced response, the first analysis does not consider the damping effect while linear forced response analysis uses Eigenvalue analysis to configure the excitation forces so that rotor vibration filed measurements can closely simulated [13].

In Figure 4—29 shows UCS map of SRDC1 rotor model Figure 4—25, hence the actual compressor 5 tilting pads journal maximum bearing stiffness coefficients are covered in the map and also the stiffness values range varying between (1.00E+06 to 1.00E+10). However, the UCS map indicates the 1st undamped critical speed approximately at 4000 rpm where the bearing stiffness interacts with the rotor 1st natural frequency, also we can see the 2^{nd} critical speed naturally damped.

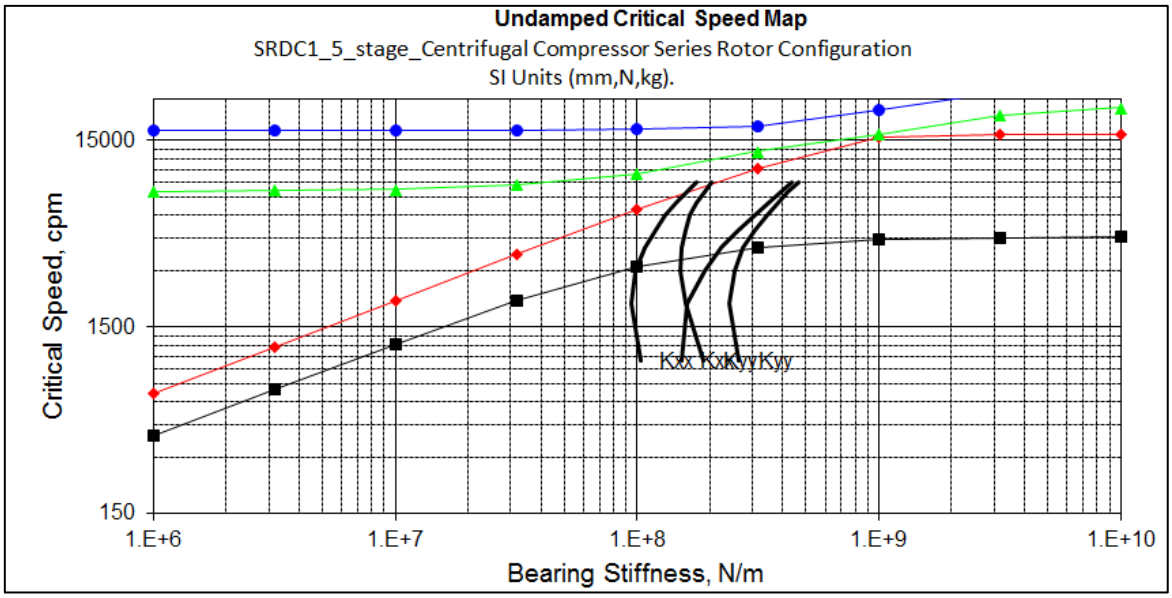

Figure 4—29 SRDC1 Undamped Critical Speed map

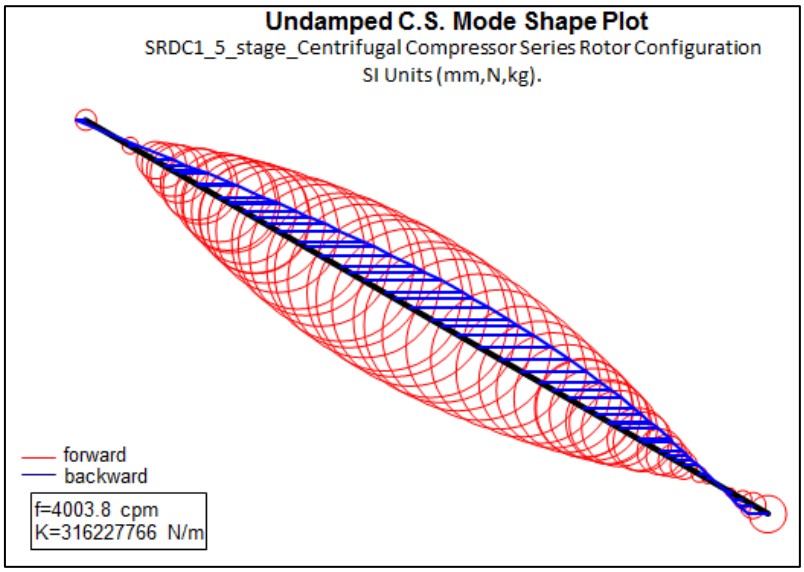

Figure 4—30 Undamped C.S. mode shape

The 1st mode unbalance rotor response calculations have been performed considering the following unbalance magnitude applied on the section of maximum deflection as determined from the undamped analysis:

$$\boldsymbol{U_1 = 4.MAX\left[6350.\left(\frac{W_{rotor}}{N}\right); 250\mu mm.W_{rotor}\right][g.mm]} \qquad 4—6$$

Based on the SRDC1 rotor mass of 1145 kg and its correspondent maximum continue speed of 8962 rpm, an imbalance mass of 3250.8 gm-mm is placed at rotor mid span station no.27. Figure 4—31 shows the response analysis of the

compressor rotor at the DE bearing, NDE bearing and rotor mid span within stations 3, 45 and 27 respectively, the results shown corresponds to the Forward probe (DE) showing a peak amplitude of approximately 19.3 microns while the After (NDE) probe is 16.6 microns and 68 microns at rotor mid span. However the first critical speed of the SRDC1 is around 4000 RPM with amplification Factor (AF) of 4.4 and the separation margin(SM) of 21.1 %.

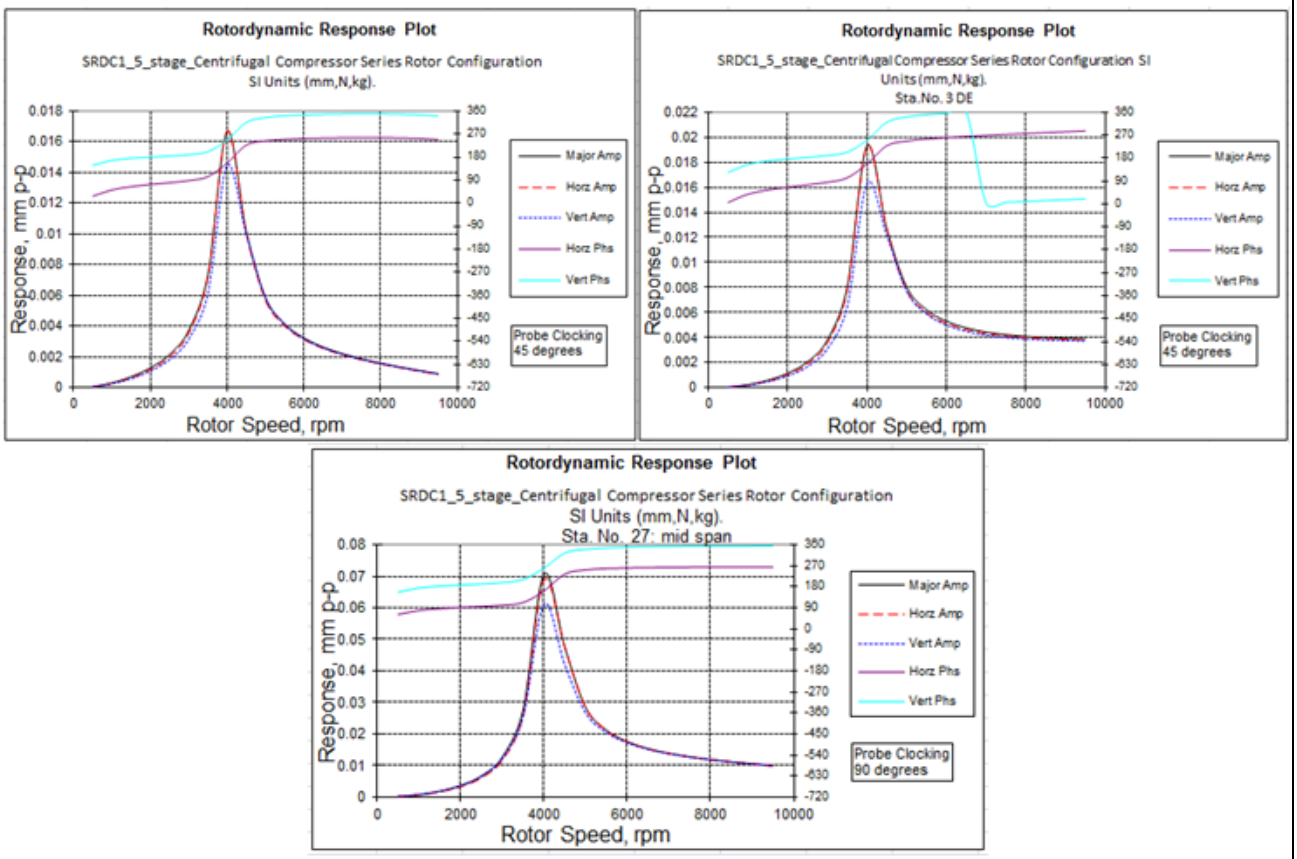

Figure 4—31 SRDC1 rotordynmic response plots

Figure 4—33 shows bode plot of Mechanical Running Test data (MRT) of SRDC1 NDE which indicates first critical speed at 4040 rpm with a correspondent AF of 3.67 and separation margin SM of 20.6 %. Based on API 617 standard the model compares well with the MRT data as the discrepancy between the MRT 1st critical speed (4040 RPM) and the model 1st critical speed (4000 rpm) is less than 5% [13]. Hence with result in table-13 the comparison between numerical model and MRT can be determined that the numerical model is capable of simulating the real compressor as the values in the table calculated from plots Figure 4—32 & Figure 4—33.

Table 13 Comparing values of MRT and Numerical model

	Operating speed (RPM)	Rotor first critical Nc1 (RPM)	Max Amplitude Ac1	AC1*0.707	Amplification Factor AF	Mode Separation margin SM
MRT	5114	4040	20.3	14.35	3.67	20.6
numerical model	5114	4000	19.3	13.6	4.4	21.13

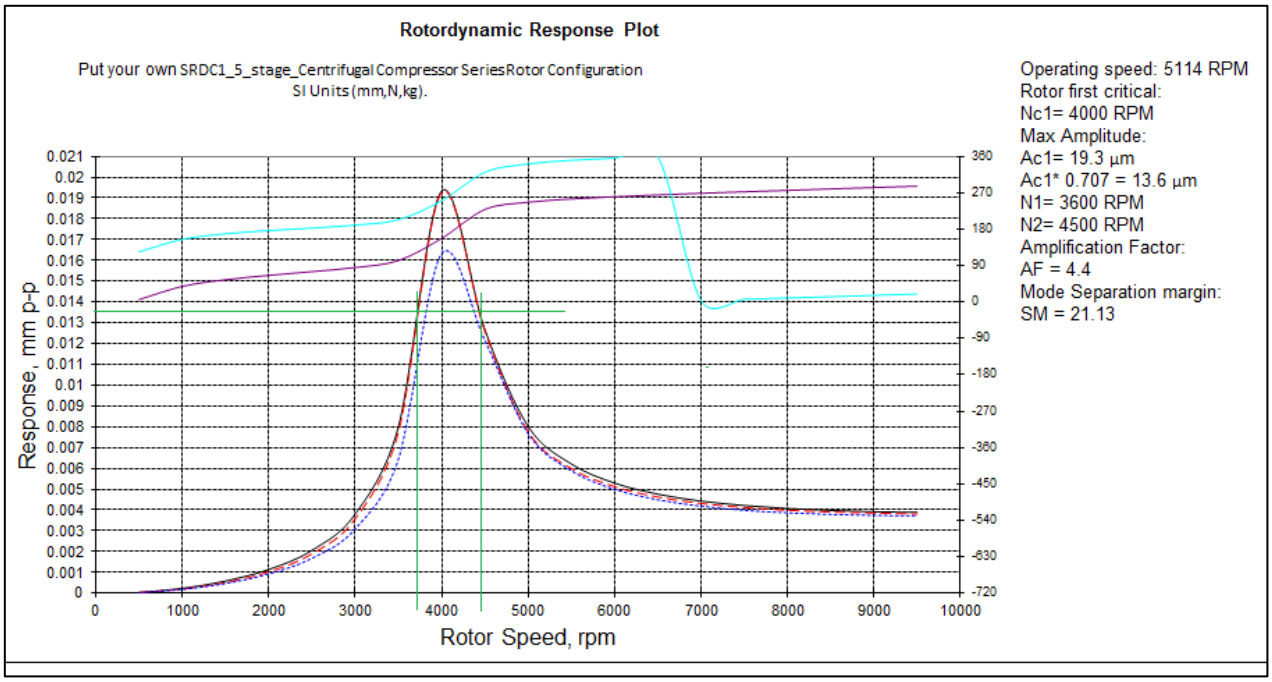

Figure 4—32 Response Plot at NDE probe within numerical model

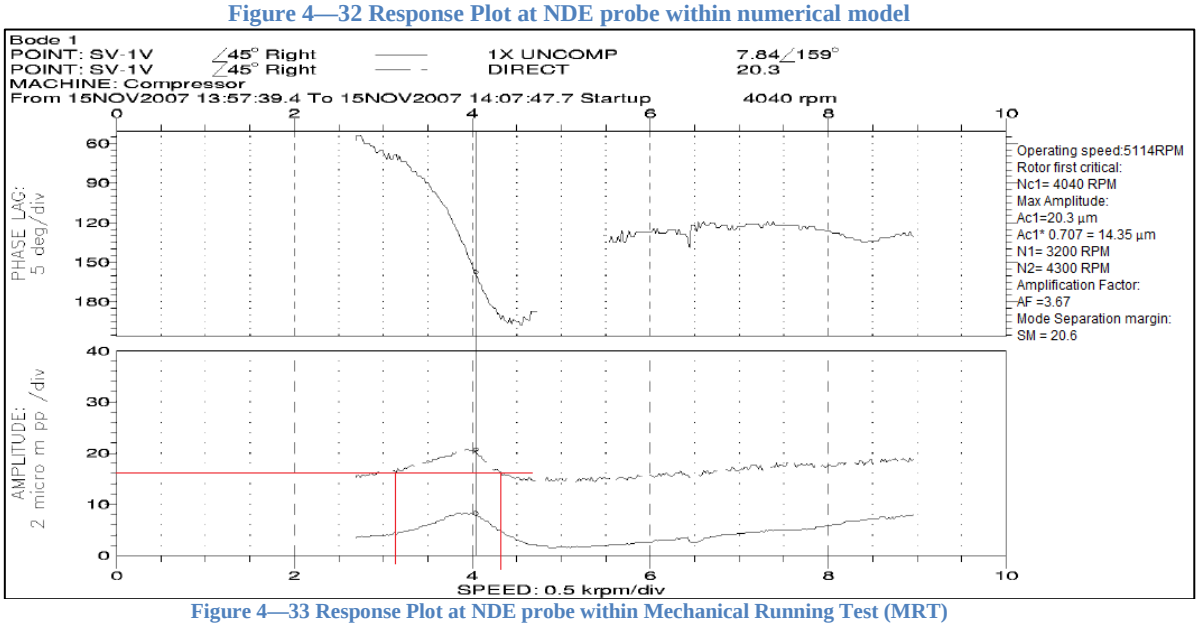

Figure 4—33 Response Plot at NDE probe within Mechanical Running Test (MRT)

To start with a basic rotor-bearing eigenvalue analysis was considered without any external aerodynamics forces, Figure 4—34 shows the damped natural

frequency map which indicates that three possible critical speeds are to be traversed by the compressor during ramp up or down which are displayed by the connection between the damped frequencies and the synchronous line. The previous response analysis showed that only one critical speed was excited at 4000 rpm while the other two modes are naturally damped as it can be seen from the root locus map (Figure 4—35). Furthermore the root locus map also illustrates that the compressor has good stability behaviour.

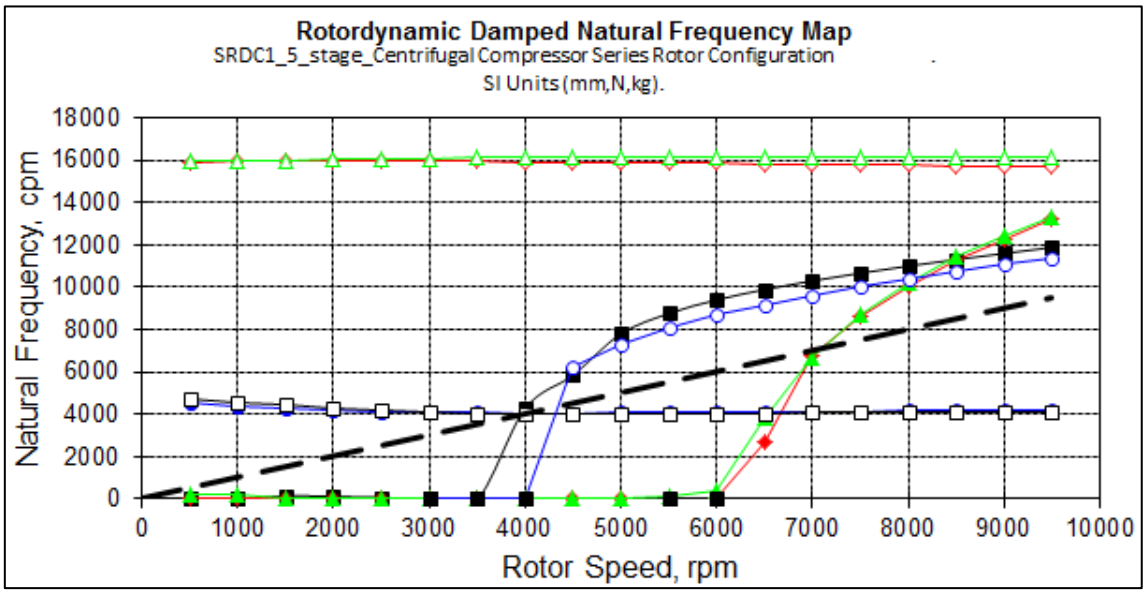

Figure 4—34 SRDC1 Compressor rotordynamic damped natural frequency map

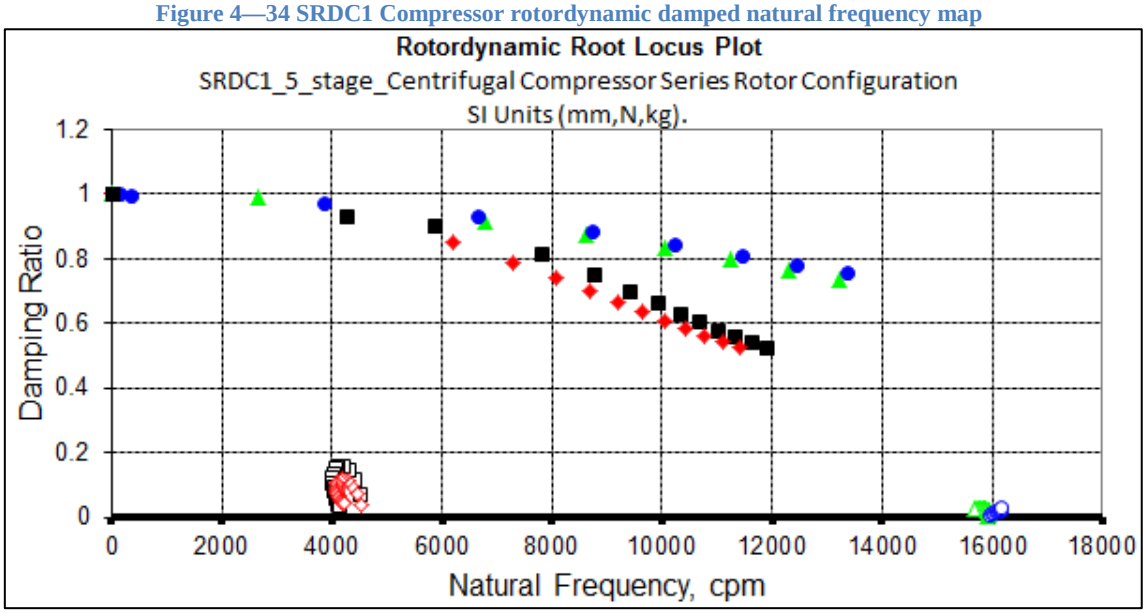

Figure 4—35 SRDC1 Compressor root locus plot with no external forces

The second analysis was to investigate the effect of cross coupling forces on the compressor rotor stability behaviour by adding SRDC1 compressor 5 impeller forces that by assumption all components are operating according to their designed performance. As seen from the root locus plot (Figure 4—36) and 1st critical speed mode (Figure 4—37), comparing between the vibration amplitude respond of no load and respond with impeller forces can identified from plots Figure 4—38 which shows the amplitudes of with impellers forces respond was more than respond without impeller force by 7um on both DE, ND bearing and rotor mid span by 22 um.

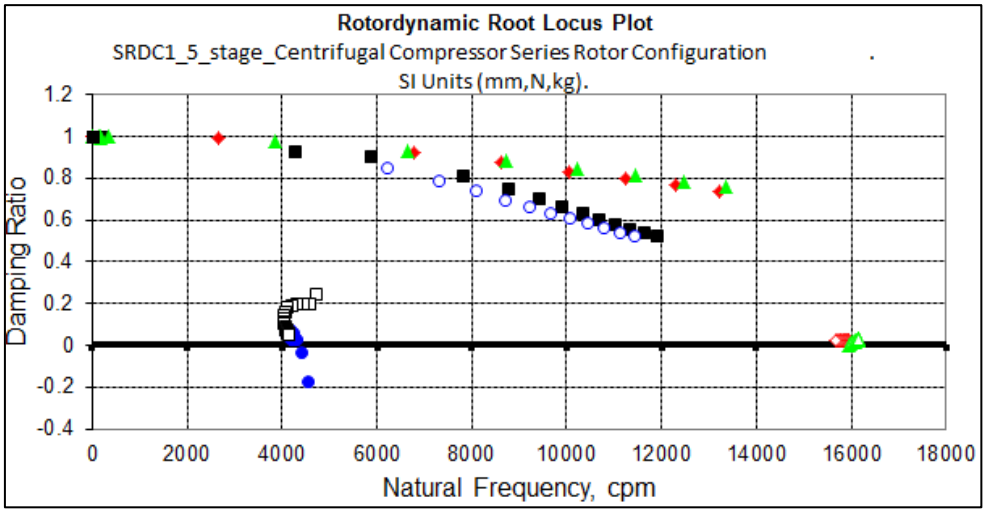

Figure 4—36 SRDC1 Compressor root locus plot with impeller forces

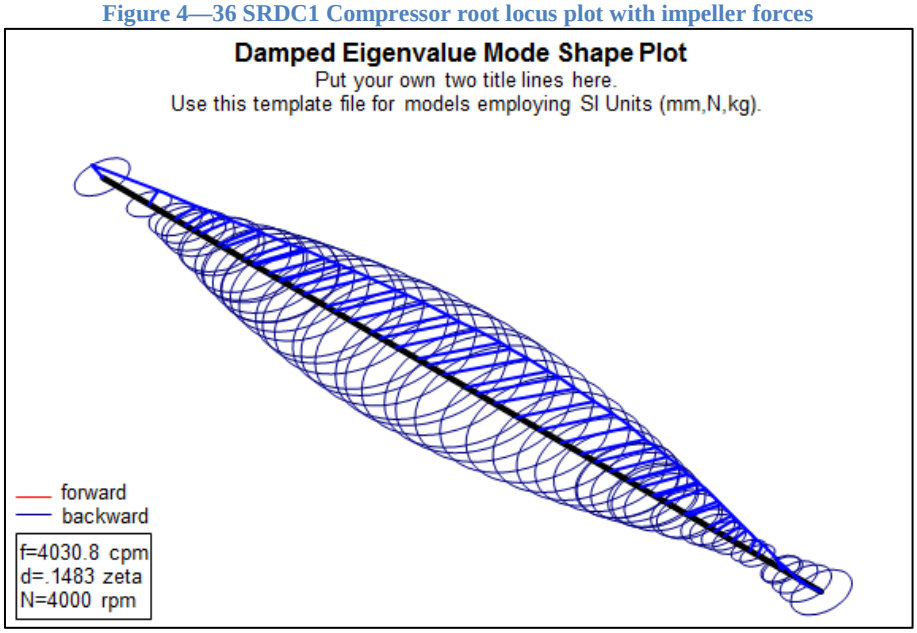

Figure 4—37 1st damped critical speed mode shape with impeller forces

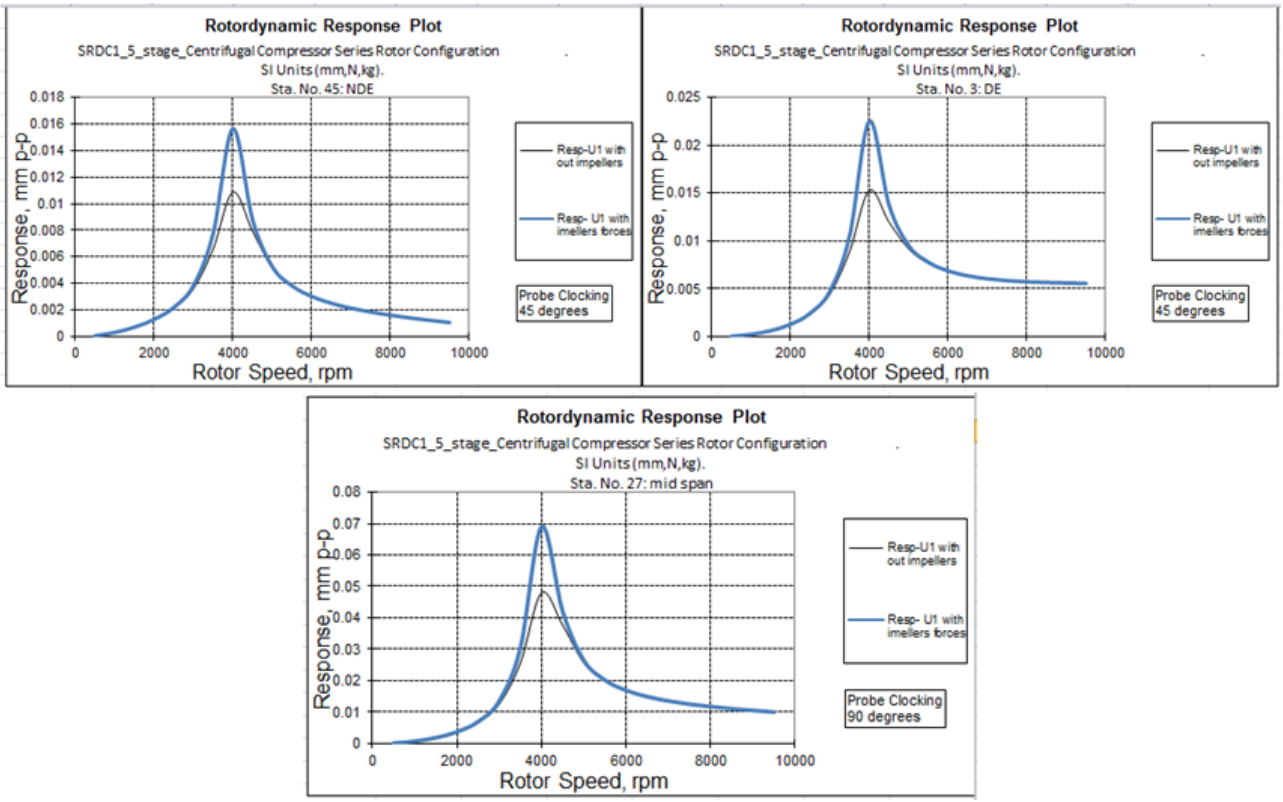

Figure 4—38 comparing plots of NDE sta.45, ND sta.3 & rotor mid span sta.27 with two seniors' analysis (no load and impeller forces)

The third analysis with considerration of all aerodynamic forces such as impellers, inter-stage seals and balance piston, first scenario was effect of maximum seals clearances, the values of clearances were provided by OEM in table-4, hence the result shows in rotordynamic root locus plot (Figure 4—39) and 1st damped critical speed mode shape load (Figure 4—40) as damping increased from second analysis by 1.3% only. Figure 4—41 shows plot of all considerations which were mentioned above as there was slightly increase on the amplitude with consideration of all aerodynamic forces when compared with the second analysis.

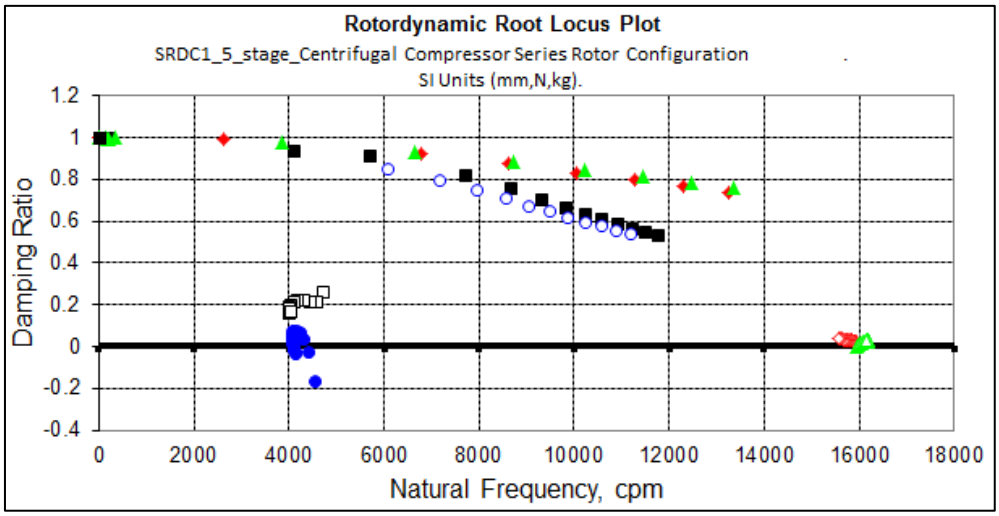

Figure 4—39 SRDC1 Compressor root locus plot at load

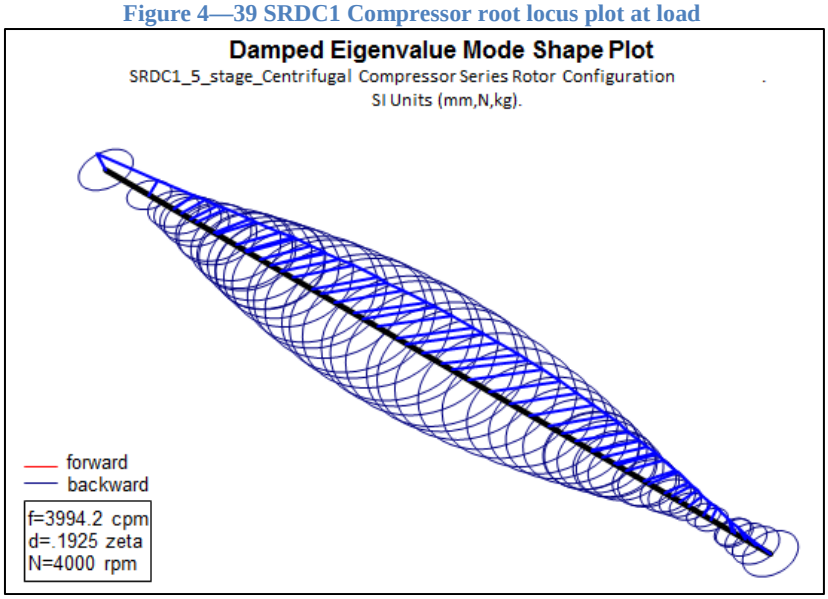

Figure 4—40 1st damped critical speed mode shape load

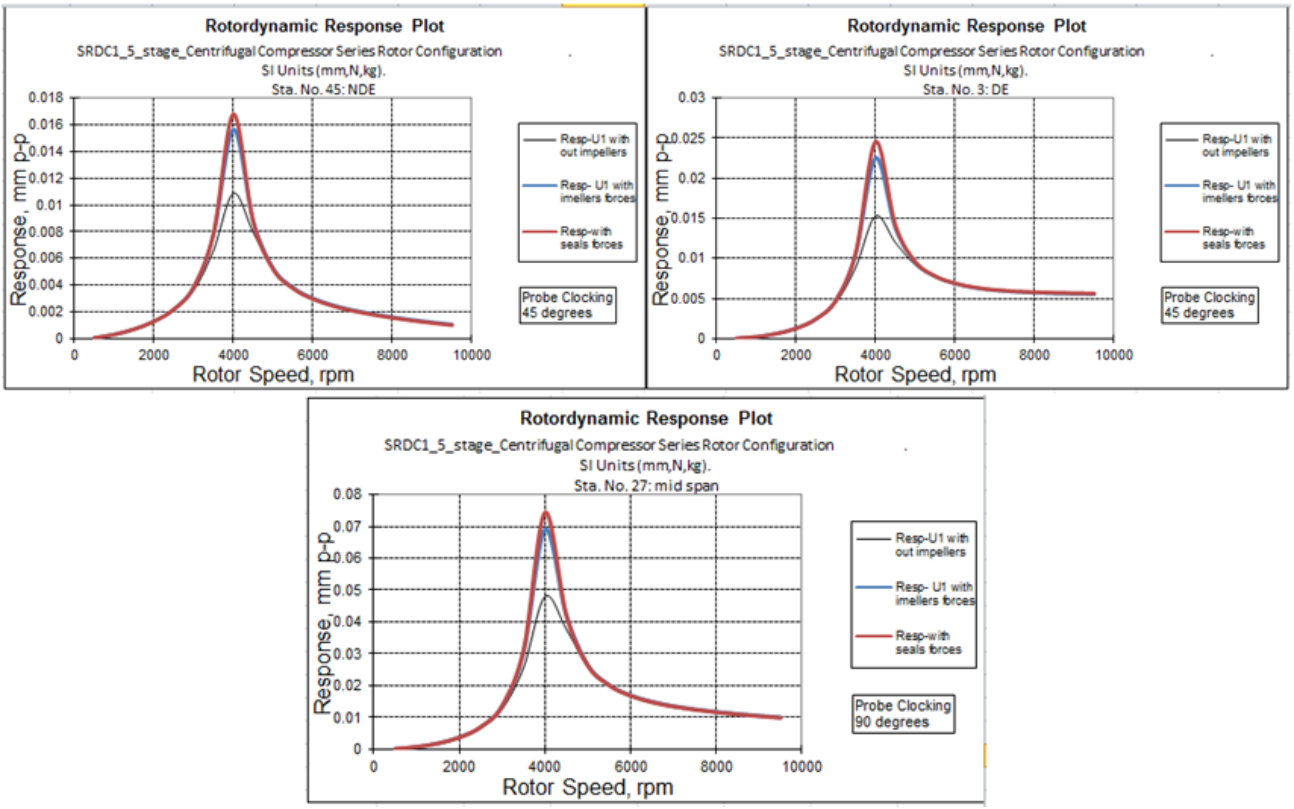

Figure 4—41 comparing plots of NDE sta.45, ND sta.3 & rotor mid span sta.27 with two seniors' analysis (no load , impeller forces

Than nominal and minimum seal clearances were considered in the fourth analysis to see the variance when compared with third analysis, the result can be seen from Figure 4—42 which indicates no much difference in terms of amplitude.

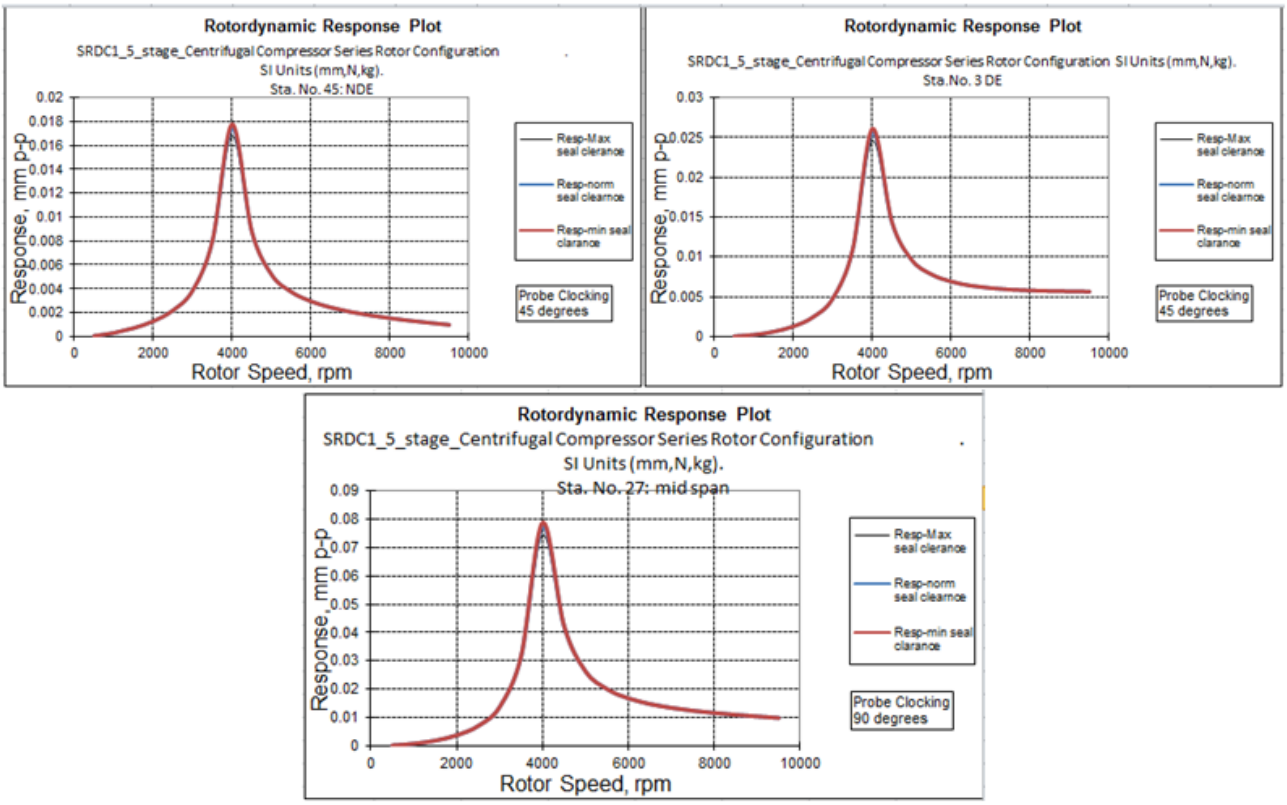

Figure 4—42 comparing plots with three conditions Max/Norm/Min seal clearances

Factory Acceptance Test (FAT) data is extra data available beside the field data and mechanical test data which gives other source to analysis the variance of SRDC1 vibration amplitudes for that comparing the all two data's (field data & FAT) in terms of 1st critical speed, Max Amplitude Ac1, Amplification factor AF and Separation margin SM with numerical model will give more assurance of accurate result.

Figure 4—43 shows the plot of SRDC1 FAT responds of DE probe which indicates the max amplitude of 28.6 um, AF of 4.59 and separation margin SM of 21.4 thus these values can considered as base of the actual compressor design as the field data's has variance on 1st critical speed vibration amplitude and most of compressor shutdown cases have similar phenomena however the compressor start-up cases have some variance as observed from field data shown in Figure 4—10 and Figure 4—11, for that one case was selected for analysis as shown in Figure 4—44.

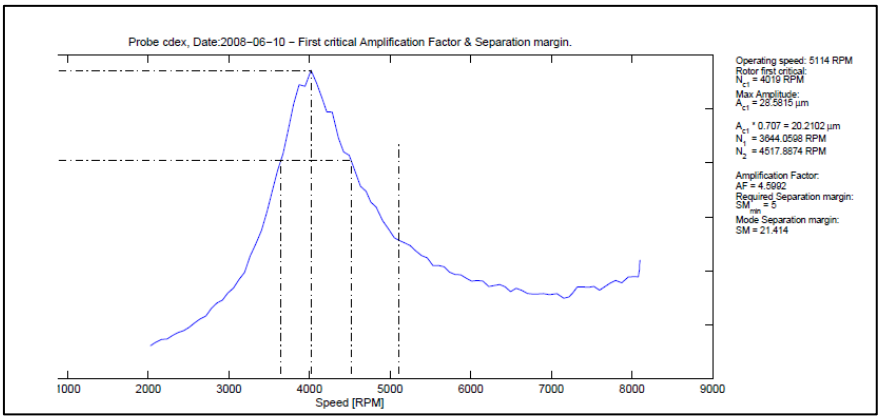

Figure 4—43 FAT responds of DE probe

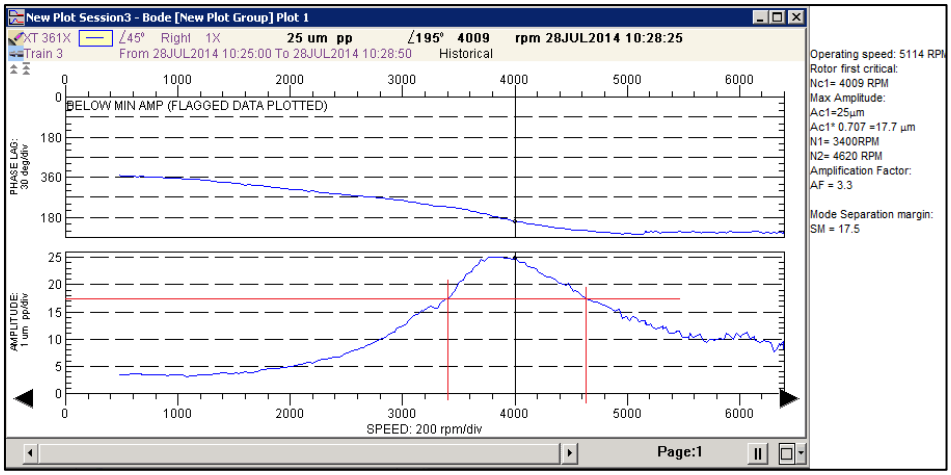

Figure 4—44 Field responds of DE probe

Having validated the model for actual conditions the next step was to simulate the condition of the SRDC1 compressor that represents the inoperable state as noted in Figure 4—43. To achieve the actual compressor design an unbalance mass (2250 gm-mm) was added on station nos. 27.Hence the result plot in Figure 4—45 shows the respond of SRDC1 numerical model DE probe compared with filed actual plot (Figure 4—44) in terms of rotor balance as the MOCS amplitude was noted from both numerical model plot and filed plot which was result max vibration amplitude of 7 um and 10 um respectively.

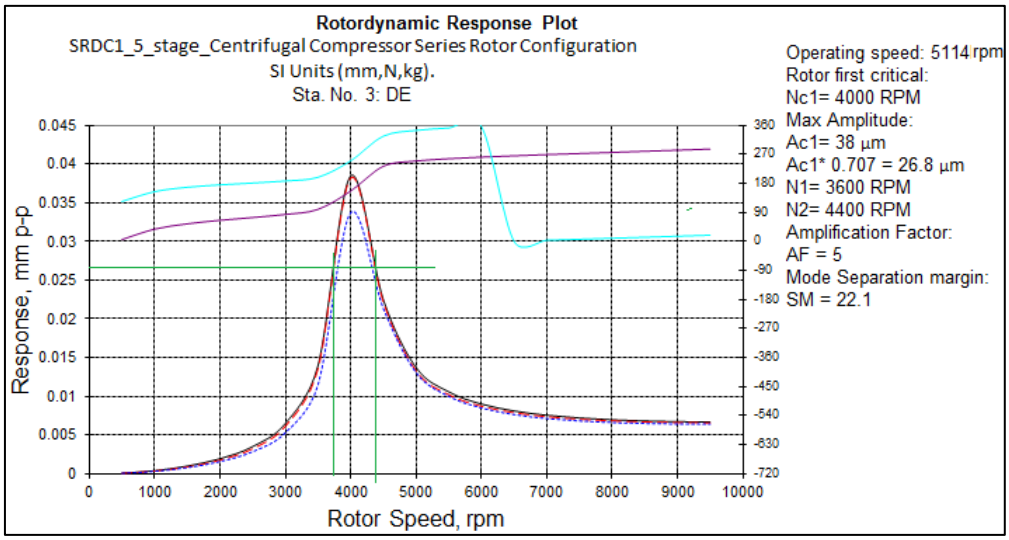

Figure 4—45 respond of SRDC1 numerical model DE probe

Table 14 is comparing values of all three responds of FAT, field data and numerical model which it considered operating speed, first critical speed, Maximum amplitude, Amplification Factor (AF) and separation margin (SM)

Table 14 Comparing values of FAT, field data and Numerical model

	Operating speed (RPM)	Rotor first critical Nc1 (RPM)	Max Amplitude Ac1	AC1*0.707	Amplification Factor AF	Mode Separation margin SM
FAT	5114	4019	28.5	20	4.6	21.4
Field data	5114	4009	25	17.7	3.3	17.5
numerical model	5114	4000	38	26.8	5	22.1

The numerical model allowed for an investigation on the effect of Inertia force, damping force and stiffness force for a defined the variance of vibration amplitudes within first critical speed.

Inertia force effect was rolled out as the field data's during hot start (high amplitude) and cold start (normal amplitude) in terms of MCOS amplitude is almost similar values as shown in tables-2, 4, 5 and 6. On the other hand the amplitude on the MCOS and Low speed were almost within close amplitude values when compered between the left plot and right plot in Figure 4—47 at an average of 11 um pk in MCOS and 7 um pk in Low speed. also the Figure 4—46 shows orbit plots of both cases of hot start and cold start (left plot and right

plot respectively) as there was no indication of unbalance, misalignment, bearing rub and rotor whirl.

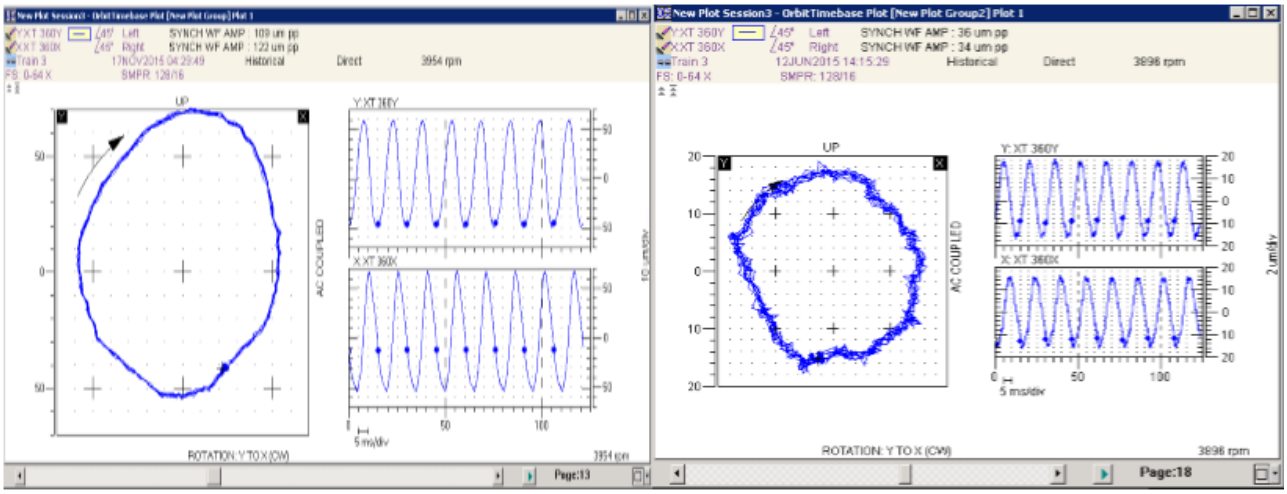

Figure 4—46 orbit plots of both cases

Considering other factors it can be seen that the lube oil temperature of both scenarios indicate similar values of 57°C as shown in Figure 4—47 and as seen in Figure 4—48 the temperature lube oil cooler downstream is around 50°C, it can be concluded that in this particular case the lube oil temperature has no influence on the observed high vibration amplitude.

.

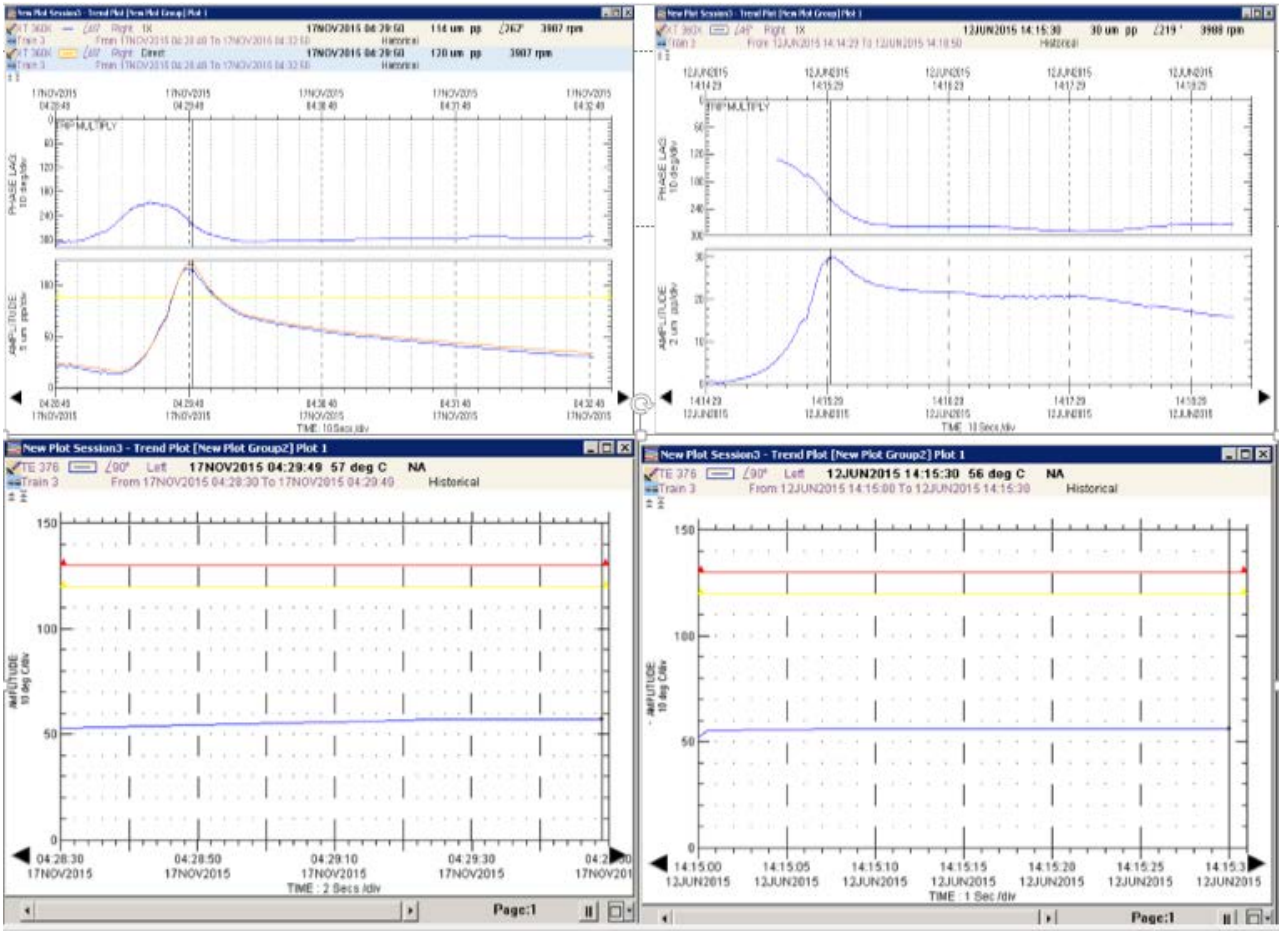

Figure 4—47 trend plots of scenarios, normal amplitude (right side) and high amplitude (left side) bottom plots shows DE bearings temperatures.

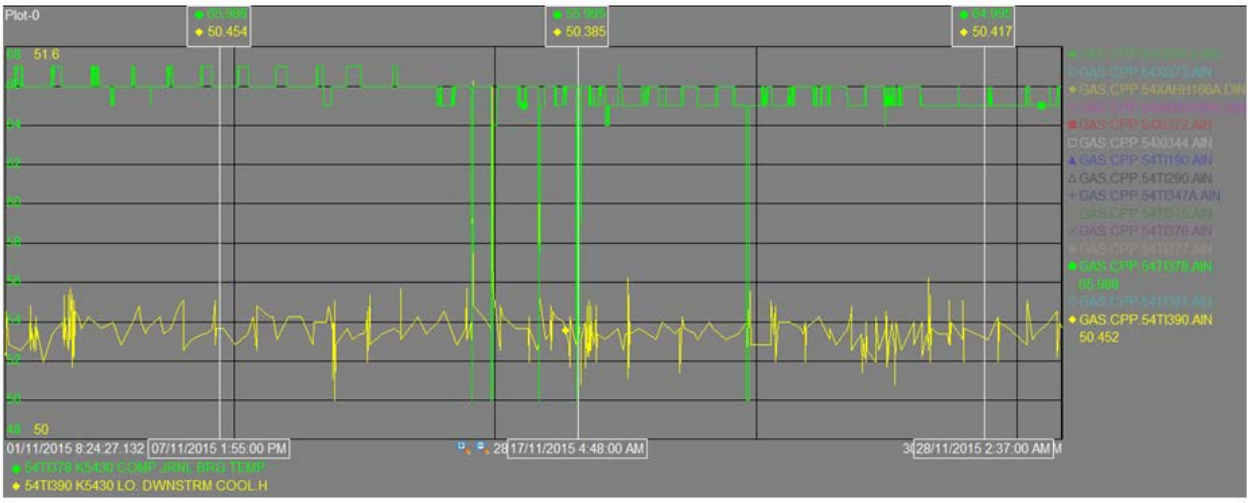

Figure 4—48 SRDC1 temperature lube oil cooler downstream

The nine cases shows in table 12 were used in the numerical analysis of investigate bearing damping effect on the 1st critical speed of SRDC1 to see the difference on the amplitude, from nine cases just minor change on the temperature as 50°C was selected against 55°C in order to compare similar filed bearing temperature as shows in Figure 4—48. Also the compressor start-up mode (with impeller forces only) was assumed because the variance in the filed data evidenced in start-up only. The observation from the result in plots Figure 4—49 are:

a) The variances in the 1st critical speed were observed which it was clearly indicating the bearing damping effect on the 1st critical speed.
b) The case 2 and case 5 (nominal bearing preload-nominal bearing clearance at 50°C and minimum preload-maximum bearing clearance at 50°C) were most closer to filed condition .
c) The amplitudes were not exceeding 35 um p-p, which it was indicating the normal field condition which it appears during cold start-up and shutdown. So bearing damping effect was rolled out in terms of the field data's during hot start (high amplitude).
d) The amplitudes at low speed 1800 rpm were almost similar for all cases which it indicates the rotor stiffness was also rolled out as effect on hot start filed case.

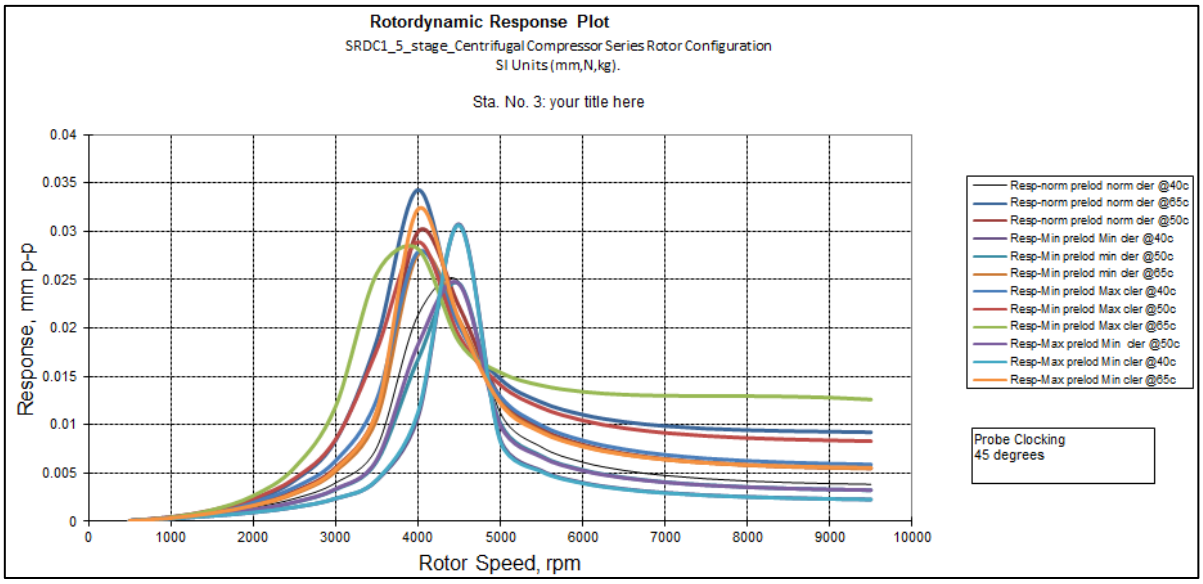

Figure 4—49 plots of DE amplitudes with different bearing conditions

The experimental data along with the numerical analysis provide a valuable combination on explaining the difference facts used to identify the main influence of the high 1X vibration amplitude at SRDC1 while traversing its 1st critical speed during hot start-up. The temporary thermal bow was suspected to be the reason of this phenomenon; therefore a detailed investigation has been conducted numerically to approve the thermal bow affect during 1st critical speed.

Many papers have been published about thermal temperature gradients across rotors influencing the rotordynamic characteristics of such critical machines particularly when the temperature across one side of the shaft and the other is high. Such variance results in frictional heating due to the physical contact between stationary and rotary parts such as labyrinth seals, impellers, slip rings, armatures, etc. However the rub generates heat locally on the shaft surface which results in shaft bow leading to additional imbalance onto residual rotor imbalance which induces an instantaneous high shaft vibration. The first paper published on this regard was by Newkirk [55] where he showed that labyrinth seals clearance are being affected by such phenomenon due to rubbing as well as shaft bending. Kellenberger (1979) investigated the synchronous rotor instability due to generator hydrogen seal rings under several combinations of

support conditions, the friction as in rub was the main driving mechanism of such hot spot on the shaft.

Morton effect is another thermal condition that can produce temperature variance in the shaft via non-uniform viscous shearing action in the oil film of a journal bearing which Keogh and Morton (1993) stated in their paper [56]. Also De Jongh (2008) has given a thorough overview on the Morton effect with explanation on how synchronous rotor instability due to non-uniform of journal bearing can happen in high speed machine [56] than Brian and Lorenz (2010) simplified analytically and mathematically of modelling bearing differential heating (Morton effect) and its influence on shaft synchronous vibration , therefore the temperature coefficient vector of sensitivity was highlighted in Brain analysis as the key missing element to predict Morton effect instability for any rotating machine [58].

Rotor bow is a condition that affects bent shaft centreline, Bently in his book (Fundamentals of Rotating Machinery Diagnostics) explained the three general categories of bow elastic, temporary and permanent. Elastic bow happens due to static radial loads on the rotor which do not exceed the yield strength hence there difference causes can be attributed to process fluid loads , internal misalignment and partial arc steam admission in steam turbines. Temporary bow can happen because of uneven heating of the rotor surface or due to anisotropic thermal material properties. Permanent bow effects if the rotor has deformed to a condition that is not self-reversing without different interference [5].

Temporary bow forms as an effect of a temporary thermal expansion of the rotor. In fact of a stopped unrestricted rotor it is at an even temperature in free space (no gravity load) (see Figure 4—50). Hence the rotor is heated from top and the bottom is cooled, compressive stresses form inside the upper half of the rotor and flexible stresses in the bottom half. These stresses produce a bending moment that bends the rotor in the warm path until the different stresses fade. After deforming the top surface is longer and the bottom surface is shorter and

no internal stresses exist in the rotor. While the cause of differential heating is removed from the rotor, the process will reverse and yield the rotor to its original profile [5].

There are two factors that cause rotor bow if both combined together during transient and uniform temperature conditions [5]:

1. Variances in thermal conductivity will contribute to an unequal temperature distribution during thermal transients.
2. Variances in the coefficient of thermal expansion in different areas will cause variation in the thermal expansion.

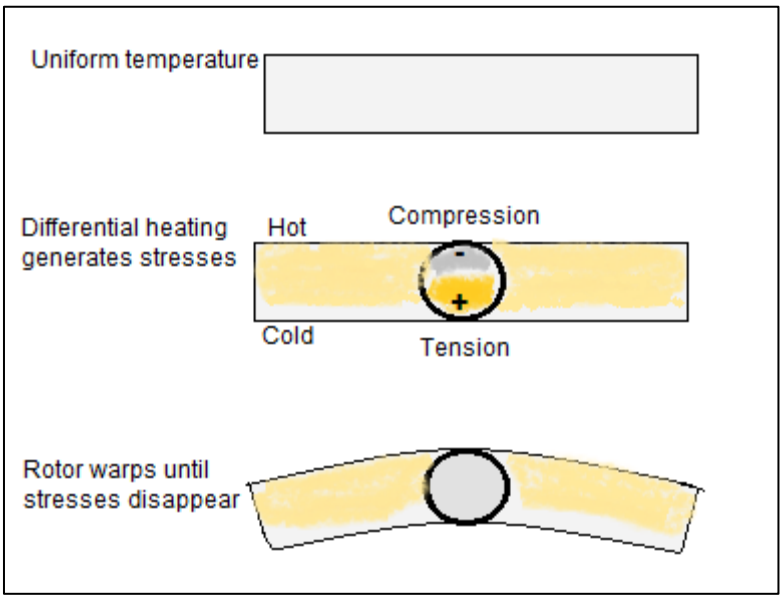

Figure 4—50 Thermal warping of a rotor, modified from Bently book [5]

Figure 4—51 shows the simulation of temperature gradient of SRDC1 compressor during operation, as the compressor arrangements design allows the big volume of natural gas to enter through compressor suction located on the non-drive end of compressor. The mechanical energy to the gas takes place with increase of the gas velocity, pressure and temperature as per ideal gas law ($PV=nRT$). The temperature increases up to 433 °F at final stage. The internal rotor thermal equilibrium suspected during long operation.

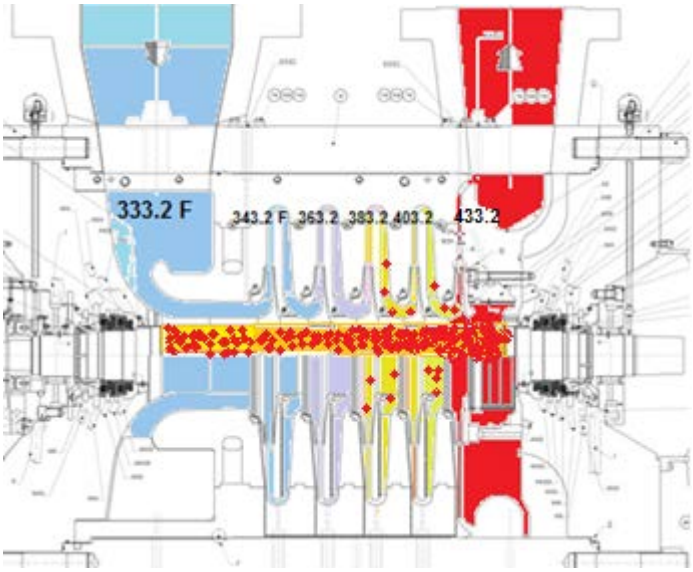

Figure 4—51 simulation of temperature gradient of SRDC1 compressor during operation.

The evidences from filed data and numerical model were not showing any of stresses in the rotor due to any internal rotor rub or temperature variance in the shaft via non-uniform viscous shearing action in the oil film of a journal bearing, as if there is an internal rub it will be considered as instability but in SRDC1 case does not have any sign of instability issue as the high vibration amplitude occurred during hot start only , on other hand the filed orbit plots (Figure 4—46) doesn't showing any unstable divergent behaviour in the compressor end bearings.

Figure 4—52 shows other simulation of temperature condition of SRDC1 compressor which was assumed occur during hot start (less than 25 minutes from last shutdown) as per the field data evidences were recorded , the possibility scenario can occur during hot start that the stopped rotor after shutdown suppose begin to cool at outer surface but because the rotor does not reach its thermal equilibrium, the huge volume (12.25 MMSCMD) of cooled natural gas(65°C) enters through suction of the compressor which is placed on NDE side resulting in sudden cooling of the NDE part of the rotor , the thermal shock occurs on that end of the rotor as the other end of rotor (DE) remain

within hottest condition thus the internal rotor stresses can build to high levels , with tension on the NDE side and compression on the DE side, the thermal stresses develop which adds stresses on the 1st critical speed unbalance mode . The more force added on the hottest end of the rotor (DE) was assumed which probably can excite the original positon of residual unbalance leading to the observed high amplitude on 1st critical speed.

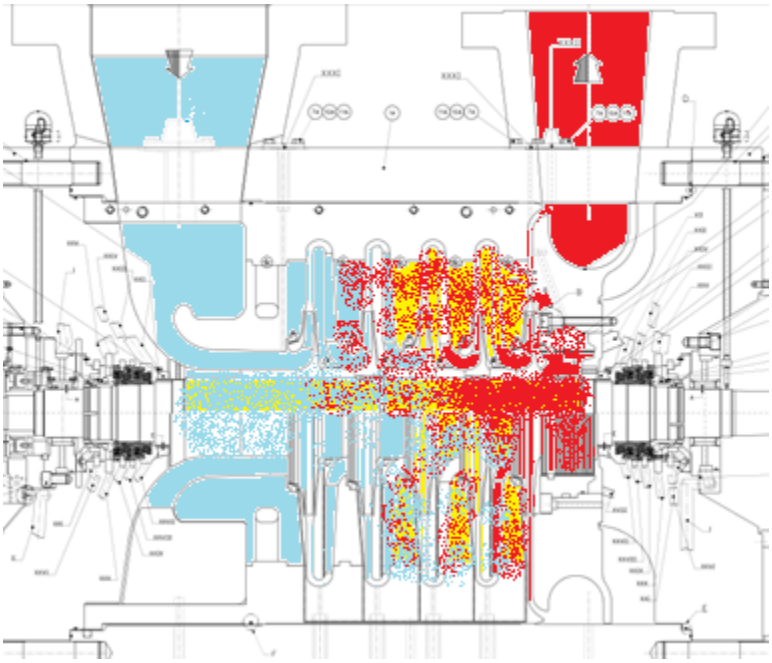

Figure 4—52 simulation of temperature condition of SRDC1 compressor which was assumed occur during hot start

The numerical model was carried out to explore the effect of additional force acting on the rotor DE side as the variance temperature between both rotor ends was assumed to induce an extra mass on the 5th impeller as it was the hottest part on the rotor Equation 4-7 shows the basic imbalance/temperature relationship presented by Brian [58] to determine how much imbalance is produced from bows due to a temperature difference between hot and cold side of the shaft.

$$\vec{U} = \vec{U_{\circ}} + \vec{C}\vec{T} \qquad 4—7$$

Where the $\vec{U}$ is total imbalance vector (oz-in, w/angle), $\vec{U_{\circ}}$ is initial mechanical imbalance vector (oz-in, w/angle), $\vec{T}$ is hot spot/ temperature vector (°F,

w/angle) and $\vec{C}$ is bow coefficient vector (oz-in/°F, w/angle). Hence the vector quantity $\vec{C}$ determines the sensitivity of imbalance to shaft temperature difference, therefore final stage temperature of 433.2 °F and unbalance mass of 3250.8 gm-mm were considered in the calculation to get the final mass. The DE shaft side diameter was assumed as effected area that the final mass result was multiplied by two thus the final mass added in the node 17 (5^{th} impeller) of the model was 13003 gm-mm.

Figure 4—53 and Figure 4—54 show the rotor response at the DE and NDE respectively, from the plots it can be seen that the similarity phenomena of filed plot Figure 4—55, the observation on DE vibration amplitude of model plot and filed plot were 101 um and 102 um respectively and the NDE vibration amplitude of model plot was 88 um and on the filed plot shows 75 um. On the other hand field data plots showed high amplitude due to the variance between the DE and NDE response by 23 um to 25 um , such results show that the used numerical model represent a close condition of the rotor condition as the variance in vibration amplitude was 13 um between DE and NDE .

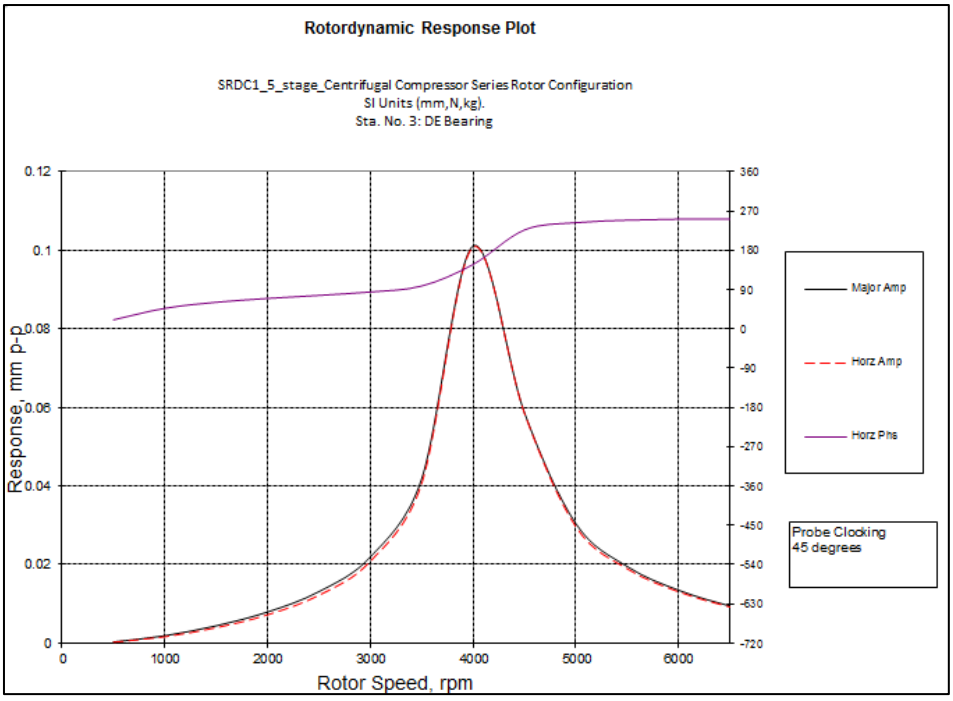

Figure 4—53 DE response plot of nurmaicl model

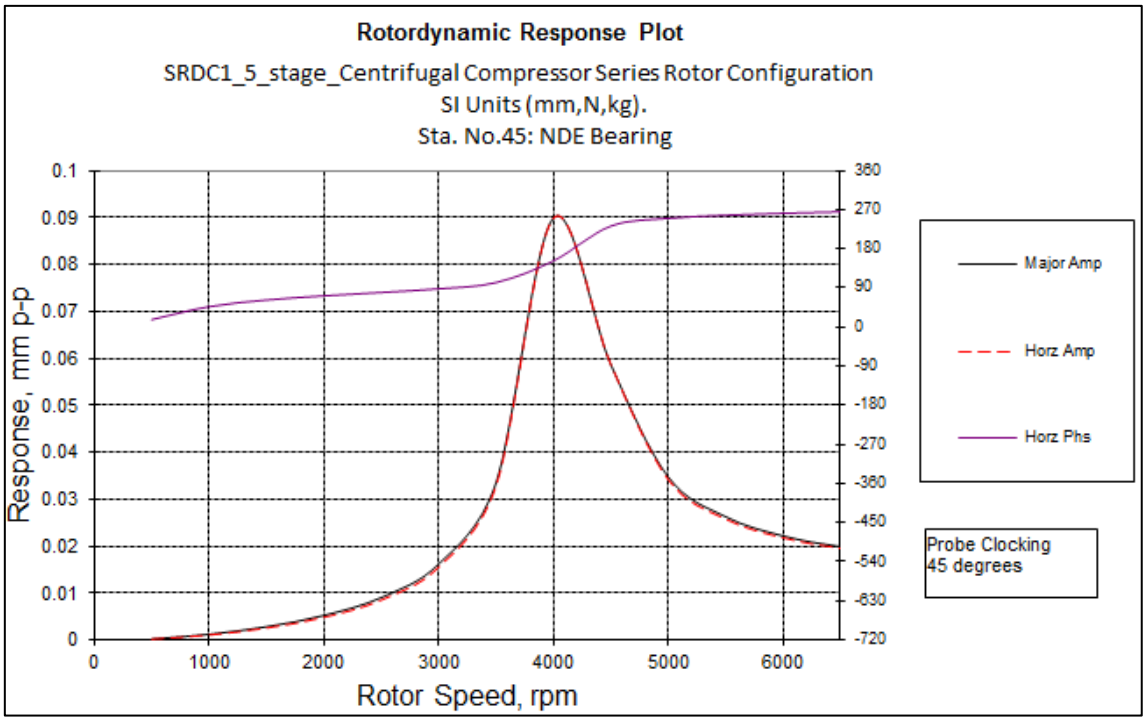

Figure 4—54 NDE response plot of nurmaicl model

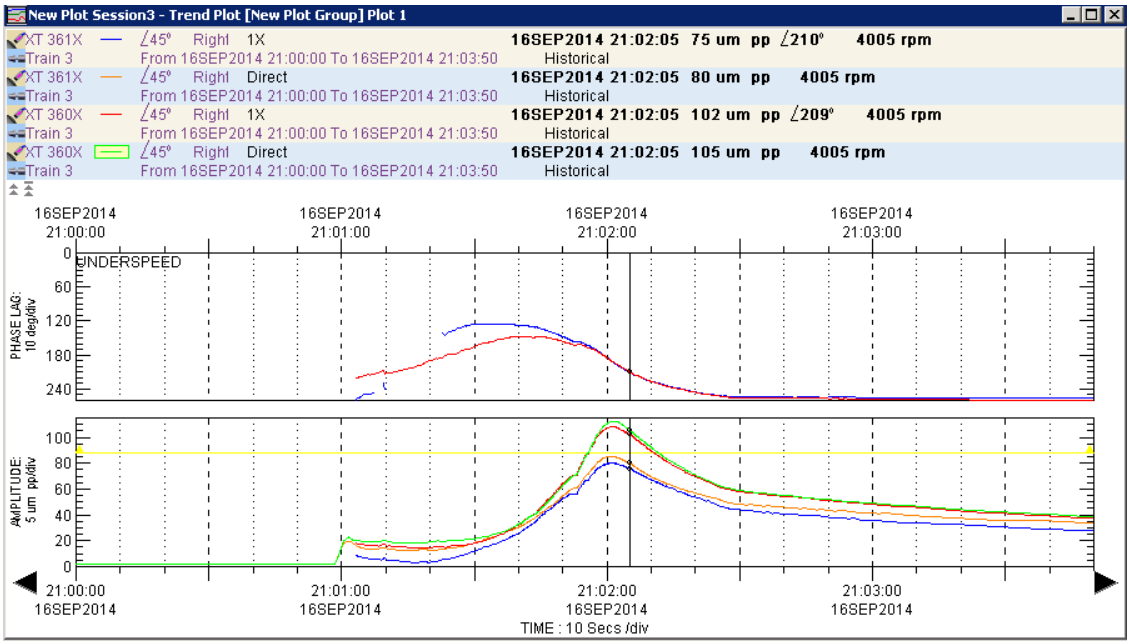

Figure 4—55 Response plots of hot start and cold start

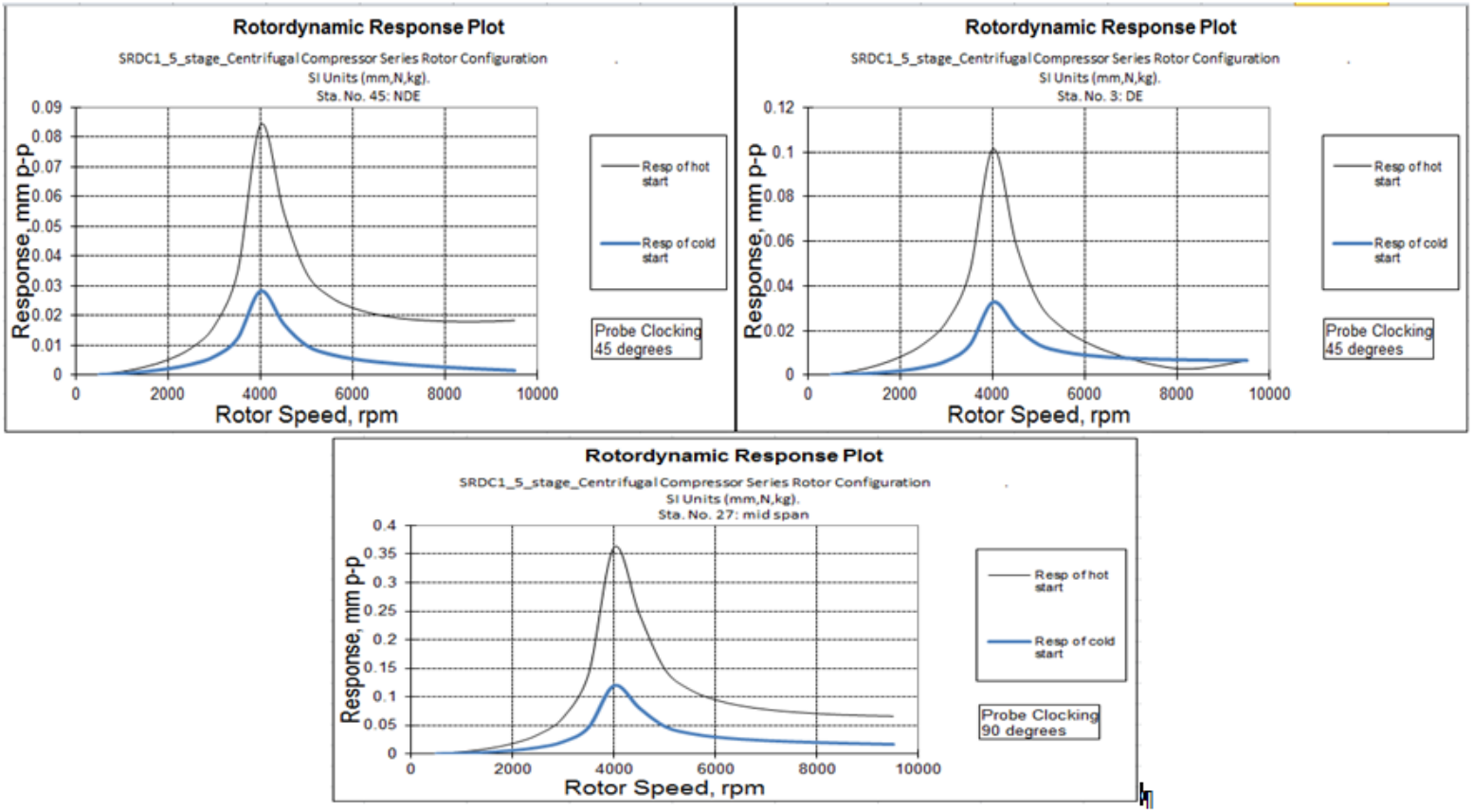

Figure 4—56 Response plots of hot start and colde start

4.2.8.5 Parametric analysis

Different bearing analysis were conducted numerically to determine the high vibration amplitude while traversing its first critical speed during hot start as the main goal to reduce the amplitudes at its critical speed (minimum; 3750 cpm, nominal; 3950 and maximum; 4200 cpm) and avoid bringing the second critical speed in the operating range (minimum operating speed is 5110 rpm and maximum operating speed is 8962 rpm). Two types of approach were considered to discover the correct and most feasible solution for this issue, first approach was modifying the current designed bearings (5 tilting pads, LBP) in terms of bearing preload, bearing temperature and bearing clearances, the second approach is testing different type of bearings such as 4 tilting pads, 6 tilting pads and 7 tilting pads.

Starting with the first approach, nine different cases in table 12 were considered taking in to account the high vibration amplitude during hot start (demonstrated in Figure 4—53) as Figure 4—57 shows different plots for different cases, all cases were showing high amplitude as the lowest amplitude was 70 um within case 1. None of the designed bearing conditions solve the existing high vibration problem (refer to table 7).

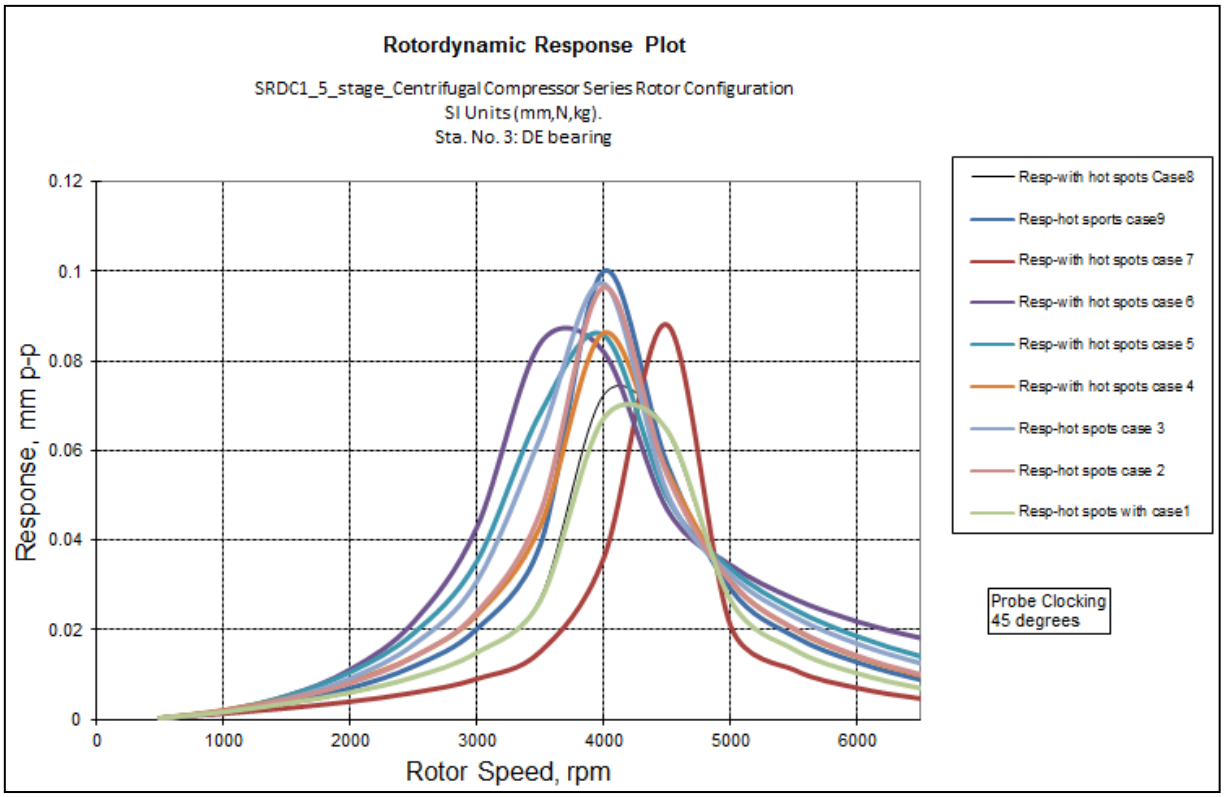

Figure 4—57 DE bearing responses of all nine cases during hot start

Figure 4—58 shows a plot of DE bearing amplitude responses considering different bearing preloads at 50 C° lube oil temperature. As it can be seen from the plot a preload of 0 and 0.1shows the lowest respond at hot start as the amplitude was reduced from 101 um of 0.6 preload to 58 um and 59 um respectively (see Figure 4—59). Other analysis were carried out with lube oil temperature of 60C° and preloads of 0 and 0.1, the results as shown in Figure 4—60 indicates highest responses compared with the responses in Figure 4—59 by 3 um and 8 um respectively .

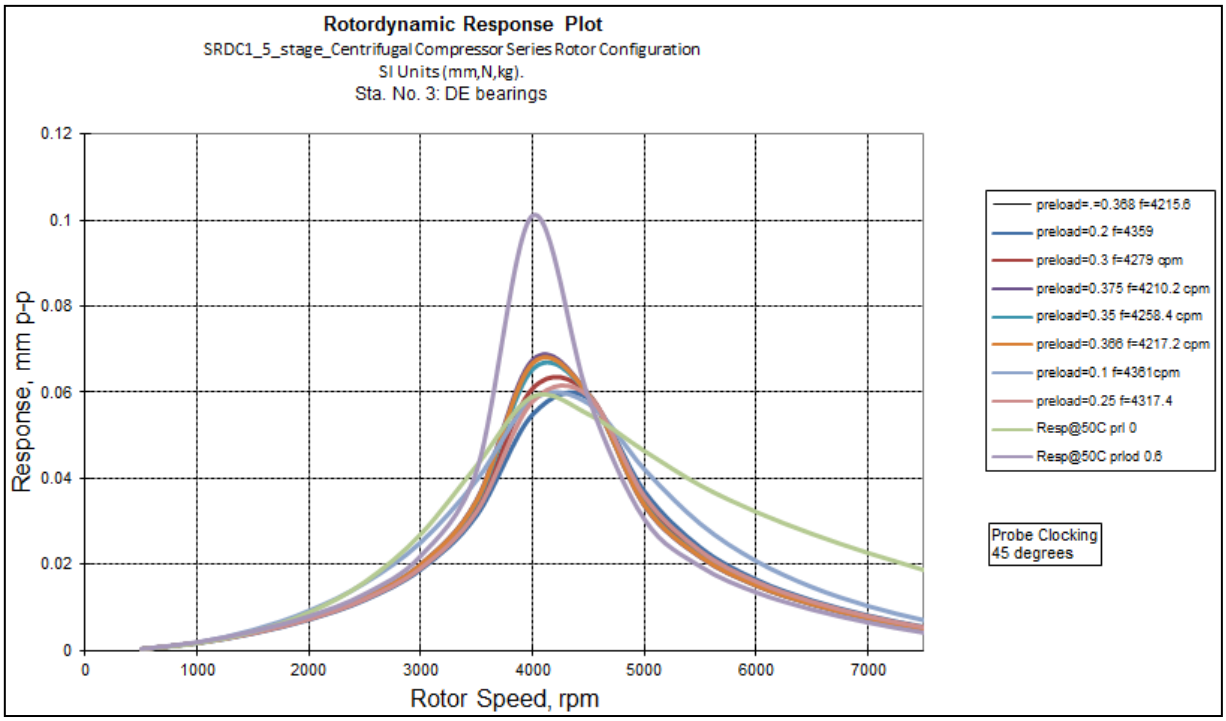

Figure 4—58 DE bearing Response plots of hot start with different bearing preload at T=50 C°

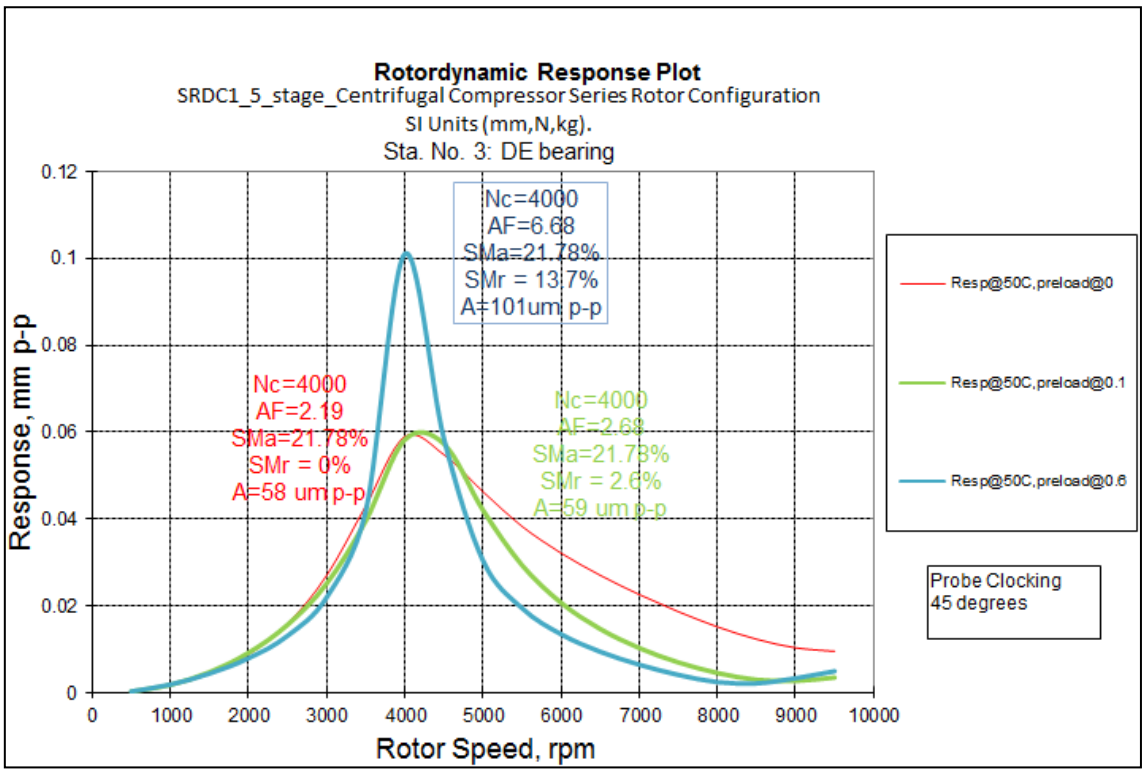

Figure 4—59 response plot of DE bearing with different preloads@ T=50 C°during hot start

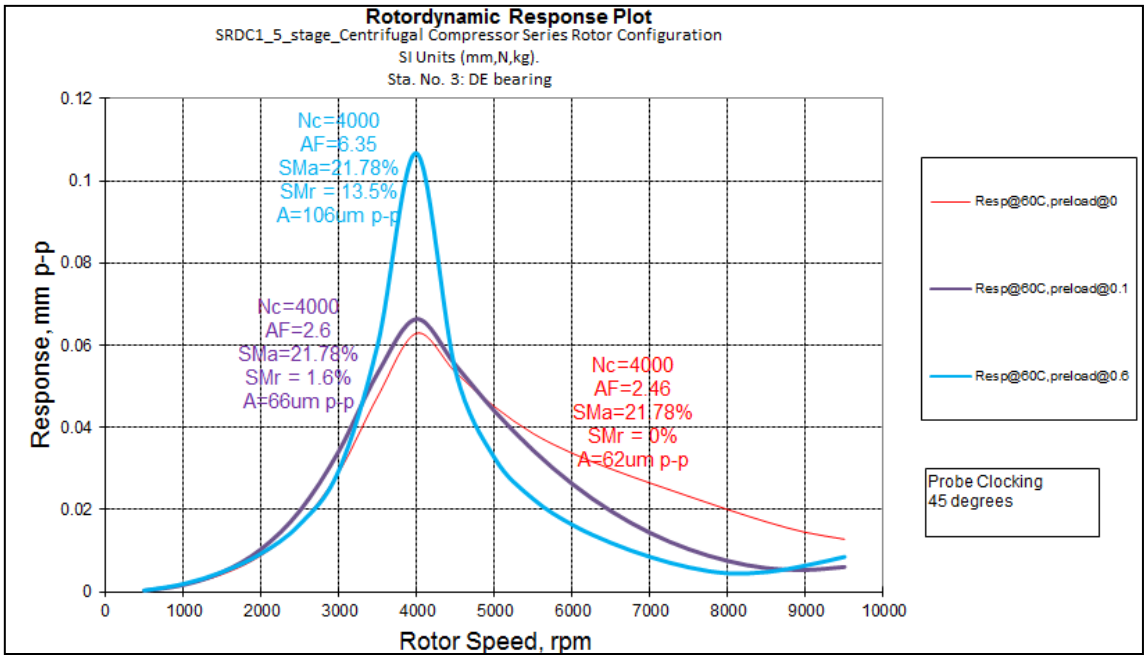

Figure 4—60 response plot of DE bearing with different preloads@ T=60 C°during hot start

Lowering the preload resulted in more effective damping which in turn reduced the amplitude without affecting the critical speed. Also observed in this analysis with both bearing preload 0 and 0.1 at lube oil temperature 50C° is the critical speed shift by 133 cpm and 320 cpm respectively see Figure 4—61 and Figure 4—62 this phenomena may occur due to lower lube oil temperature (higher viscosity) which leads to more effective damping while the bearing stiffness remains approximately constant as the variance is negligible [8] , on the other hand the analysis with bearing preloads 0 and 0.1 at 60 C° temperature resulted in the critical speed being reduced for both preloads by 178 cpm and 185 cpm respectively see Figure 4—63 and Figure 4—64 which supports the confirms that this is mainly due to oil viscosity becoming less due to oil temperature increment.

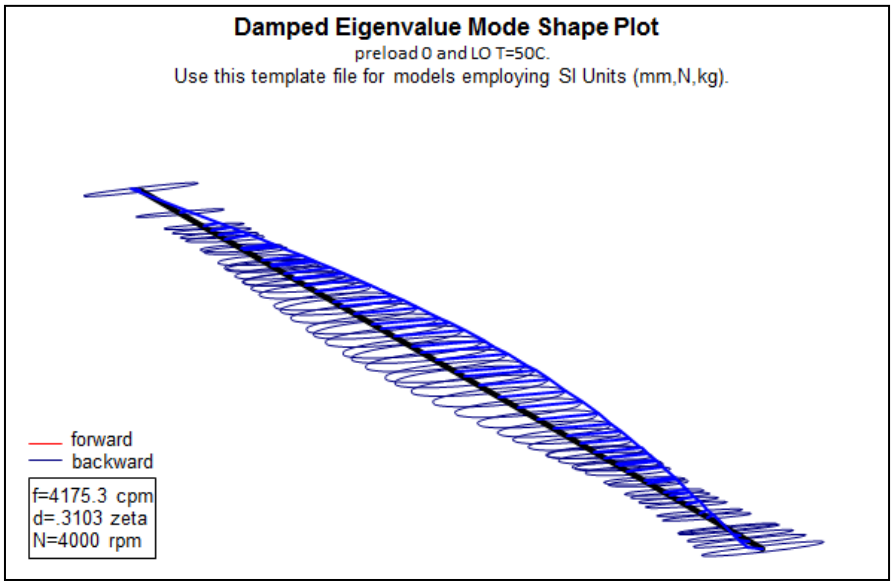

Figure 4—61 damped Eigenvalue mode shape plot of DE bearing with preload 0, temperature 50C during hot start

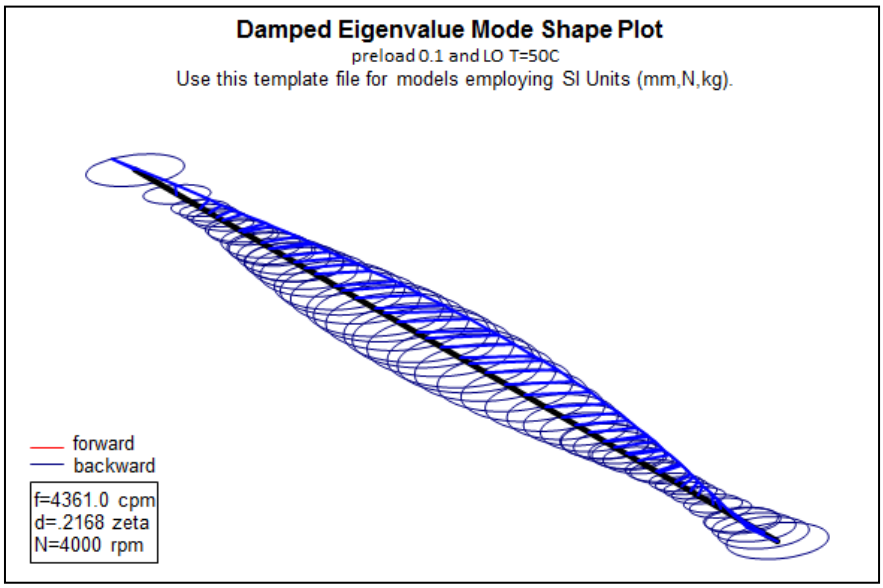

Figure 4—62 damped Eigenvalue mode shape plot of DE bearing with preload 0.1, temperature 50C during hot start

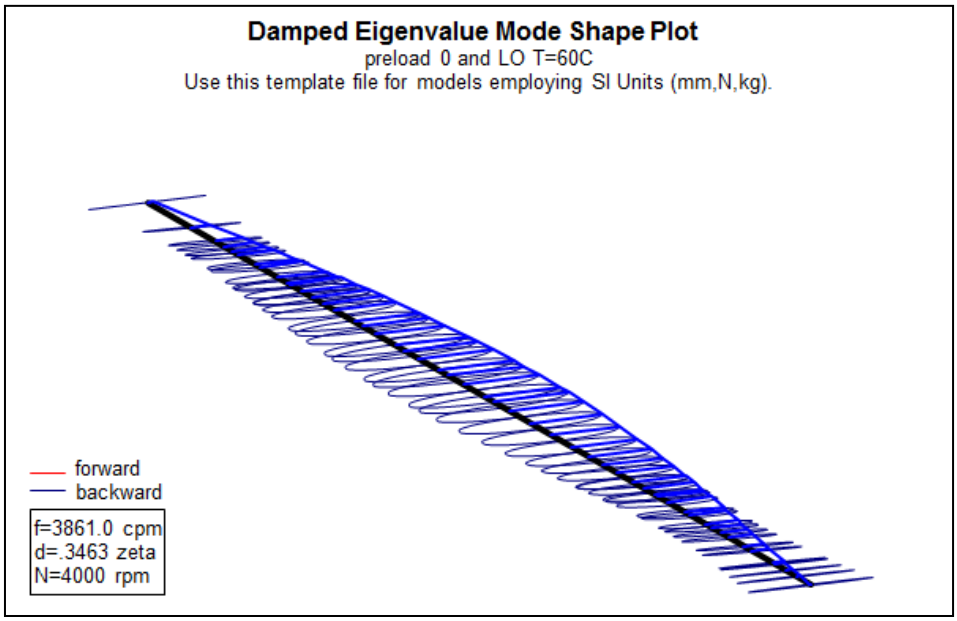

Figure 4—63 damped Eigenvalue mode shape plot of DE bearing with preload 0, temperature 60C during hot start

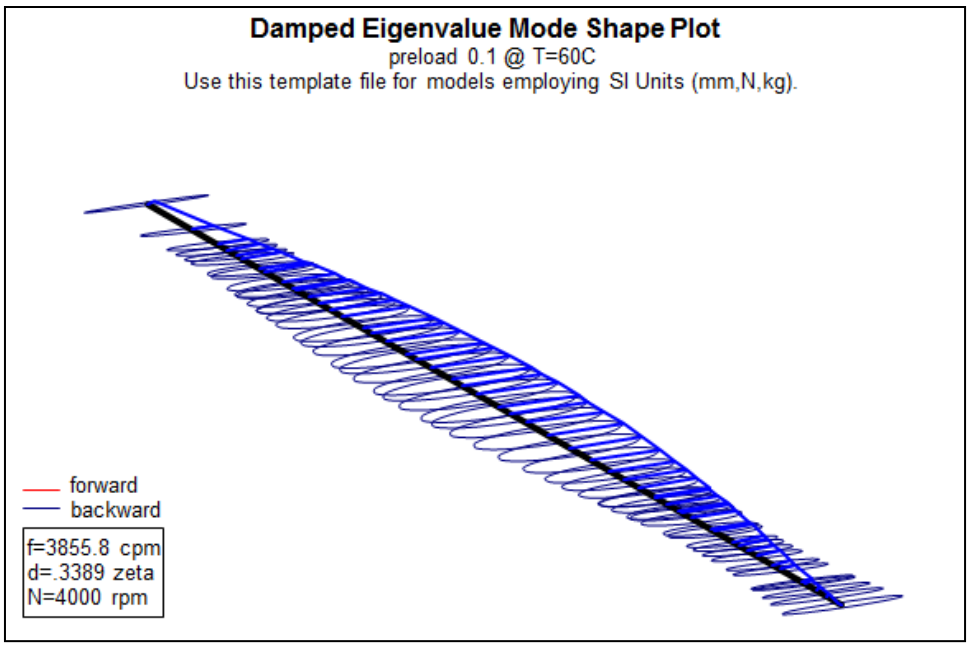

Figure 4—64 damped Eigenvalue mode shape plot of DE bearing with preload 01, temperature 60C during hot start

Figure 4—65 shows the numerical response of the DE bearing during shutdown using a bearing preload of 0.1 at LO temperature of 50C, the vibration amplitude improved when compared before the modification as it was around

35 um and after modification it is 22 um, this is due to bearing effective damping being increased as well as the damping from the aerodynamic load.

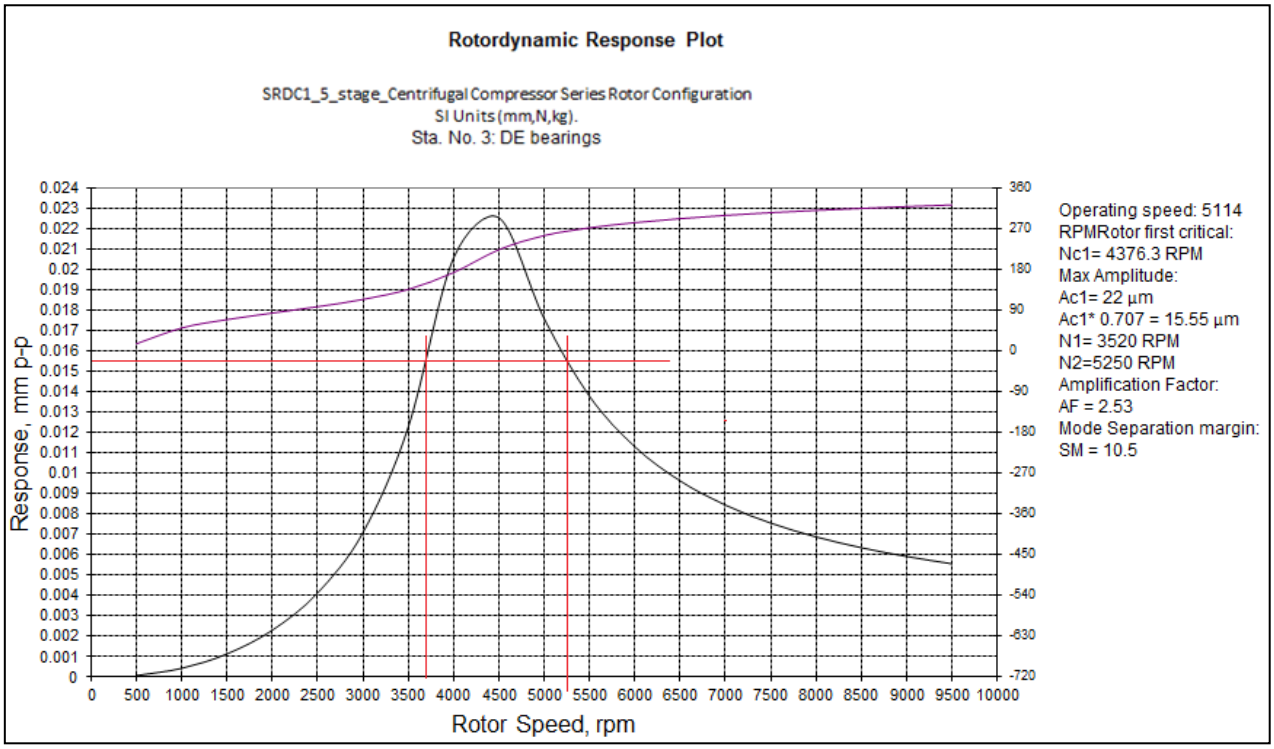

Figure 4—65 response of DE bearing during shutdown consider the bearing modified with preload 0.1

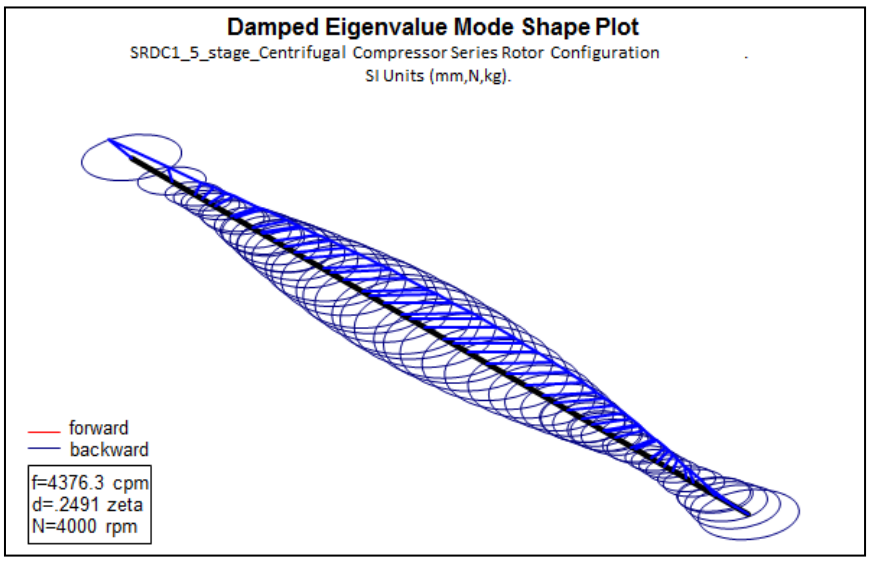

Figure 4—66 Damped Eigenvalue mode shape during shutdown consider the bearing modified with preload 0.1 and temperature 50C

Indeed the lowest amplitude response was observed at a bearing preload of zero but a bearing preload 0.1 at lube oil temperature 50C is recommended using to solve the issue as below reasons:

1. Zero preload has disadvantages, first the tolerance range on the journal diameter, the pad radius of curvature and the assembled bearing clearance can all contribute to creating a negative preload, second problem is the loss of damping when the top pads become unladed which could affect the top unloaded pads flutter, the fluttering pad may cause rotor vibration [8].
2. The response will have faster vice versa as the Amplification Factor of bearing preload 0.1 higher than AF of bearing preload zero.

The second approach was implemented numerically to identify any possibilities for other different type of bearings to provide more positive results to reduce the vibration amplitude during hot start. To achieve this variance bearings were selected to examine them numerically, Figure 4—67 response plot of DE bearing with different types of bearing shows the result from this analysis.

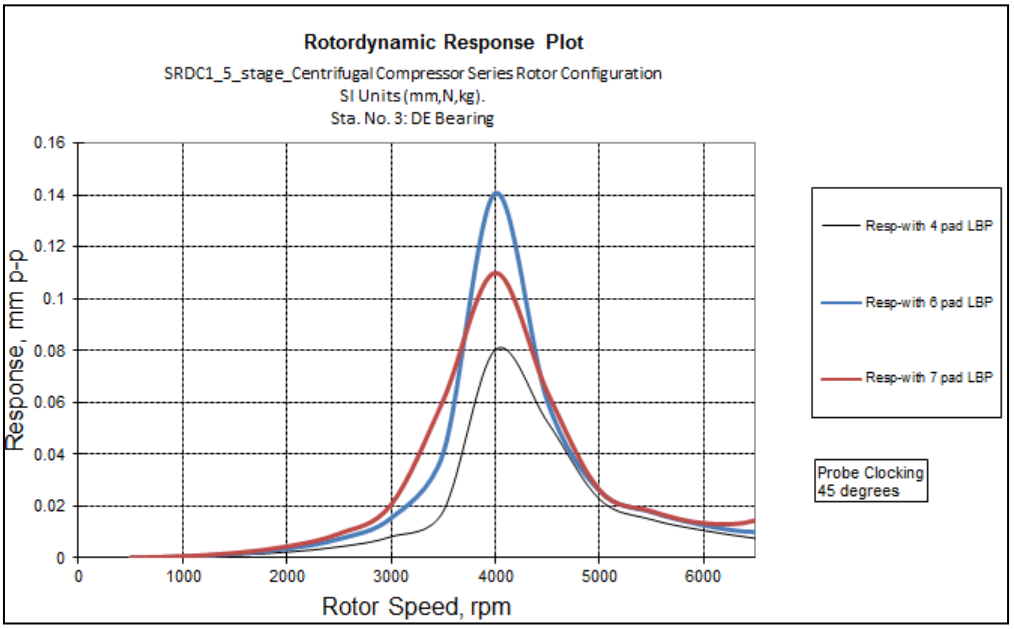

Figure 4—67 response plot of DE bearing with different types of bearing

4.2.8.6 Case-2: Field Observation on high vibration was gradually appearing on gearbox pinion bearing side of SRDC1 compressors during operating speed.

All four compressors (K-5410-KC, K-5420-KC, K-5430-KC and K-5440-KC) have been commissioned in May 2010 and since then there were many trips occurred due to high vibration on gearbox pinion bearing side for all compressors. The Field data of all compressors which observed from Bentley Nivada system 1 were showing similar phenomena thus two compressors (K-5420 and K-5430) data were selected to shows the behaviour of rotordynamics as below observations:

1. High vibration amplitude on Gear box output shaft bearing with probe tags of 54-XI-247X and 54-XI-347X (Figure 4—68 indicates probe location) appeared within compressor speed between 7481 rpm – 7795 rpm as shows in compressor trend plots Figure 4—69 and Figure 4—70.

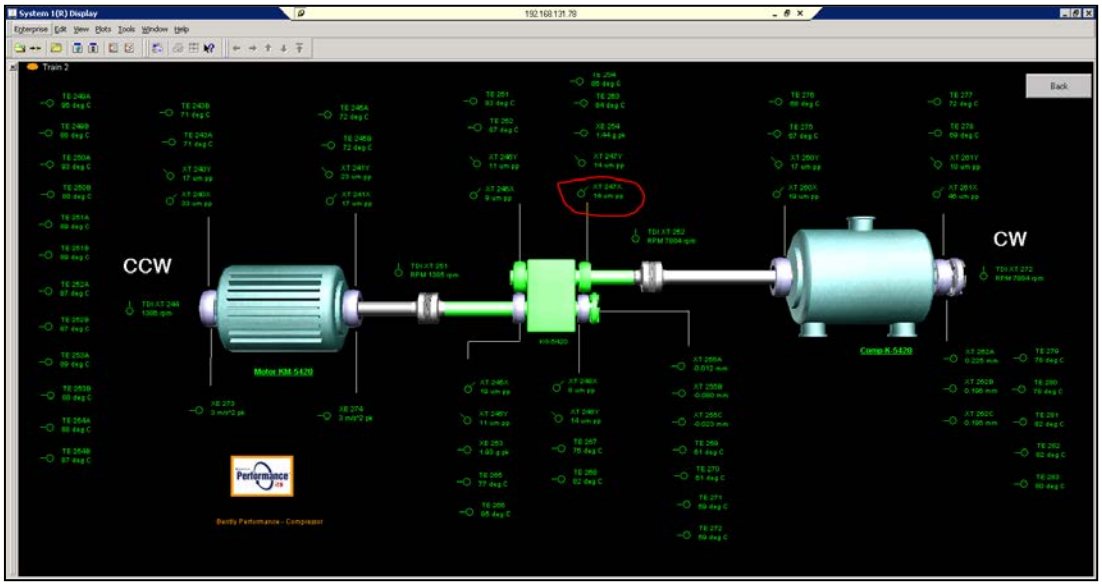

Figure 4—68 compressor remote desktop overview from BN system 1

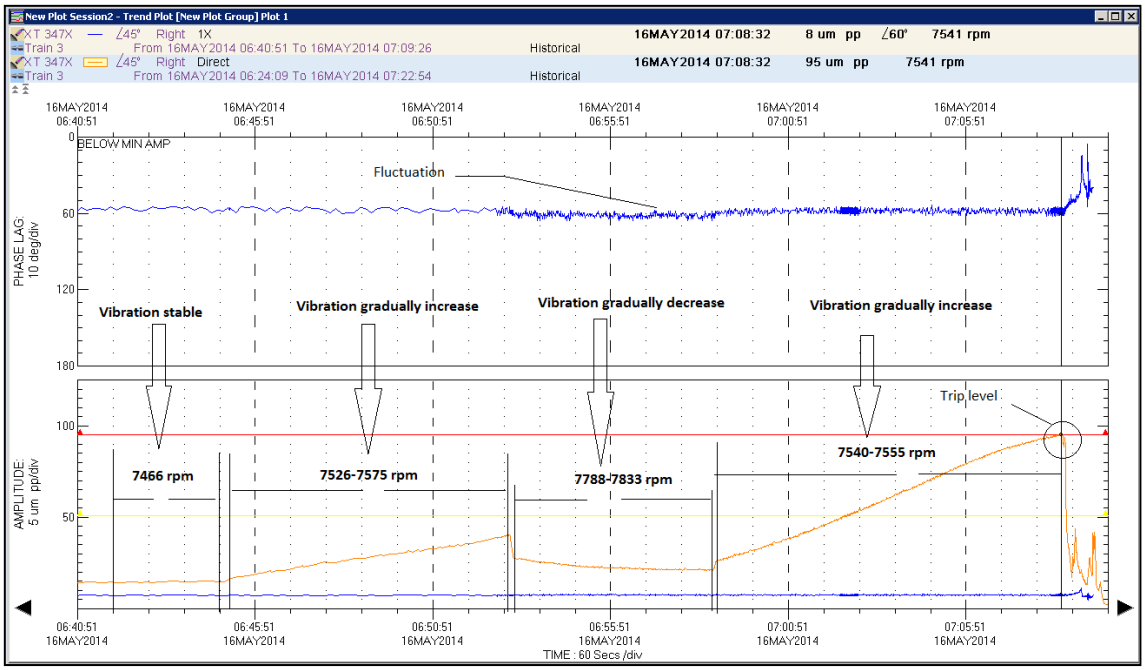

Figure 4—69 K-5430 Trend plot

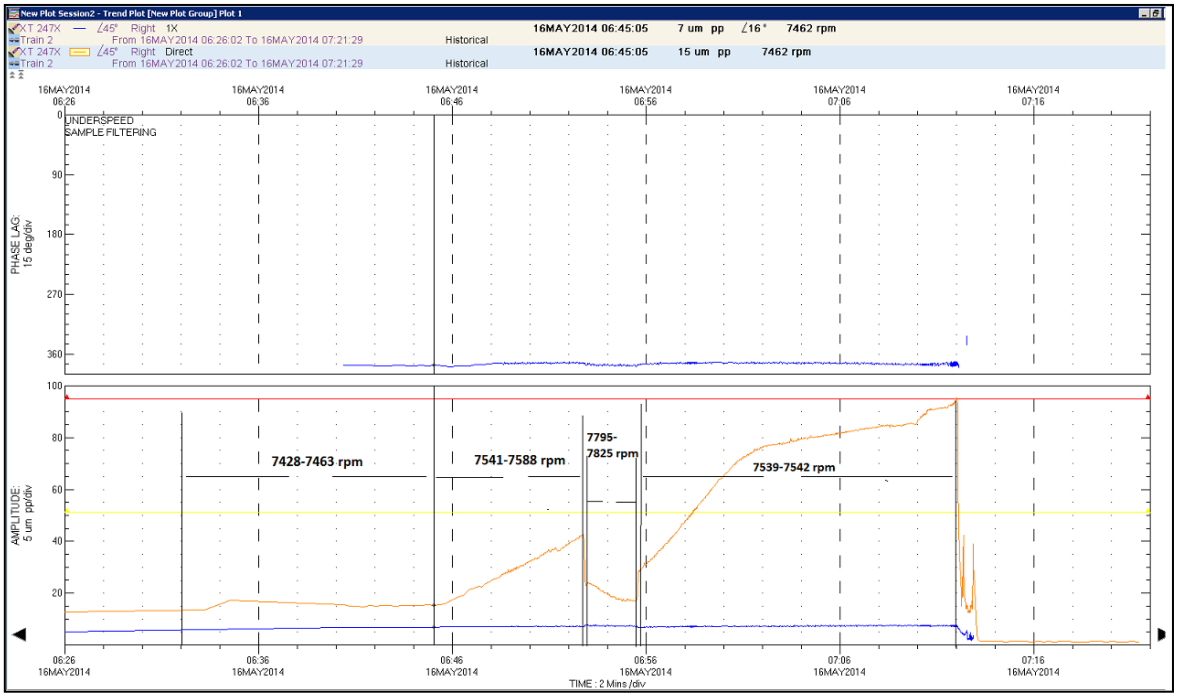

Figure 4—70 K-5420 Trend plot

2. Also within same probes mentioned in the first point , the high vibrations were appeared during compressor start-up , Figure 4—71 shows vibration trends of K-5420 and K-5430 as the top trends show the high vibration amplitude at speed around 1728 rpm and 3230 rpm , the bottom trend shows almost similar vibration amplitude at speed around 1740 rpm and 3229 rpm.

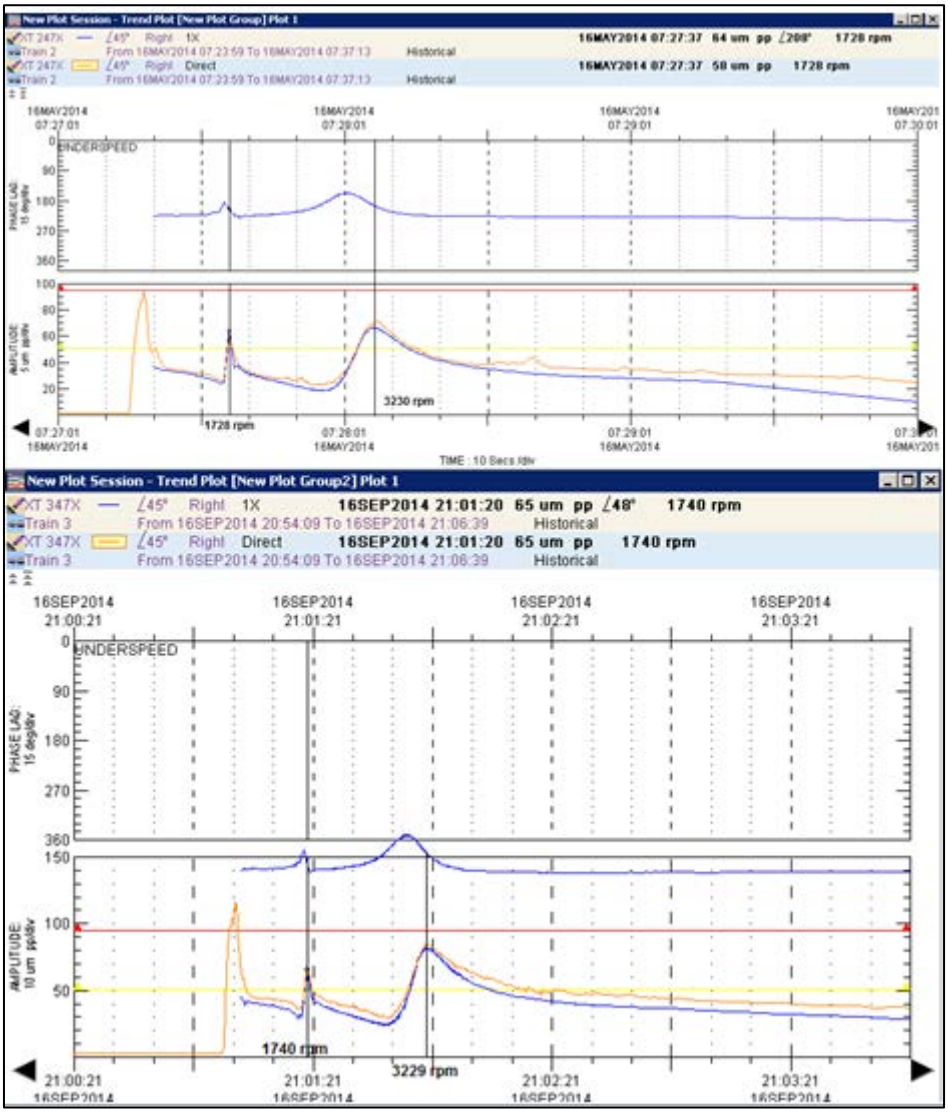

Figure 4—71 Top plotof K-5420 and bottom plot for K-5430

3. Figure 4—72and Figure 4—73 show spectrum plots of the same probes indicating many frequencies, both plots with almost similar values such as 22Hz, 28Hz, 53Hz and 125Hz.

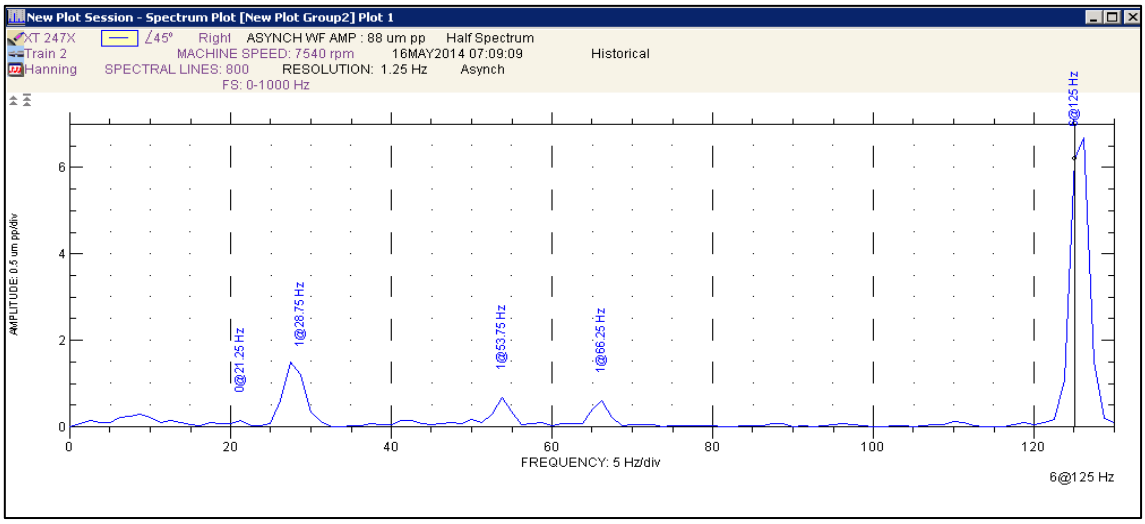

Figure 4—72 Specturm plot for K-5420

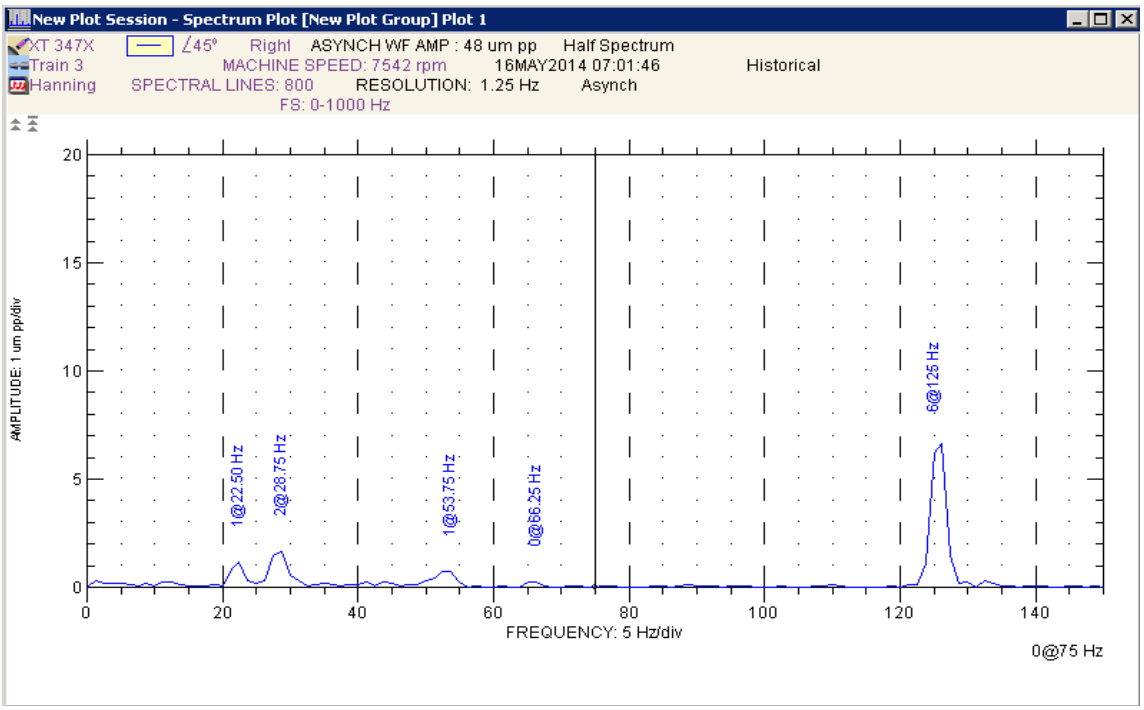

Figure 4—73 Specturm plot for K-5430

4. The frequencies which are mentioned in previous point were clearly indicated in the waterfall plots in Figure 4—74 and Figure 4—75 , also other new frequencies appeared in those plots such as 102Hz in top plot and 105Hz in bottom plot.

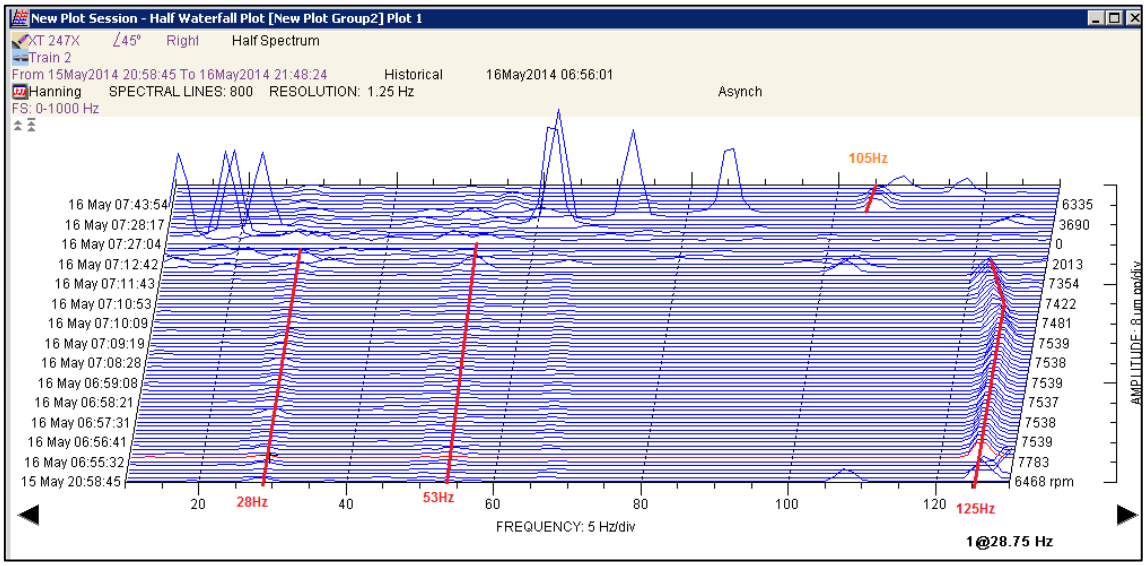

Figure 4—74 waterfall plot for K-5420

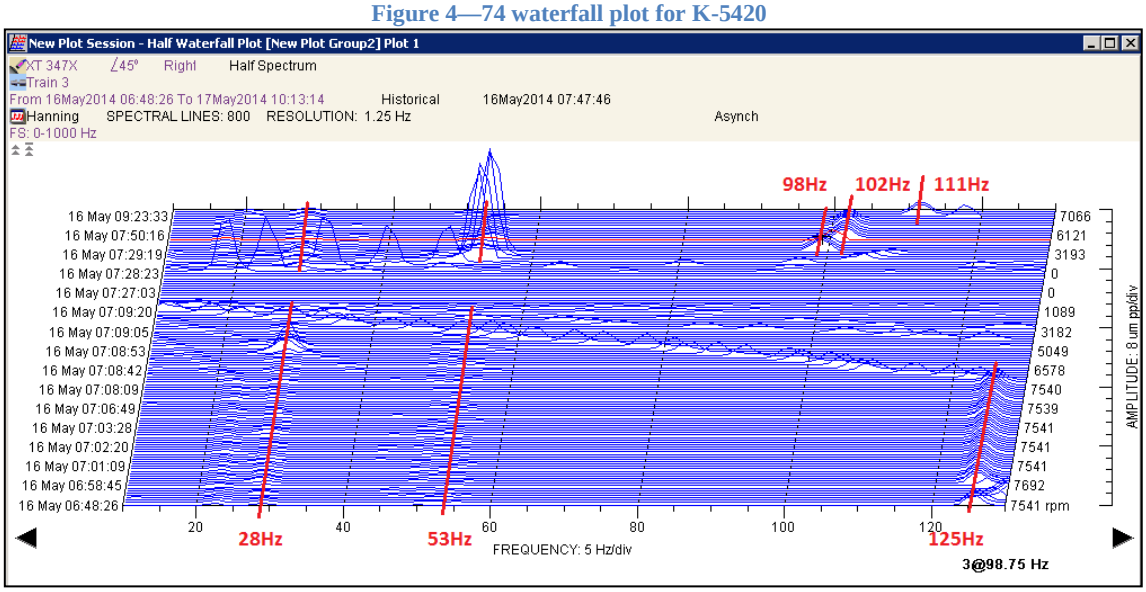

Figure 4—75 waterfall plot for K-5430

4.2.8.7 Compressor rotordynamic model – Torsional analysis

The field data observations which are highlighted in the previous section highlight the possibility of torsional problems due to the variance in the frequencies being recorded also due to the train configuration which is prone to such problems. Moreover the likelihood of torsional pulsations in SRDC compressors are high because the units are driven by VFD motor which is well known for its torsional excitation source, VFD motors play vital role in coupling failure [60]. Also in many cases the torsional oscillations can be seen as lateral

vibrations on gear or pinion, the relationship between the lateral and torsional explained by Kita, Hataya and Tokimasa [59]. Hence the torsional analysis is conducted to assess the likelihood of any correlation between the high amplitude response observed at the Gear box output shaft bearing and possible torsional natural frequencies excitation.

Torsional analysis needs the whole train unit i.e. Motor, Low Speed coupling, pull Gear, pinion Gear, High speed Coupling and Compressor (see Figure 4—7) to be modelled. A numerical model of SRDC train was generated as showing in Figure4—76

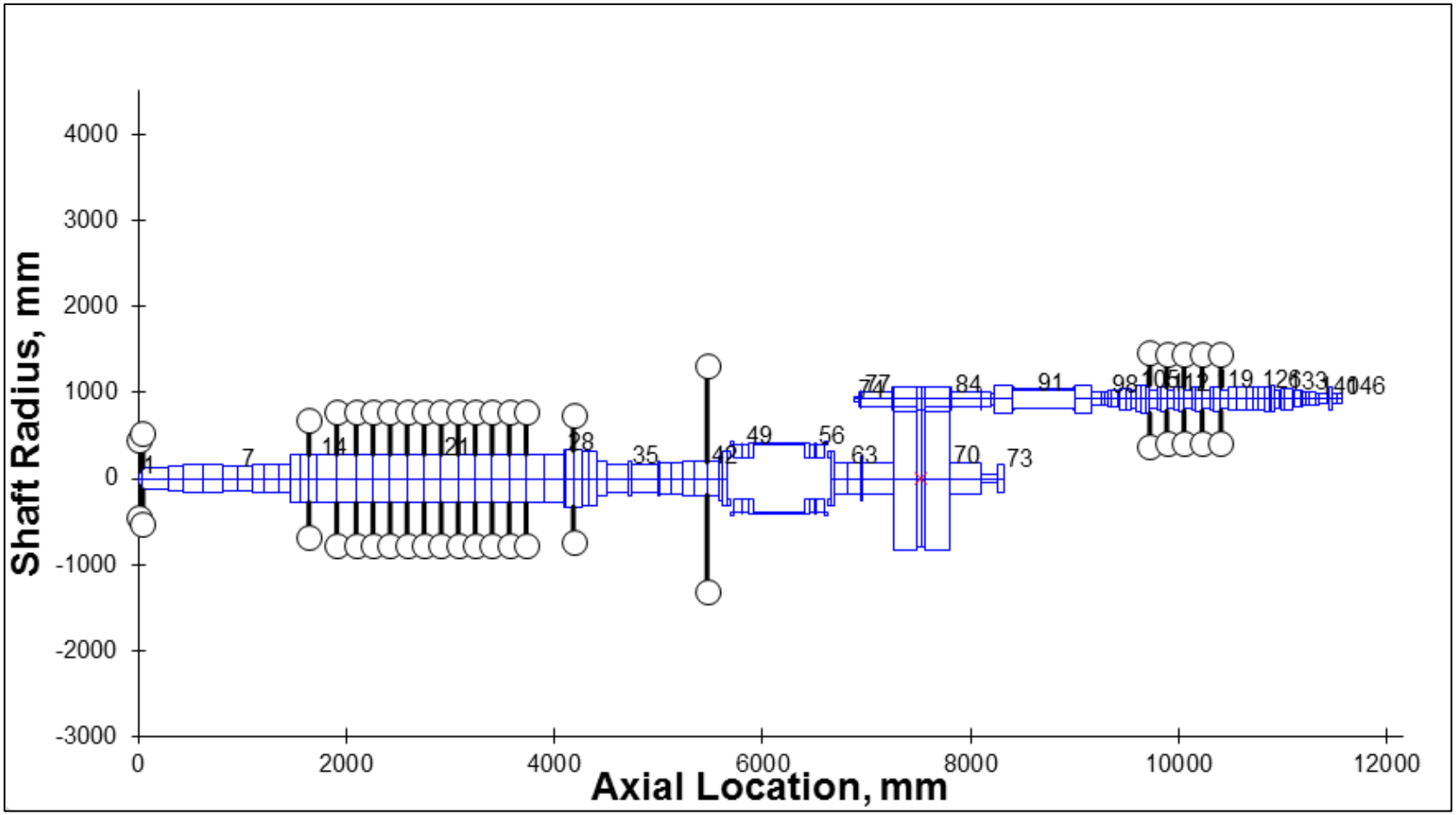

Figure 4—76 complete train numerical model

Torsional interference diagram was generated to discover the possibility of any torsional frequency being the root cause of the high peak observed in the Gear box output shaft bearing during initial train start-up and during the operating running speed. Figure 5-93 shows the complete train torsional map, from the diagram it can be observed that many torsional frequencies allocated within all three orders, in order 1 the frequencies appeared 35Hz, 87Hz and 105Hz, in second order the frequencies appeared 16.6Hz, 42Hz and 53Hz, the frequencies 28Hz and 35Hz appeared in order 3.

However the waterfall plots in Figure 4—74 and Figure 4—75 were clearly showing some of the frequencies existed similar to what it appears in the numerical model (Figure 4—77) such as 28Hz, 53Hz and 105Hz. The frequencies of 125 Hz did not appear in the numerical model.

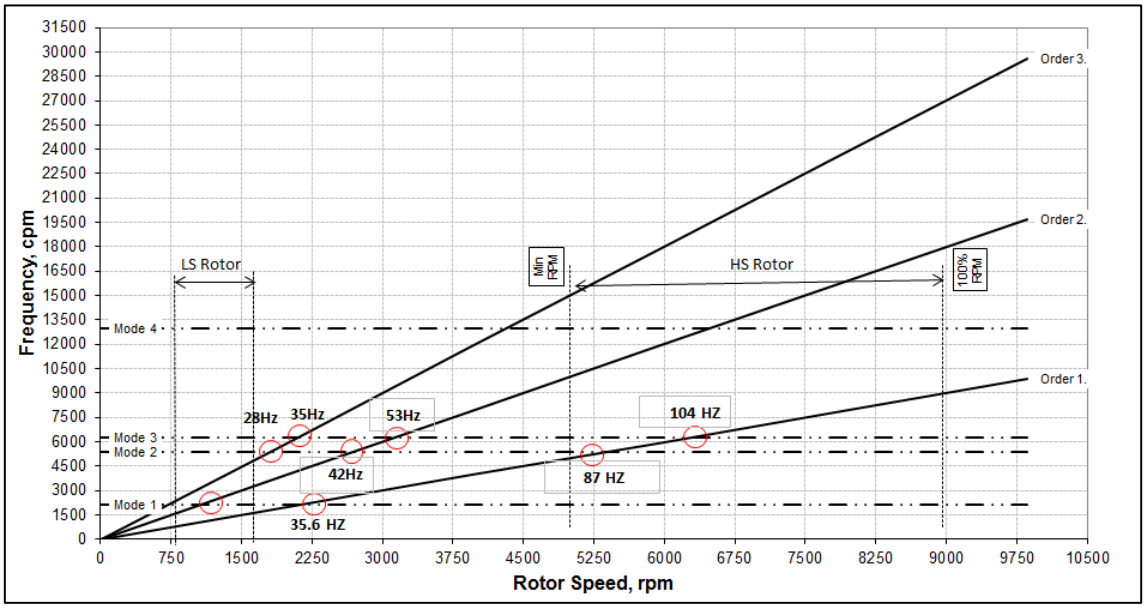

Figure 4—77 SRDC Torsional interference diagram

5 Conclusion and recommendations

5.1 Conclusion

The influence of centrifugal compressor system components such as bearing, seal, rotor system assembly and thermal temperature gradients across rotors have direct impact on turbomachinery rotordynamics behaviour in terms of performance and stability. The numerical analysis and experimental data from the field were used to verify and demonstrate the influence of those factors on centrifugal compressor rotordynamics. Different bearing analysis were conducted during this thesis which shows how bearings have direct influence on rotating machines , for that the consideration of bearing design is vital for having reliable machine during operation period and also while solving rotordynamics problems.

Aerodynamics forces generated by the balance piston seal, impeller seal and shaft seal affect the efficiency, performance and rotordynamics behaviour of the compressor.

Compressor's Rotor is the main part in centrifugal compressor which consists of a solid shaft, impellers, spacers (sleeves), thrust collar and balance piston. Normally there are two methods using to assembly the rotor components into the shaft; these are thermal fit and hydraulic shrink fit process. Hydraulic fit method is mostly used for single stage rotor assembly / disassembly because most designs consider impeller disassembly for seal, the thermal fit method is used for all multistage rotor assembly which is assembled vertically for ease of assembly and to reduce residual shaft stresses, also the rotor mounting methods play a main role in stiffening the compressor rotor which has direct impact on critical speed.

The rotor thermal effect is a hidden factor which influences the rotordynamics behaviour as the field data along with the numerical analysis provide a valuable combination on explaining the influence of the high 1X vibration amplitude while traversing its 1^{st} critical speed during centrifugal compressor hot start-up.

The four identical centrifugal compressors each one is designed at rated flow of 12.25 MMSCMD of wet gas with suction pressure varying from 35 bara to 65 bara and discharge pressure of 100 bara . Those compressors have identical rotordynamic problems which is the high levels of rotor vibration while traversing its first critical speed during hot start only, also the sudden high vibration appearing on the gearbox pinion bearing side during MOCS, the two different phenomena's were divided in this thesis in to two different cases to investigate them numerically. The results of those analyses conclude that the observed rotordynamic problems are related to design issue.

The first case of high amplitude vibration occurred while traversing its 1^{st} critical speed during hot start was investigated numerically. The different rotordynamic affects were rolled out in terms of direct influence on this case such as force coefficients (direct and cross-coupled coefficients) and rotor unbalance effect. The temporary thermal bow was suspected to be the reason of this phenomenon; therefore a detailed investigation has been conducted numerically to investigate the thermal bow effect at 1^{st} critical speed. The evidences from filed data and numerical model were not showing any phenomena of internal rotor rub or any sign of Morton effect which both are mainly caused by rotor thermal bow (refer to section 4.2.12) so the effect of rotor rub and Morton effect were rolled out either .

SRDC1 case does not have any sign of instability issue as the high vibration amplitude occurred during hot start only and at critical speed, on the other hand orbit plots don’t show any unstable behaviour in the compressor end bearings. the possible scenario can occur during hot start that the stopped rotor after shutdown begins to cool at outer surface but because the rotor does not reach its thermal equilibrium, the huge volume (12.25 MMSCMD) of cooled natural gas(65°C) enters through suction of the compressor which is placed on NDE side resulting in sudden cooling of the NDE part of the rotor , the thermal shock occurs on that end of the rotor as the other end of rotor (DE) remains within hottest condition thus the internal rotor stresses can build to high levels , with tension on the NDE side and compression on the DE side, the thermal

stresses develop which adds forces (unbalanced) on the 1st critical speed mode.

For that the numerical model was carried out to explore the effect of additional force acting on the rotor DE side as the variance temperature between both rotor ends was assumed to induce an extra mass on the 5th impeller as it was the hottest part on the rotor. Equation [58] was used to determine how much imbalance is produced from bow due to temperature difference between hot and cold side of the shaft. The results from the numerical model shows similar phenomena of that observed on the site as the DE vibration amplitude of model plot and field plot were 101 um and 102 um respectively and the NDE vibration amplitude of model plot was 88 um and on the field plot shows 75 um . On the other hand field data plots showed high amplitude due to the variance between the DE and NDE response by 23 um to 25 um , such results show that the used numerical model represent a close condition of the rotor condition as the variance in vibration amplitude was 13 um between DE and NDE .So with all evidences of this study confirm that the main reason of high amplitude vibration occurred while traversing its 1st critical speed during hot start was a result of thermal bow, the huge cold gas volume enters on NDE side while the rotor still hot in equilibrium mode and with sudden thermal shock occurs on that end of the rotor as the other end of rotor (DE) remain within hottest condition thus the internal rotor stresses can build to high levels , with tension on the NDE side and compression on the DE side, the thermal stresses develop which adds stresses on the 1st critical speed unbalance mode. Force response analysis was conducted to solve this issue; the bearing is the simplest part to investigate through it to reduce the high amplitude response. Finally the conclusion to solve this issue is to change the bearing preload from 0.6 to 0.1 with same inlet lube oil temperature (50°C) resulting in the response amplitude being reduced to 59 um from 101 um,

The second case of high vibration appeared on gearbox pinion bearing side of SRDC1 compressors during start-up and operating speed was investigated numerically. The torsional interference diagram Figure 4—77 indicated some of

natural frequencies which it could be excited by different harmonics that may be excited by the VFD motor. So a torsional harmonic response analysis must be considered to evaluate the severity of such mode on the rotordynamics behaviour of the train.

5.2 **Recommendations**

If the results and conclusion of this research are to be considered to solve PDO SRDC compressors rotordynamic issues the below recommendations should be implemented:

In case 1:

1. For short term solution, all four SRDC compressors should not start with hot condition as the filed data's show the high amplitude observed in 1st critical speed during start up within period less than 40 minutes from last shutdown so that thermal equilibrium is ensured
2. For long term solution, the bearings preload should be modified reduced from 0.6 to 0.1
3. For future consideration, the hot start test during Factory Acceptance Test should be performed specially for compressor with specification of single stage, long rotor span and hug gas volume.

In case 2:

Since the train designed with many torsional natural frequencies, the following points could be considered to mitigate the existing problem:

1. VFD motors generate many harmonics which could excite the natural frequencies, therefore harmonics filter is recommended to isolate the excitation frequencies
2. Implement critical speed skip bands on all 4 VFDs (tag numbers K5410, K5420, K5430, K5440) as shown in the below table to avoid torsional excitation to the system.

Speed BANDs	Motor Speed Rang (RPM)	Corresponding to Compressor Speed Rang (RPM)
BAND 1	305-567	1740 - 3230
BAND 2	1330 – 1370	7481 – 7795
BAND 3	1420 -1440	8079 - 8193

5.3 **Recommendations for future work:**

Further study is required to approve theoretically the rotor thermal effect which influences the rotordynamics behavior, indeed in this research the field data along with the numerical analysis provide a valuable combination on explaining the influence of the high 1X vibration amplitude while traversing its 1st critical speed during centrifugal compressor hot start-up.

Also more effort is required to study the Torsional vibration which is influenced with different force such as VFD motors harmonics surrounding the compressor.

6 REFERENCES

[1] " Petroleum development Oman, Training package PTP 11, Reciprocating Compressor,2002.", .

[2] Rolls-Royce plc 1986 ,fifth edition , reprinted 1996 with revisions, The Jet Engine, © Rolls-Royce plc , (1986), fifth ed, Rolls-Royce, England.

[3] "Petroleum Development Oman, Training Package PTP 11, Centrifugal Compressors,2002", (2002), .

[4] DEP SPECIFICATION , DEP 31.29.40.10-Gen, September 2011, COMPRESSORS – SELECTION, TESTING, AND INSTALLATION ,Copyright Shell Group of Companies.(September 2011), , Copyright Shell Group of Companies. ed., shell, U.S. government.

[5] Bently, D. E. and Hatch, C. T. (2002), Fundamentals of rotating machinery diagnostics, Amer Society of Mechanical.

[6] Kirk, R. and Miller, W. (1979), "The influence of high pressure oil seals on turbo-rotor stability", ASLE transactions, vol. 22, no. 1, pp. 14-24.

[7] Ludtke, K. H. (2004), "Process centrifugal compressors", chapters 1&2 Springer-Verlag Berlin Heidelberg, .

[8] Nicholas, J. C. and Wygant, K. (1995), "Tilting pad journal bearing pivot design for high load applications", Proceedings of the 24th turbomachinery symposium, Vol. 1, pp. 179.

[9] San Andres, L. (2009), "Notes 11. High pressure floating ring seals", Available electronically from http://hdl.handle.net/1969, vol. 1, pp. 93251.

[10] Scharrer, J. K. and Pelletti, J. M. (1995), "Leakage and Rotordynamic Effects of Compressible Annular Seals", Proceedings of the Twenty-Fourth Turbomachinery Symposium, pp. 175.

[11] Semanate, J. and San Andres, L. (1994), "Thermal analysis of locked multi-ring oil seals", Tribology International, vol. 27, no. 3, pp. 197-206.

[12] Semanate, J. E. and Andres, L. S. (1993), "Analysis of multi-land high pressure oil seals", Tribology Transactions, vol. 36, no. 4, pp. 661-669.

[13] Standard, A. (2002), "617, 2002,“", Axial and Centrifugal Compressors and Expander-Compressors for Petroleum, Chemical and Gas Industry Services,” Seventh Edition, American Petroleum Institute, Washington, DC, .

[14] Whalen, J. K., Alvarez, E. and Palliser, L. (2004), "Thermoplastic Labyrinth Seals for Centrifugal Compressors", Proceedings of the Thirty-Third Turbomachinery Symposium, Houston, TX, September, pp. 20.

[15] Zeidan, F. Y., Perez, R. X. and Stephenson, E. M. (1993), "The Use of Honeycomb Seals in Stabilizing Two Centrifugal Compressors", Proceedings of the Twenty-Second Turbomachinery Symposium, pp. 3.

[16] Richards, Robert L., et al. "Using a damper seal to eliminate subsynchronous vibrations in three back-to-back compressors." Proceedings of the 24th Turbomachinery Symposium. 1995.

[17] El-Gamal, H. A., Awad, T. H. and Saber, E. (1996), "Leakage from labyrinth seals under stationary and rotating conditions", Tribology International, vol. 29, no. 4, pp. 291-297

[18] Vance, J., Zeidan, F. and Murphy, B. (2010), machinery vibration and rotordynamics, John Wiley & Sons, Inc, Hoboken, New Jersey.

[19] Eldin, Ahmed Mohamed Gamal. Leakage and rotordynamic effects of pocket damper seals and see-through labyrinth seals. Diss. Texas A&M University, 2007.

[20] Camatti, Massimo, et al. "Instability of a High Pressure Compressor Equipped With Honeycomb Seals." Proceedings of the 32nd Turbomachinery Symposium, Turbomachinery Laboratory, Texas A&M University, College Station, TX, September. 2003.

[21] Moore, J. Jeffrey, et al. "Investigation of a Rotordynamic Instability in a High Pressure Centrifugal Compressor Due to Damper Seal Clearance Divergence." Seventh IFToMMConference on Rotor Dynamics, Vienna, Austria (2006).

[22] Rodrigues Rodrigues, Margarita. "Improving performance and rotordynamic characteristics of injection compressors via much longer balance-piston and division-wall seals." Master's thesis, Texas A&M University. Available electronically from http://hdl. handle. net/1969 1 (2006).

[23] Sprowl, T. B. and Childs, D. W. (2007), "A study of the effects of inlet preswirl on the dynamic coefficients of a straight-bore honeycomb gas damper seal", Journal of Engineering for Gas Turbines and Power, vol. 129, no. 1, pp. 220-229.

[24]Kocur, J., and G. Hayles. "Low Frequency Instability in a Process Compressor." Proceedings of the 33rd Texas A&M University Turbomachinery Symposium. 2004.

[25]Smalley, Anthony J., et al. "Dynamic characteristics of the diverging taper honeycomb-stator seal." Journal of turbomachinery 128.4 (2006): 717-724.

[26] Wygant, Karl D., Lloyd E. Barrett, and Ronald D. Flack. "Influence of Pad Pivot Friction on Tilting-Pad Journal Bearing Measurements—Part II: Dynamic Coefficients©." Tribology transactions 42.1 (1999): 250-256.

[27] Brechting, Robert, et al. "Load Direction Effects in Measured Static and Dynamic Operating Characteristics of Tilting Pad Journal Bearings." Australian Journal of Mechanical Engineering 2.2 (2005): 143.

[28] Pettinato, Brian, and Pranabesh De Choudhury. "Test Results of Key and Spherical Pivot Five-Shoe Tilt Pad Journal Bearings—Part I: Performance Measurements." Tribology transactions 42.3 (1999): 541-547.

[29] Yang, Seong Heon, Chaesil Kim, and Yong-Bok Lee. "Experimental study on the characteristics of pad fluttering in a tilting pad journal bearing." Tribology international 39.7 (2006): 686-694.

[30] Fillon, Michel, and Douglas Hargreaves. "Analysis of a Tilting Pad Journal Bearing to Avoid Pad Fluttering." Tribiology International 40.4 (2006): 607-612.

[31] Kim, Sung-Gi, and Kyung-Woong Kim. "Influence of pad–pivot friction on tilting pad journal bearing." Tribology International 41.8 (2008): 694-703.

[32] Zeidan, Fouad Y., and Bernard S. Herbage. "Fluid film bearing fundamentals and failure analysis." Proceedings of the 20th Turbomachinery Symposium. 1991.

[33] Walid Jouri Senior Consultant of Glomacs “Advanced Vibration Analysis "Conducted for Petroleum Development Oman(PDO). June 2013

[34] Wachel, J. C. "Nonsynchronous Instability of Centrifugal Compressors." ASME paper 75-PET (1975): 22.

[35] Wilcox, Ed. "UNEXPECTED ROTORDYNAMIC INSTABILITY."

[36] Childs, Dara W., Matthew Graviss, and Luis E. Rodriguez. "Influence of groove size on the static and rotordynamic characteristics of short, laminar-flow annular seals." Journal of tribology 129.2 (2007): 398-406.

[37] Bill Forsthoffer, W. E. (2005), "16 - Centrifugal compressor rotor design", in Forsthoffer's Rotating Equipment Handbooks, Elsevier Science, Oxford, pp. 169-178.

[38] Newkirk, B.L., 1924, “Shaft Whipping”, General Electric Review, 27(3), pp.169-178

[39] Jeffcott, H.H., 1919, “The Lateral Vibration of Loaded Shafts in the Neighbourhood of a Whirling Speed: The Effect of Want of Balance,”Philosophical Magazine, Ser.6, 37, pp.304

[40] Kimball, A.L. Jr., 1924, “Internal Friction Theory of Shaft Whirling”, General Electric Review, 27(4), pp.244-251

[41] Jafri, S., Shrink Fit Effects on Rotordynamic Stability: Experimental andTheoretical Study. Thesis, Texas A&M University, August 2007.

[42] Gunter, Edgar J., and P. R. Trumpler. "The influence of internal friction on the stability of high speed rotors with anisotropic supports." Journal of Manufacturing Science and Engineering 91.4 (1969): 1105-1113.

[43] Walton, J., Artilles, A., Lund, J., Dill, J., Zorzi, E., 1990, “Internal Rotor FrictionInstability”, Mechanical Technology Incorporated Report, 88TR39

[44] Walton Jr, James F., and Michael R. Martin. "Internal Rotor Friction Induced Instability in High-Speed Rotating Machinery." ASME Vibration of Rotating Systems 60 (1993): 297-305.

[45] Kimball, A.L. Jr., 1925, “Measurement of Internal Friction in a Revolving Deflected Shaft,”, General Electric Review, 28, pp.554-558

[46] Kimball, A.L. Jr., Lovell, D.E., 1926, “ Internal Friction in Solids,” Transactions of ASME, 48, pp.479-500

[47] Black, H. F. "The stabilizing capacity of bearings for flexible rotors with hysteresis." Journal of Manufacturing Science and Engineering 98.1 (1976): 87-91.

[48] Ehrich, F.F., 1964, “Shaft Whirl Induced by Rotor Internal Damping”, Journal of Applied Mechanics, 31, pp. 279-282

[49] Vance, J.M., Ying, D., “Effects of Interference Fits on Threshold Speeds of Rotordynamic Instability”, Paper No. 2007, Proceedings of the International Symposium on Stability Control of Rotating Machinery, August 20-24, 2001, South Lake, Tahoe, California

[50] Mir, Mohammad M., “Effects of Shrink Fits on Threshold Speeds of Rotordynamic Instability”, MS thesis, 2001, Texas A&M University, College Station

[51] Srinivasan, A., “Effects of Shrink fits on Threshold Speeds of Rotordynamic Instability”, MS thesis, 2003, Texas A&M University, College Station

[52] Murphy, B.T., “Eigenvalues of Rotating Machinery”, PhD dissertation, 1984,Texas A&M University, College Station

[53] Muszynska, A. "Rotor-to-Stationary Part Rubbing Contact in Rotating Machinery. Rotor Dynamics." (2005): 555-710.

[54] Rao, J. S. (1991), ROTOR DYNAMICS, Second ed, WILEY EASTERN LIMITED, New Delhi, India.

[55] Newkirk, B. L., 1926, “Shaft Rubbing,” Mechanical Engineering, 48, pp. 830-832.

[56] De Jongh, F. M., 2008, “The Synchronous Rotor Instability Phenomenon – Morton Effect,” Proceedings of the 37th Turbomachinery Symposium, Turbomachinery Laboratory, Texas A&M University, College Station, Texas

[57] Alford, J. S. "Protecting turbomachinery from self-excited rotor whirl." Journal of Engineering for Power 87.4 (1965): 333-343.

[58] Murphy, Brian T., and Joshua A. Lorenz. "Simplified Morton effect analysis for synchronous spiral instability." Journal of Vibration and Acoustics 132.5 (2010): 051008.

[59]Kita, Masayuki, Takeshi Hataya, and Yasunori Tokimasa. "Study of a rotordynamic analysis method that consider torsional and lateral coupled vibrations in compressor trains with a gearbox." Proceedings of the thirty-sixth turbomachinery symposium. 2007.

[60]Corcoran, J. P., J. A. Kocur, and M. C. Mitsingas. "Preventing undetected train torsional oscillations." Proceedings of the Thirty-ninth Turbomachinery Symposium. Houston, Texas. USA: Texas A&-M U-niversity. 2010.

[61]Wu, Xi, et al. "Finite element analysis of coupled lateral and torsional vibrations of a rotor with multiple cracks." Proceedings of ASME Turbo Expo. 2005.

[62]Sihler, Christof, et al. "Torsional mode damping for electrically driven gas compression trains in extended variable speed operation." Proc. 38th Turbomachinary Symposium. 2009.

[63]Murphy, B. T. and Vance, J. M., "Labyrinth Seal Effects on Whirl Stability," Number C306-80, ImechE Proceedings, pp. 369-373 (1980)

[64]Reynolds, Osborne. "On the Theory of Lubrication and Its Application to Mr. Beauchamp Tower's Experiments, Including an Experimental Determination of the Viscosity of Olive Oil." Proceedings of the Royal Society of London 40.242-245 (1886): 191-203.